Study on Gold Nanoparticles for Biological Applications

Yinan Zhang

A thesis presented in partial fulfilment

of the requirements for the degree of

Doctor of Philosophy

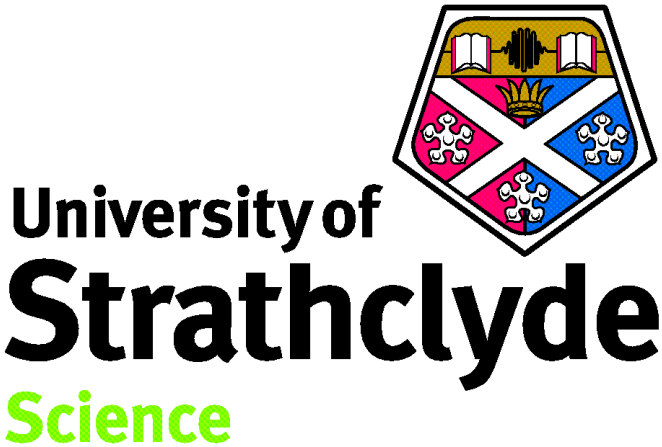

Department of Physics

University of Strathclyde

March 2013

This thesis is the result of the author's original research. It has been composed by the author and has not been previously submitted for examination which has led to the award of a degree.

Signed:

Date:

Acknowledgement

I sincerely thank my supervisor Dr. Yu Chen and second supervisor Prof. David Birch for their help, guidance and support all through my PhD project.

I would like to express my gratitude to EPSRC for providing me with a PhD studentship.

I would also like to thank Dr. Jun Yu, Dr. Alastair Wark, Dr. Jens Sutter, Dr. Jan Karolin, Ms. Dan Xu, and Ms. Alison McLintock for their special and kind support in my research work. And I am really appreciate all the great help provided by members from the Photophysics group. Moreover, I would like to thank Dr N. Lidgi-Guigui and Prof. R. E. Palmer in Birmingham University for providing samples of size-selected gold nanoclusters.

Finally I would thank my parents, without whom I would never have had the opportunity to finish my PhD study.

Abstract

Gold nanoparticles have attracted much attention in the field of biological research, especially in biological imaging and sensing due to their unique physical properties. Fluorescence is a highly-sensitive, non-invasive biological study method and has been widely used in a variety of research topics. The aim of this thesis is to study the unique optical properties of gold nanoparticles and demonstrate their application in biological imaging and sensing through fluorescence microscopic and spectroscopic techniques.

An introduction of gold nanoparticles and fluorescence techniques used in this project is given in Chapter 1.

In Chapter 2, the synthesis method of gold nanoparticles, dependence of optical properties on particle size and shape, the unique spectroscopic characterization and microscopic application of gold nanorods are discussed.

Fluorescence lifetime imaging microscopy (FLIM) based on two-photon luminescence lifetime from gold nanorods in cell culture, and the advantages of this method in biological imaging are demonstrated in Chapter 3.

In Chapter 4, the energy transfer between a DNA dye, 4'-6-Diamidino-2-phenylindole (DAPI), and different types of gold nanoparticles in solution is demonstrated using FLIM. Biological imaging application based on energy transfer between gold particles and DAPI in cell culture is discussed as well in this chapter.

A study on energy transfer process concerning different excitation conditions is reviewed in Chapter 5. Furthermore, application of fluorescence resonant energy transfer (FRET) based FLIM method in the research of intracellular pathway of gold nanoparticles in cells is demonstrated.

Chapter 6 presents a systematic study on the cytotoxicity of gold nanorods in cell culture using MTT (3-(4, 5-Dimethylthiazol-2-yl)-2,5-diphenyltetrazolium bromide) method. The effects of particle shape, surface conditions, dosage, incubation time on the cytotoxicity and the mechanism of cytotoxicity are discussed.

In Chapter 7, a brief summary and outlook to future work are presented.

Contents

List of figures and tables

Chapter 1 Introduction

1.1 Gold nanoparticles

Metal nanoparticles have attracted much attention due to their unique physical properties, especially the surface plasmon resonance (SPR), which is the collective oscillation of free electrons in response to the resonant incidence electromagnetic field. The SPR leads to great enhancement in the optical properties of nanoparticles, such as scattering and absorption.[1, 2] Among all types of nanostructure, there have been substantive literature focused on gold nanorods, as they have special SPR structure. Compared to gold nanospheres (GNSs), the surface plasmon band of GNRs splits into two bands: one locates around 520nm and the other one can range from visible light to near-infrared (NIR) region.[3, 4,] As the NIR band permits photons to penetrate organic tissues with relatively high transmittivity, gold nanorods have great application potential in biological research, including bioimaging,[5-9] biosensing[10-12] and photothermal therapy.[13-15] For bioimaging, GNRs can emit two-photon luminescence (TPL) with strong intensity (58 times bigger than that from Rhodamine).[16] Furthermore TPL microscopy has excellent spatial resolution due to its quadratic dependence on incidence light intensity.[17] TPL from gold nanorods is sensitive to the polarization of the incident excitation.[16, 18] For the application in biosensing, as the SPR wavelength depends critically on the dielectric constant of surrounding medium, gold nanoparticles is sensitive to the change of environment of nanoparticles hence can be used for sensing.[19] By monitoring the spectroscopic change of dye molecule-nanoparticle pair, gold nanoparticles can be utilized in distance dependent sensing applications, such as fluorescence resonant energy transfer.[20] For the photothermal application, gold nanoparticles can also convert radiative energy into heat, endowing them with intense photothermal properties and has been proven to be localized, targeted, high efficacy, and lack of side effects.[21] Such localized heating effects can be directed toward the eradication of diseased tissue, providing a non-invasive alternative to surgery.[22, 23] Nanorods with well-

defined shapes and sizes can be synthesized by seeded growth methods, and their longitudinal plasmon resonances can be finely tuned as a function of aspect ratio (long axis of nanorod divided by short one).[24, 25] Moreover, there are numerous measures for conjugating gold nanorods with biomolecule labels for cell targeting or intracellular delivery,[26] such as folic acid,[22] antibodies,[27] and DNA,[28] introduced by surface functionalization processes. By assembling single gold nanoparticles into functional structure, they can be even more useful in sensing and detection of a variety of analytes including environmental toxins and biomarkers.[29]

1.1.1 Theory on surface plasmon resonance of gold nanoparticles

The surface plasmon oscillation is the coherent excitation of free electrons within the conduction band, leading to an in-phase oscillation. The electric field of incident light induces a polarization of the free conduction electrons. As the ionic core is much heavier than the free electron, net charge will occur at the nanoparticle boundaries acting as a restoring force. Then a dipolar oscillation of electrons is created. An illustration of surface plasmon of metal particles is shown in Fig.1.1.

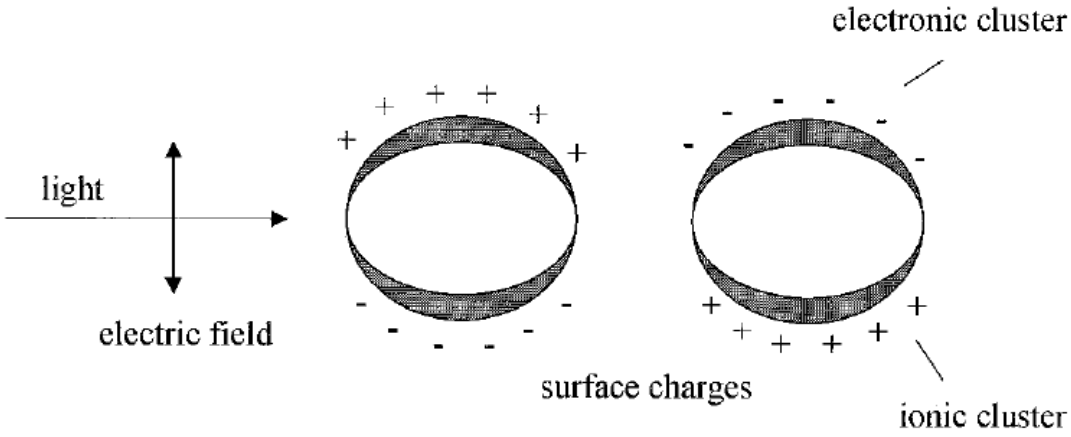

Fig.1.1 Illustration of the excitation of the dipole surface plasmon oscillation.[30]

The absorption of nanoparticles in optically and spatially homogeneous solution, with the intensity denoted by *I*, particle density by *N* and beam path length by *x*, can be expressed as:

$$\frac{dI(x)}{dx} = -NC_{ext}I(x)$$

(1.1)

where C_{ext} is the extinction coefficient. By integrating the above equation, the absorption of particle solution is given by:

$$I(x) = I_0 \exp(-NC_{ext}x)$$

(1.2)

The above equation shows that the absorption of particles is proportional to the particle extinction coefficient C_{ext}, particle density N and the beam transmission length x.

For spherical particles, the surface plasmon induced absorption can be described by Mie theory. The expressions are displayed below.[30]

$$\sigma_{ext} = \frac{2\pi}{|k|^2}\sum_{L=1}^{\infty}(2L+1)Re(a_L + b_L)$$

(1.3)

$$\sigma_{abs} = \frac{2\pi}{|k|^2}\sum_{L=1}^{\infty}(2L+1)Re(|a_L|^2 + |b_L|^2)$$

(1.4)

$$\sigma_{abs} = \sigma_{ext} - \sigma_{sca}$$

(1.5)

$$k = 2\pi\frac{\sqrt{\varepsilon_m}}{\lambda}$$

(1.6)

$$a_L = \frac{m\psi_L(mx)\psi_L'(x) - \psi_L'(mx)\psi_L(x)}{m\psi_L(mx)\eta_L'(x) - \psi_L'(mx)\eta_L(x)}$$

(1.7)

$$b_L = \frac{\psi_L(mx)\psi_L'(x) - m\psi_L'(x)\psi_L(x)}{\psi_L(mx)\eta_L'(x) - m\psi_L'(x)\eta_L(x)}$$

(1.8)

Here, σ_{ext}, σ_{sca} and σ_{abs} represents extinction, scattering and absorption cross-section separately. a_L and b_L, the scattering coefficients, are functions of wavelength λ and the medium dielectric function ε_m. The dielectric function of particles $\varepsilon(\omega)=\varepsilon_1(\omega)+i\varepsilon_2(\omega)$. $m=n/n_m$, where n is the complex refractive index of the particle and n_m the real refractive index of the medium. k is the wave-vector and $x=|k|r$ with r representing the radius of the nanoparticle. ψ_L and η_L are the Ricatti-Bessel cylindrical functions. The prime indicates differentiation. L is the summation index of the partial waves. L=1 corresponds to the dipole oscillation, and L=2 is associated with the quadruple oscillation and so on.

The extinction cross-section can be normalized to give the extinction cross-section per unit area:

$$Q_{ext} = \frac{\sigma_{ext}}{\pi r^2}$$

(1.9)

where r is the particle radius, and can be conveniently transferred to commonly used extinction coefficient in the units of $M^{-1}cm^{-1}$ as following:

$$\varepsilon(M^{-1}cm^{-1}) = \frac{3 \times 10^{-3} V_m Q_{ext}}{4 \times 2.303 r}$$

(1.10)

where $V_m(cm^3mol^{-1})$ represents the molar volume of the metal.

For nanoparticles much smaller than the wavelength of incidence light, only the dipole oscillation contributes significantly, with a_1 and b_1 expressed as:

$$a_1 = -\frac{i2x^3}{3}\frac{m^2-1}{m^2+1} - \frac{i2x^5}{5}\frac{(m^2-2)(m^2-1)}{(m^2+2)^2} + \frac{i4x^5}{9}\left[\frac{m^2-1}{m^2+2}\right]^2 + O(x^7) \tag{1.11}$$

$$b_1 = -\frac{i2x^5}{15}\frac{m^2-1}{2m^2+2} + O(x^7) \tag{1.12}$$

The Mie theory can be reduced to the following equation:

$$\sigma_{ext}(\omega) = 9\frac{\omega}{c}\varepsilon_m^{3/2}V\frac{\varepsilon_2(\omega)}{[\varepsilon_1(\omega)+2\varepsilon_m]^2+\varepsilon_2(\omega)^2} \tag{1.13}$$

with V being the particle volume, ω the angular frequency of the incidence light and c the speed of light. The resonance condition is fulfilled when $\varepsilon_1(\omega)$=-$2\varepsilon_m$ only if ε_2 is weakly dependent on ω. The above equation can be used to explain the absorption spectra of small gold nanoparticles. For large particles, the dipole approximation is not valid and higher-order modes of oscillation have to be taken into account, which will cause the absorption spectrum peaking at lower energies.

1.1.2 Surface plasmon resonance of gold nanorods

For gold nanorods, the absorption spectrum splits into two bands with one at around 500nm corresponding to the oscillation of the electrons perpendicular to the long axis and the other at lower energy representing the oscillation of the free electrons along the long rod axis. These two modes are referred to as the transverse and longitudinal

plasmon surface absorption. The scheme of surface plasmon induced absorbance bands is shown in Fig.1.2.

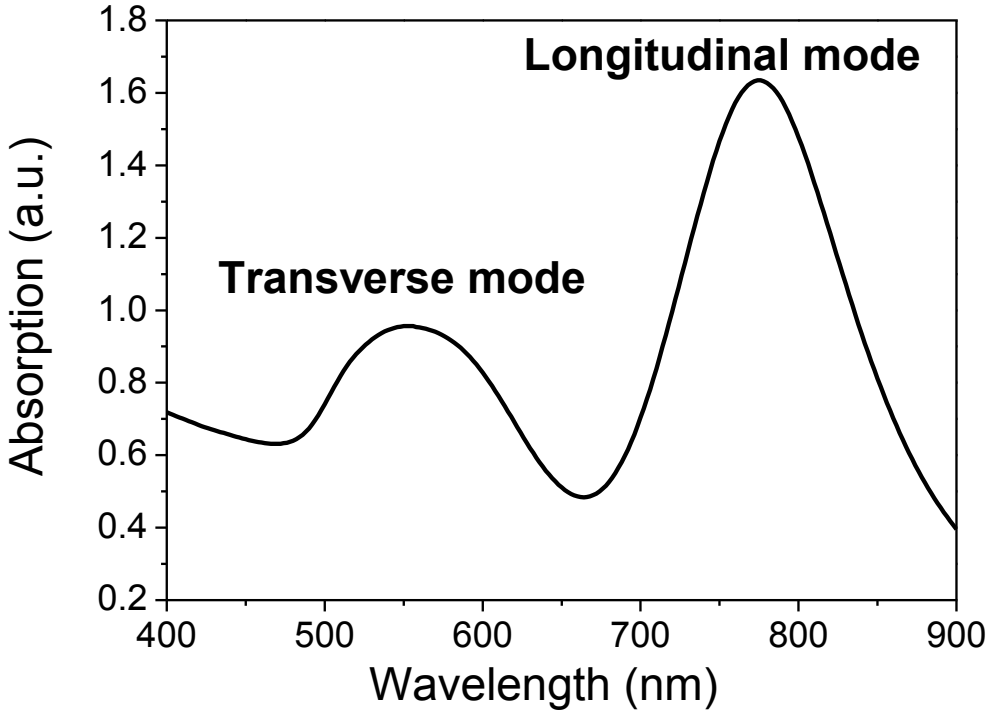

Fig. 1.2 An absorption spectrum of gold nanorods showing two surface plasmon modes.

Mie theory as described above is strictly applicable only to spherical particles. By extending Mie's theory, the optical absorption of randomly oriented gold nanorods can be described by Gans's theory, Within the dipole approximation, according to Gans's theory, the extinction cross-section is,[30]

$$\sigma_{ext}(\omega) = \frac{\omega}{3c} \varepsilon_m^{3/2} V \frac{(\frac{1}{P_j^2})\varepsilon_2}{\{\varepsilon_1(\omega) + [\frac{1-P_j}{P_j}]\varepsilon_m\} + \varepsilon_1^{\,2}} \qquad (1.14)$$

where P_j are the depolarization factors along the three axes A, B and C of the nanorod with A>B=C, defined as

$$P_A = \frac{1-e^2}{e^2}[\frac{1}{2e}\ln(\frac{1+e}{1-e}) - 1],$$

(1.15)

$$P_B = P_C = \frac{1-P_A}{2},$$

(1.16)

$$e = [1-(\frac{B}{A})^2]^{1/2}$$

(1.17)

In analogy with the absorbance of spheres, the plasmon resonance condition is:

$$\varepsilon_1(\omega) + (\frac{1-P_j}{P_j})\varepsilon_m = 0$$

(1.18)

Gansg's theory can explain how the surface plasmon band reacted to the influence from the aspect ratio of particle, the solvent medium and shell layer. As discussed above, the peak position of surface plasmon band depends on the shape parameter, Pj: a small change in the aspect ratio will lead to a drastic change in the absorption spectrum, or the surface plasmon structure. The extinction spectrum of GNRs with different aspect ratios is shown in Fig.1.3.[31] As the aspect ratio varies from 2.65 to 3.65, the longitudinal band red shifts more than 100nm. There have been reports indicating that the peak position and aspect ratio follow a linear relationship (shown in Fig.1.3 (b)). As the peak position is a function of the surrounding medium refractive index as well (shown in Fig.1.3 (c)), GNRs change colour when dissolved in different solvents. Based on the dependence of the surface plasmon resonance

structure to both geometric and dielectric effects, gold nanoparticles have promising applications as sensors.

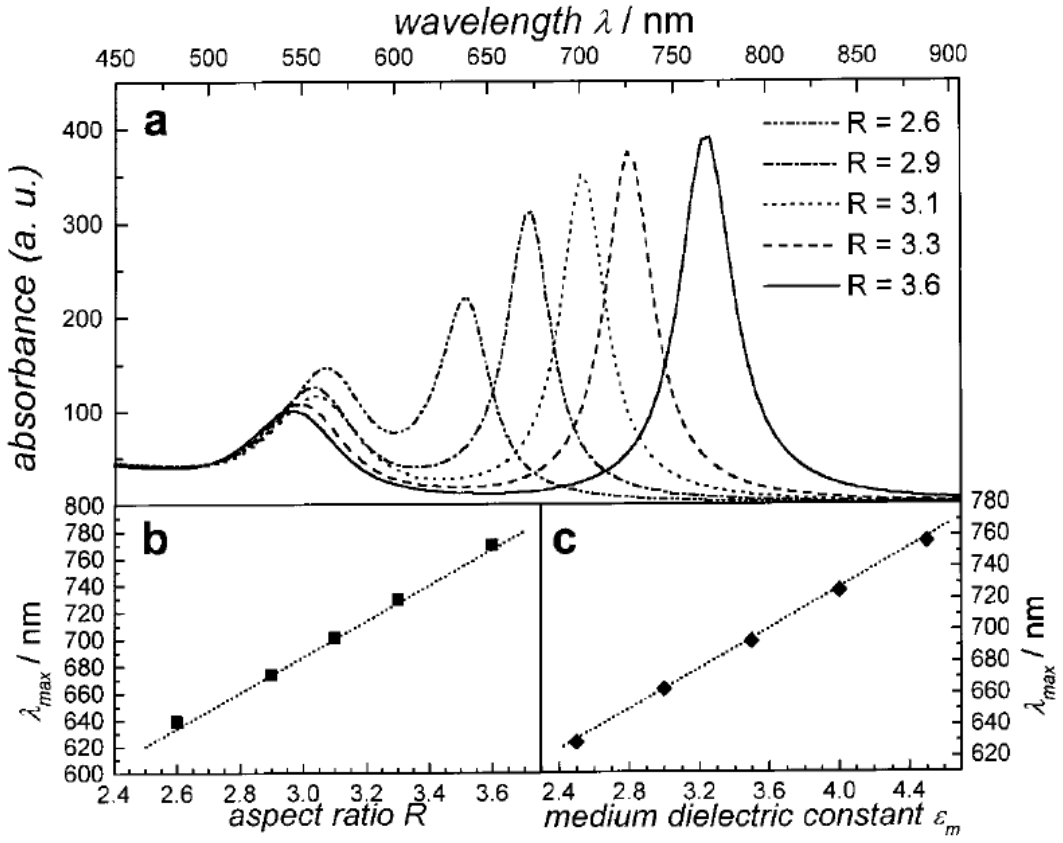

Fig.1.3 (a) Calculation with Gans's theory of absorption of gold nanorods as a function of aspect ratio R; (b) and (c) The dependence of maximum longitudinal absorption peak on aspect ratio and medium dielectric constant. [31]

1.2 Fluorescence

1.2.1 Fluorescence process

Luminescence is the emission of light from excited states of any substance. As shown in Fig.1.4, luminescence is divided into two categories: fluorescence and phosphorescence, depending on the nature of the excited state involved in the process. The electron in the excited singlet state has the opposite spin to the second electron in the ground state, which means that the return to ground state is spin allowed and will occur rapidly. The emission rates of fluorescence are typically $10^8 s^{-1}$, so that a typical fluorescence lifetime is around 10ns. Compared to fluorescence,

phosphorescence is the emission of light from an excited triplet state. Transition to the ground state is forbidden as the electron in the excited state has the same spin as the ground state electron. Therefore, the emission rate of phosphorescence is low and the lifetime is usually in the rage of milliseconds to seconds.[32]

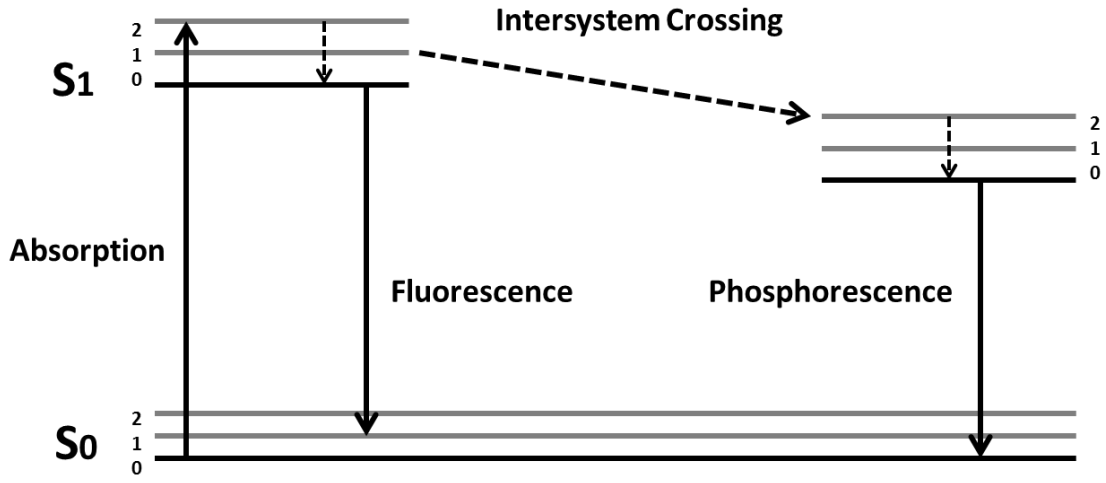

Fig.1.4 Diagram of luminescence phenomenon.

The fluorophores can return to the ground state by either a radiative (emitting photons) or non-radiative process, as shown in Fig.1.5. The fluorescence quantum yield is the ratio of the number of emitted photons to the number absorbed, and is defined by the following equation,

$Q=\Gamma/(\Gamma+k_{nr})$,

(1.19)

where Q, Γ, and k_{nr} represents the quantum yield, the emission rate and the non-radiative decay rate of fluorophore, respectively.

The lifetime of the excited state is defined by the average time the fluorophore molecules stay in the excited state before return to the ground state; for a single ground-excited state system, it can be expressed as,

$\tau=1/(\Gamma+k_{nr})$.

(1.20)

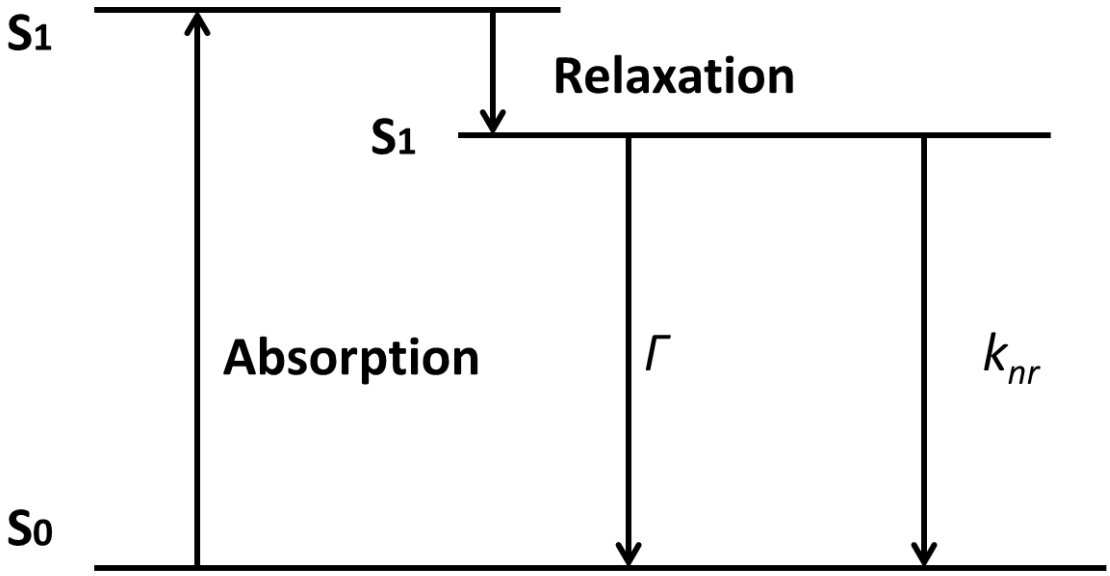

Fig.1.5 Diagram demonstrating fluorescence lifetime and quantum yield.

Fluorescence emission is a random process, and few molecules emit their photons at $t = \tau$. The lifetime is an average value of the time spent in the excited state. The lifetime of the fluorophore in the absence of non-radiative process is called the intrinsic or natural lifetime, and can be given by,

$$\tau_n = 1/\Gamma. \tag{1.21}$$

The natural lifetime can be calculated from the absorption spectra, extinction coefficient, and emission spectra of the fluorophore. The radiative decay rate Γ can be calculated by the following equation,

$$\Gamma \cong 2.88 \times 10^9 n^2 \frac{\int F(\bar{\nu})d\bar{\nu}}{\int \frac{F(\bar{\nu})d\bar{\nu}}{\bar{\nu}^3}} \int \frac{\varepsilon(\bar{\nu})}{\bar{\nu}} d\bar{\nu}$$

$$= 2.88 \times 10^9 n^2 < \bar{\nu}^{-3} > \int \frac{\varepsilon(\bar{\nu})}{\bar{\nu}} d\bar{\nu} \tag{1.22}$$

where $F(\bar{\nu})$, $\varepsilon(\bar{\nu})$, and n is the emission spectrum, absorption spectrum in wavenumber unit and the refractive index of the medium respectively. This

expression assumes no interaction with the solvent, and *n* is considered to be constant over the absorption and emission band.

The natural lifetime can be calculated from the measured lifetime and quantum yield

$\tau_n = \tau / Q.$

(1.23)

In practice, suppose after excitation, n_0 of fluorophores are excited to the excited sate, then the excited-state population will decay with a rate $\Gamma + k_{nr}$ as discussed above (Eqn.20),

$$\frac{dn(t)}{dt} = (\Gamma + k_{nr})n(t)$$

(1.24)

Where *n(t)* is the number of excited fluorophores at time t after excitation. Emission is a random event, and each excited fluorophore has the same probability of emitting in a given period of time. This results in an exponential decay of the excited sate population,

$n(t) = n_0 exp(-t/\tau).$ (1.25)

In a practical fluorescence experiment, it is the fluorescence intensity rather than the excited molecule population will be detected. Therefore, the above equation can be written in terms of the time dependent fluorescence intensity *I(t)*.

$I(t) = I_0 exp(-t/\tau),$

(1.26)

where I_0 is the initial intensity at time 0.

The lifetime τ can be determined by fitting the intensity-time curves to decay models, normally the multi-exponential model:

$$I(t) = \sum_i \alpha_i \exp(-t/\tau_i) \tag{1.27}$$

Where α_i is normalized to unity.

For a single exponential decay, 63% or 1/e of the molecules return to ground state prior to t= τ.

1.2.2 Two-photon luminescence (TPL)

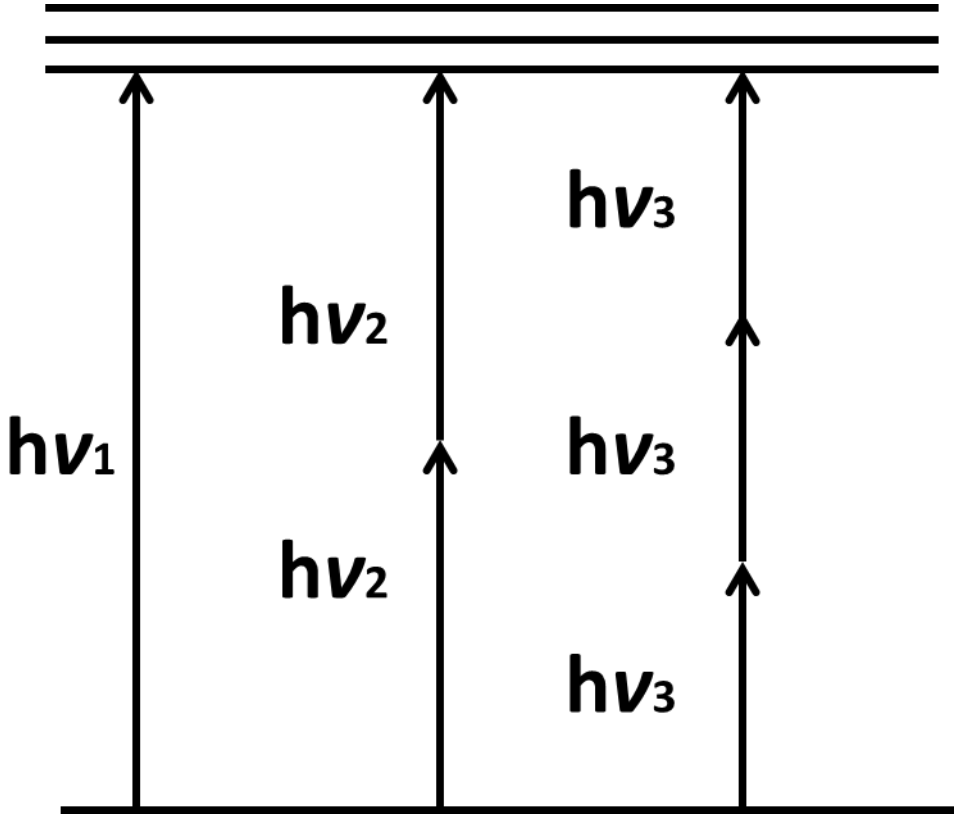

Fig.1.6 Diagram of single and multi photon excitations.

Multi-photon luminescence is a process in which a fluorophore absorb more than one incident photons with lower energy and emit photons with higher energy. The two-photon excitation (TPE) fluorescence is related to the simultaneous absorption of two lower-energy photons, which cooperatively provide the energy needed for the fluorescence process. The illustrating diagram of multi-photon luminescence is shown in Fig.1.6. Properties of TPE can be discussed following a simple way with an assumption that the probability of a molecule undergoing n-photon absorption is proportional to the probability of finding n photons within the volume it occupies at any moment in time.[4]

We consider a laser beam passes through a cube of side *s*, much smaller than the beam width. The mean energy E_m in this cube, for a beam of wavelength λ is

$$E_m = mhc/\lambda, \tag{1.28}$$

where *m* corresponds to the mean number of photons. Since the cross-sectional area is s^2, and the time needed for each photon to cross the cube is s/c, then the power density *I*, of the laser beam is

$$I = \frac{E_m}{s^2 \times s/c} = \frac{mhc^2}{\lambda s^3} \tag{1.29}$$

with *c* representing the speed of light.

Considering $V=s^3=V_m/N_a$, where for a molecule the mean volume occupied is the molar volume V_m divided by Avogadro's constant N_a, we obtain

$$m = \frac{IV_m\lambda}{N_a hc^2} \tag{1.30}$$

For a 750nm laser with intensity GWcm^{-2} into a molecular volume of the order of 10^{-4}m^{3}mol^{-1}, the value of m is of the order of 10^{-5}.[4]

In order to find the probability p_n which means that n photons are in the molecular volume, we use a Poisson distribution, resulting in

$$P_n = \frac{m^n}{n!} e^{-m} \tag{1.31}$$

Since *m* is small, the exponential can be expanded in Taylor series and only the first term taken into account. Therefore, the probability for TPE, *n*=2, p_2 is[4]

$$p_2 = \frac{1}{2} m^2 \propto \gamma I^2 \tag{1.32}$$

where γ is a proportionality factor. The dependence of TPE on I^2 is obtained.

The quadratic dependence of TPE on the incident intensity has great advantages to microscopy imaging. Since the amount of light absorbed is proportional to the square of the intensity, focusing the beam decreases its size but increase its intensity, as shown in Fig. 1.7. As a result the amount of light absorbed is not constant across the beam passing direction, but reaches a maximum at the focal plane where the incident intensity is the highest. This effect results in strong localized excitation, leading to a better depth resolution and a reduced photodamage to the fluorophores than one photon excitation.[4, 33-37]

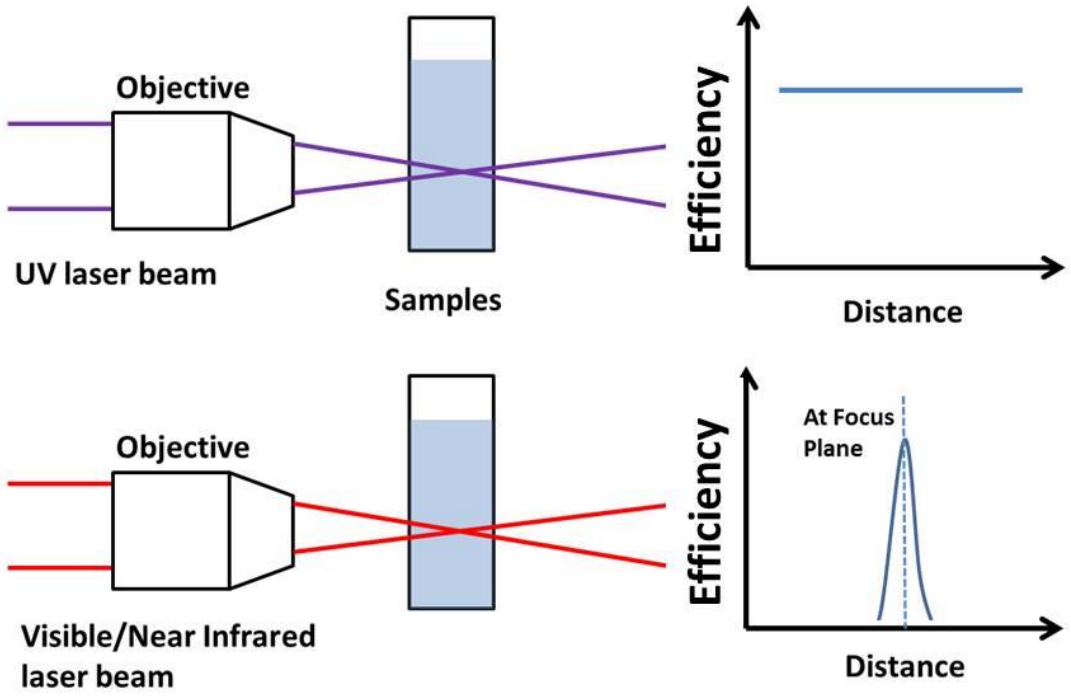

Fig.1.7 Illustration of excitation efficiency on beam pathway into specimen under single and two-photon excitation.

1.3 Time domain measurement and time-correlated single photon counting (TCSPC)

Photon counting techniques follows the concept that the detector reacts to a random sequence of pulses corresponding to the detection of individual photons. The light intensity is represented by the density of the pulses, not by their amplitude. The intensity of the light signal is obtained by counting the pulses in subsequent time channels.[38, 39]

Time-correlated single photon counting, or TCSPC, is based on the concept that the probability of detecting a single photon at time *t* is proportional to the fluorescence intensity at that given time. By accurately measuring the arrival time of every single photon, the decay waveform can be reconstructed. . The principle of TCSPC is shown in Fig. 1.8. After excitation, when a single emitting photon from the fluorophore is detected, the arrival time of the corresponding photon to the detector

is measured, which adds ‘1’ count in a memory location with an address proportional to the detection time. After many signal periods, a large number of photons have been detected, and the distribution of the photons over the time in the signal period builds up. The result represents the ‘waveform’ of the optical pulse. [38, 40-42]

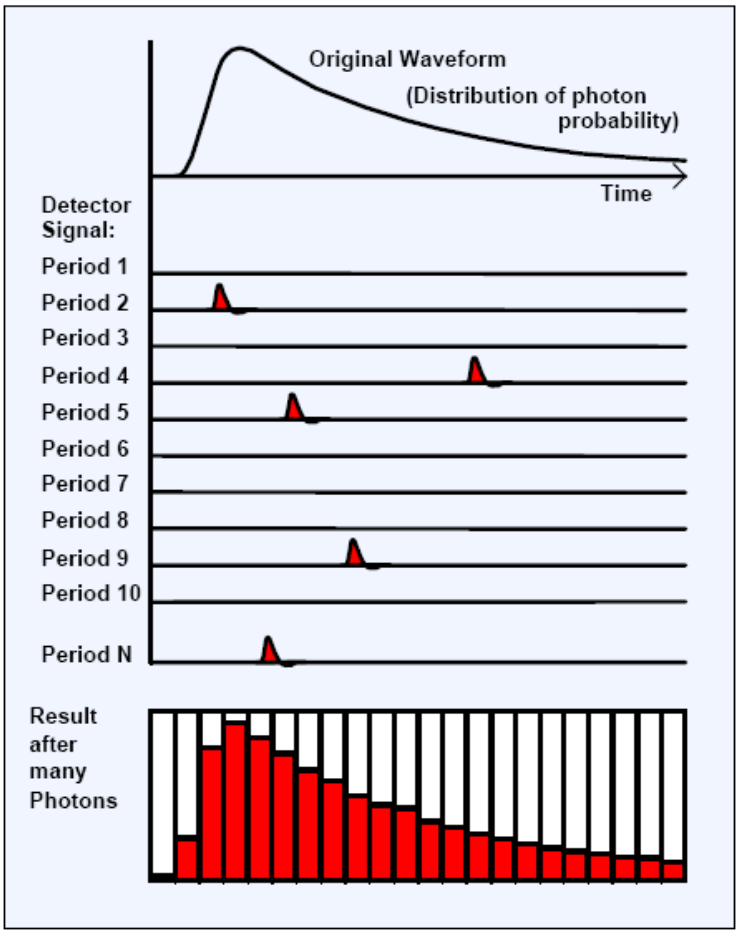

Fig.1.8 The concept of TCSPC technique.[38]

A typical TCSPC setup is shown in Fig1.9. In a TCSPC measurement process, the pulse excitation light source sends a reference signal pulse (the start pulse) to the time-to-amplitude converter (TAC). The TAC accordingly generates a voltage which increases linearly with time. After the sample is excited by the excitation source, the detector will record a single emission photon and generate a pulse to the TAC as well (the stop pulse), which will terminate the voltage increasing at TAC. The voltage now is proportional to the time delay between the excitation and emission signals, or between the start and stop pulse. The voltage then is amplified by a biased amplifier (the AMP) and converted to a numerical value by the analog-to-digital converter

(ADC). The ADC output is used as an address word for the measurement data memory. When a photon is detected, the ADC output word addresses a memory location corresponding to the time of the photon. By incrementing the data contents of the addressed location the photon distribution over time is built up. There is a 'Constant Fraction Discriminator', CFD, implemented before both start and stop pulses going through TAC. The CFD is used to avoid pulse-height induced timing jitter thus the arrival time of pulses can be accurately measured.

In a practical TCSPC setup, usually a 'reverse mode' is applied. In the reverse mode, the pulse from the detector will work as the start pulse to TAC while the pulse from excitation source will work to stop the TAC voltage increasing. This is because in modern TCSPC setup, the light source normally has a very high repetition rate, inducing many pulse periods in which no photons are detected. In these periods the TAC is started but not stopped. Consequently, there must be a circuit in the TAC that detects the out-of-range condition, and resets the TAC frequently. As the emission pulses are much less frequent than the excitation ones, using the reverse mode will be much more efficient.

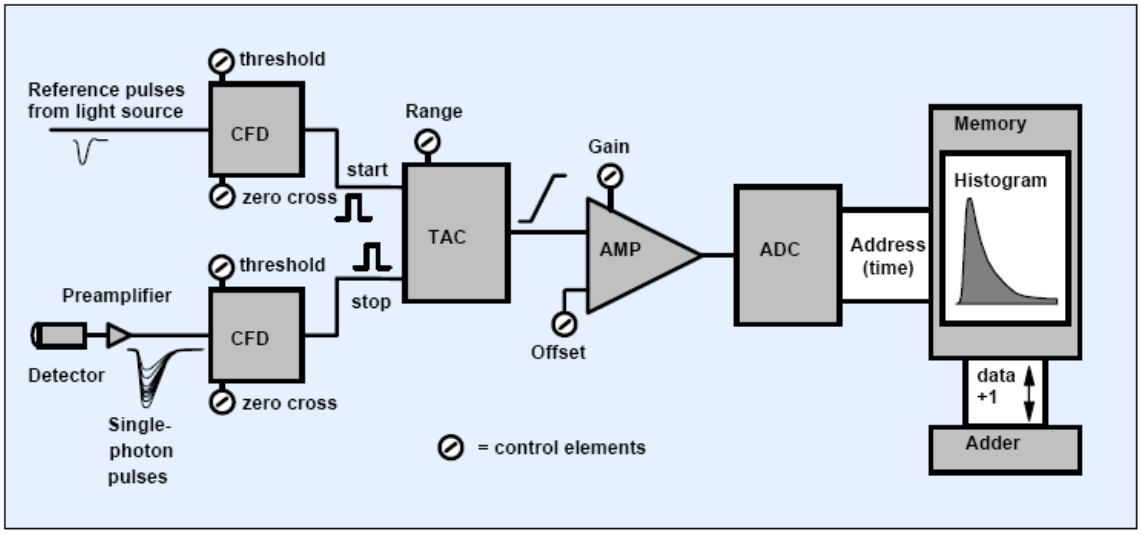

Fig.1.9 Schematic setup of a typical TCSPC lifetime measurement unit. [38]

Fig.1.10 shows the schematic experimental setup of a TCSPC lifetime measurement unit from Horiba Jobin Yvon IBH. As described above, a reverse mode is applied, and both emission and excitation monochromators and polarizers have been implemented. All components, including the FluoroHub (or the control box) are controlled by the Data Station software provided by Horiba IBH.

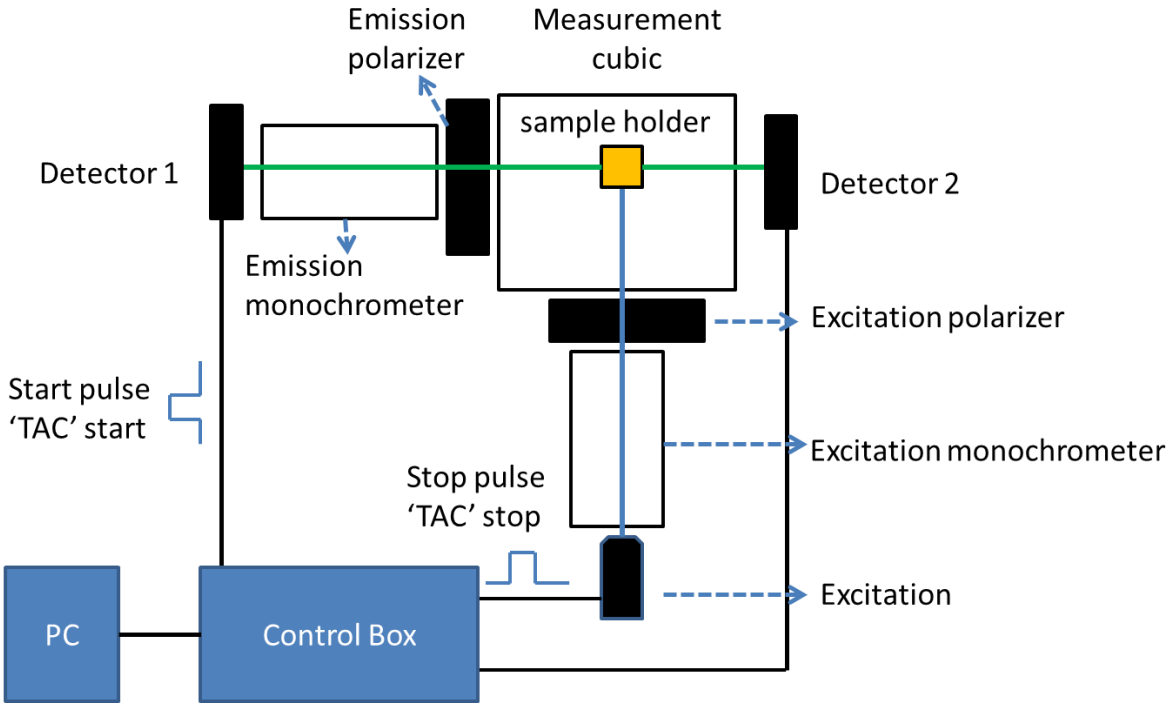

Fig.1.10 Schematic setup of Horiba Jobin Yvon IBH TCSPC fluorescence lifetime measurement unit.

1.4 Data analysis of fluorescence lifetime measurement

1.4.1 The convolution process

Practical experimental data from a TCSPC measurement is complex, as the measured intensity decay is a convolution with the excitation function, which is not exactly a δ-impulse. However, the excitation pulse can be seen as a series of δ -functions with different amplitudes. Each of these δ-functions excites an impulse response from the sample, with the intensity proportional to the height of the δ-function. The measured intensity can be seen as the sum of all these exponential decays, starting with

different amplitudes and different times. [39]The concept of convolution thus can be expressed as:

$$I_k(t) = L(t_k)I(t - t_k)\Delta t(t > t_k) \tag{1.33}$$

in which each δ-function excitation is assumed to excite an impulse response at time t_k. The amplitude of the impulse response function excited at time t_k is proportional to the excitation intensity $L(t_k)$. The term $(t- t_k)$ appears because the impulse response is started at $t=t_k$, and it is understood that there is no emission from $I(t_k)$ before excitation ($t< t_k$). The measured decay $N(t_k)$ is the sum of the impulse responses created by all the individual δ-function excitation pulses occurring until t_k, thus

$$N(t_k) = \sum_{t=0}^{t=t_k} L(t_k)I(t - t_k)\Delta t \tag{1.34}$$

This equation can be expressed in integral form:

$$N(t) = \int_0^t L(t')I(t - t')dt' \tag{1.35}$$

The equation above shows that the experimental intensity at time *t* is determined by the sum of all the intensities expected for all the -function excitation pulses occurring until *t*. There will be new intensity decays excited as long as there is non-zero intensity in $L(t_k)$. This is the reason why the measured decay depends on the instrument response function (IRF) shape.

1.4.2 The least squares analysis

Least squares analysis is used to test whether a given mathematical model is consistent with the experimental data, and to determine the parameters for the model having the highest probability of being correct. Least squares analysis provides the best estimate for parameters if the data satisfy a reasonable set of assumptions listed below:[43]

1. All the experimental uncertainty is in the dependent variable.
2. The uncertainties in the dependent variable (measured values) have a Gaussian distribution, centred on the correct value.
3. The assumed fitting function is the correct mathematical description of the system. Incorrect models yield incorrect parameters.
4. The data points are individually independent observations.
5. There are a sufficient number of data points so that the parameters are over determined.

For a given model, a least-squares analysis is accomplished by minimizing the goodness of fit parameter, given by

$$\chi^2 = \sum_{k=1}^{n} \frac{1}{\sigma_k^2} [N(t_k) - N_c(t_k)]^2$$

$$= \sum_{k=1}^{n} \frac{[N(t_k) - N_c(t_k)]^2}{N(t_k)} \qquad (1.36)$$

where $N(t_k)$, $N_c(t_k)$ and σ_k represents the measured data, calculated decay and standard deviation respectively. In the expression the sum extends over the number (n) of channels or data points used for a particular analysis. In TCSPC, the standard deviation is known to be the square root of the number of photon counts, $\sigma_k = \sqrt{N(t_k)}$. The relationship between the standard deviation and the number of photons is true only when there are no systematic errors and counting statistics is the only source of uncertainty in the data. If the data contains only Poisson noise then the relative uncertainty in the data decreases as the number of photons increases. The value of χ^2 is the sum of the squared deviations between the measured data $N(t_k)$ and

expected values $N_c(t_k)$, each divided by squared deviations expected for the number of detected photons. For a multi-exponential decay model, during least square analysis the values of all parameters will be varied until χ^2 reaches minimum. But it is not convenient to interpret the values of χ^2 because it depends on the number of data points. The value of χ^2 will be larger for data sets with more data points, for this reason reduced χ^2 has been introduced:

$$\chi_R^2 = \frac{\chi^2}{n-p} = \frac{\chi^2}{v} \tag{1.37}$$

where n is the number of data points, p is the number of floating parameters, and $v=n-p$ is the number of degrees of freedom. For TCSPC the number of data points (numbers of channels, typically several thousand) is much larger than the number of parameters (α_i, τ_i), therefore v is approximately equal to n. If only random errors contribute to χ_R^2, then this value is expected to be near unity. If the model does not fit, the individual values of χ_R^2 and χ^2 are both larger than that expected for random errors. This is why the value of χ_R^2 can be used to judge the goodness of fitting. When the experimental uncertainties σ_k are known, the value of χ_R^2 is expected to be close to unity. This is because each data point is expected to contribute σ_k^2 to χ^2, the value of which is in turn normalized by the $\sum \sigma_k^2$, so the ratio is expected to be near unity. If the model does not fit the data, then χ_R^2 will be significantly larger than unity.

1.5 Fluorescence microscope and confocal microscope

Fluorescence microscope has been applied to a variety of research fields since invention. [44, 45] The concept of a conventional optical setup is displayed in Fig. 1.11, the excitation light is blue and the emission fluorescence is green. The microscope is equipped with a dichromatic (or dichroic) mirror to reflect light shorter than a certain wavelength (the excitation) but transmits light of longer wavelength (the emission). Thus, the light from the excitation source can be reflected and passes through the objective to the sample, while the longer-wavelength emitting light from

the specimen can pass through both the objective and the dichroic mirror to the detector.

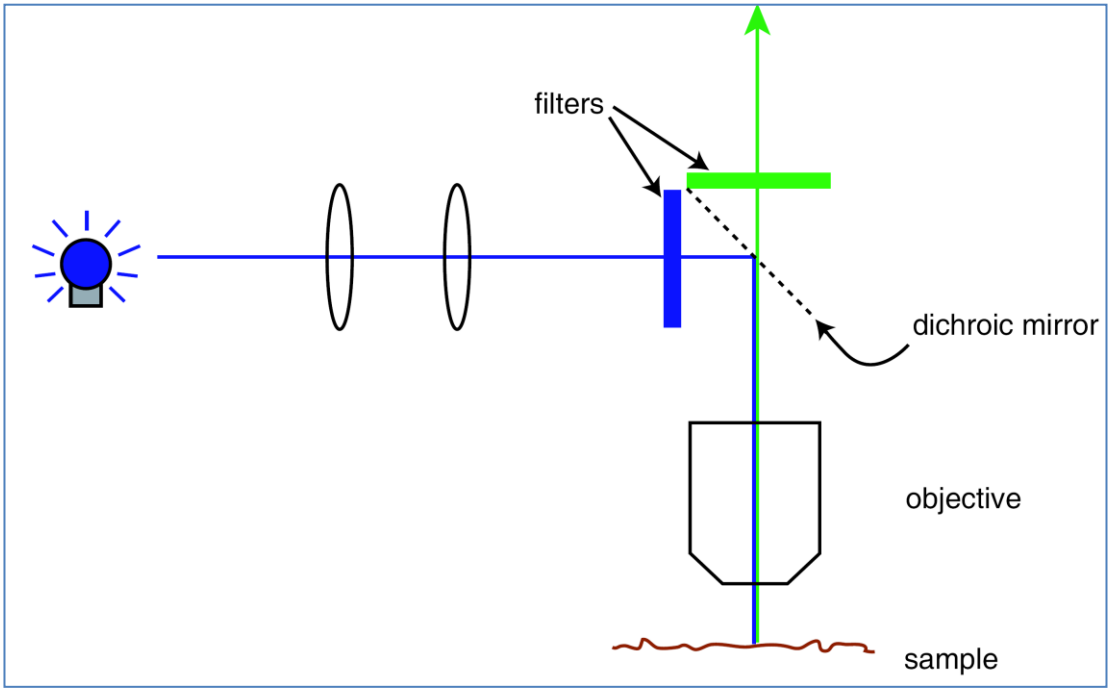

Fig.1.11 Schematic setup of conventional fluorescence microscope.[44]

Different from the conventional optical microscope, the confocal microscope makes use of point-by-point illumination of the specimen and rejection of out-of-focus light. The mechanism of a confocal microscope is illustrated in Fig. 1.12. The dark and light blue rays represent light from points in and out of the focus plane respectively. The image of the light blue point is not at the same location as the image of the dark blue point. In confocal microscopy, the aim is to exclude the out-of-focus plane points (the light blue ones) and see only the signal from the focus plane (the dark blue point). Accordingly, if a screen with a pinhole is placed at the detector side of the microscope system, then all of the light from the dark blue point will pass through the pinhole. Note that at the location of the screen the light blue point is out of focus. Moreover, most of the light will get blocked by the screen, resulting in an image of the light blue point that is significantly attenuated compared to the image of the dark blue point. In fluorescence microscopy the entire field of view of the specimen is completely illuminated, making the whole region fluoresce at the same time. The highest intensity of the excitation light is at the focal point of the lens, but

the other parts of the specimen do get some of the excitation light and they do emit fluorescence. Thus, light at a ‘‘dark blue’’ point may include light that has been scattered from other ‘‘light blue’’ points, thereby obscuring its fluorescence. To reduce this effect the confocal microscope focuses a point of light at the in-focus dark blue point by placing a pinhole aperture in front of the light source. Thus, the only regions that are illuminated are a cone of light above and below the focal (dark blue) point.

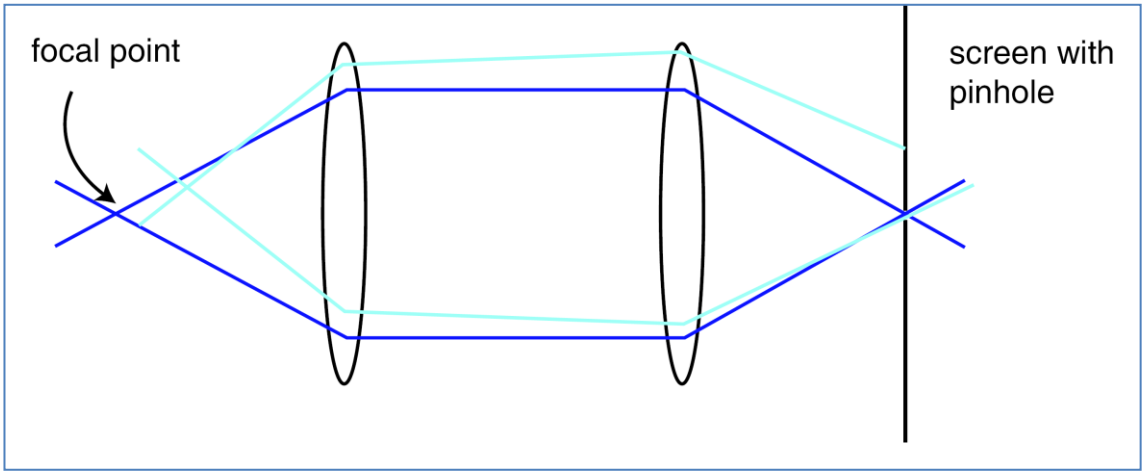

Fig.1.12 Mechanism of a pinhole in confocal microscope. [44]

Fig.1.13 shows the optical setup of confocal system, Zeiss LSM 510, used in this project. The excitation source includes a pre-set Argon laser (wavelength option 471nm, 488nm, and 514nm), a He-Ne laser (wavelength 540nm) and a separate Coherent Chameleon Ti:Sapphire laser (wavelength ranging from 690nm to 1040nm). After going through the beam splitter, only the excitation light at specific wavelength will transmit the objective to the specimen. We have three Olympus objectives in use, a 10x air objective, a 40x oil emersion one and a 63x water emersion objective. The emission light is collected by the same objective and penetrates the beam splitter to detectors. There are two detection channels, allowing take a single confocal fluorescence image with either detectors or a multi-channel emerge image with two detectors at a same time. Filters applied to channel one are longpass filters mainly designed for the Argon laser system while on channel two bandpass filters are equipped so that one can chose specific energy window to take confocal image.

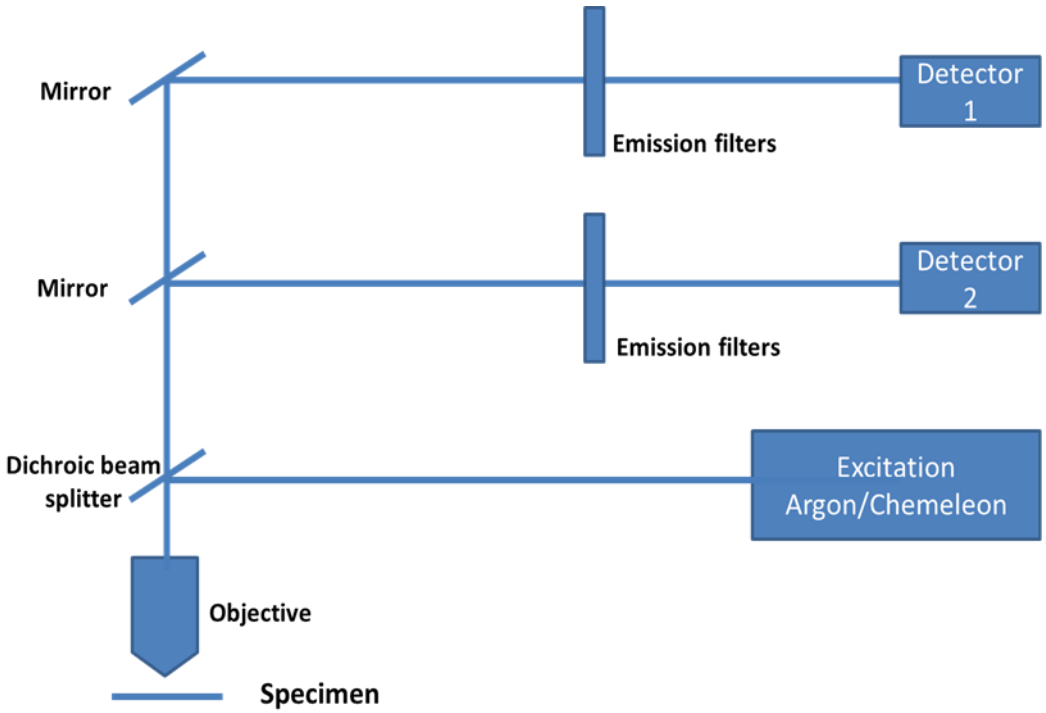

Fig.1.13 Optical setup of Zeiss LSM-510 confocal microscope.

1.6 Fluorescence lifetime imaging microscopy (FLIM)

1.6.1 Introduction to FLIM

Traditional microscopy relies on the contrast that can be achieved from absorption, polarization, phase *etc.*. Commonly fluorescence intensity is measured. FLIM provides contrast according to the fluorescence decay time.

Lifetime does not change on intensity variations, therefore lifetime measurements are not dependent on the local concentration of fluorophores, bleaching, the optical path, of the microscope, the local excitation light intensity, or on the local luminescence detection efficiency. The fluorescence decay time depends on the intrinsic characteristics of the fluorophore and also on the local environment. The local viscosity, pH, or refractive index, as well as interactions with other molecules, such as collision or energy transfer, can all affect the fluorescence lifetime.[46-57] Thus, as well as being able to distinguish spectrally similar fluorophores, imaging of the fluorescence lifetime can be used to probe the surroundings of a fluorophore.

FLIM technologies can be divided into two categories: (i) confocal scanning or multi-photon excitation FLIM where the image is acquired pixel-by-pixel using a non-imaging detector , and (ii) wide-field camera-based FLIM.[46, 58-62] The time-resolved information is obtained either in the time domain by exciting the sample with a short optical pulse and observing the decay of the fluorescence intensity (with time-correlated single photon counting (TCSPC), gating, or a streak camera), or in the frequency domain by modulating the excitation source and/or the detector to calculate the fluorescence decay time from the demodulation and the phase shift of the fluorescence.[63]

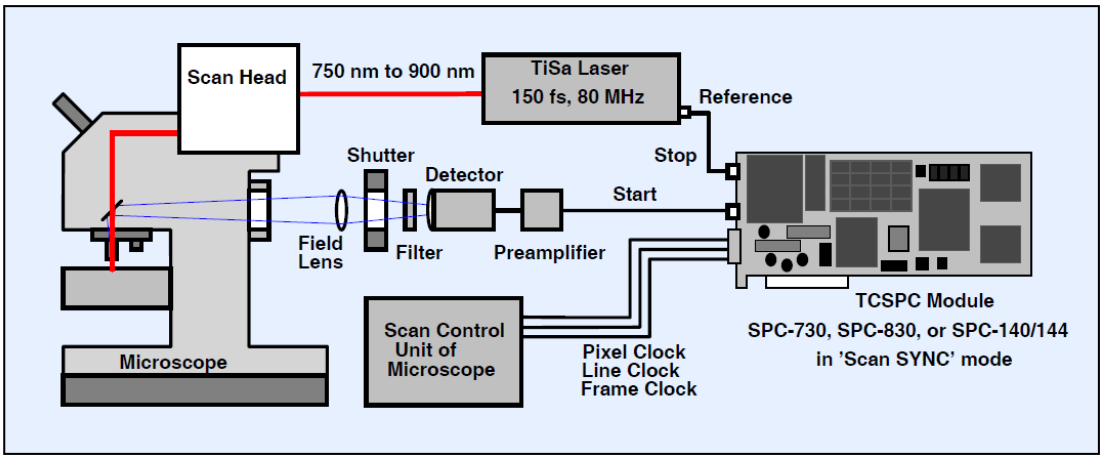

Fig.1.14 Setup of Confocal microscope equipped with FLIM module.[63]

The FLIM system used in this project is shown in Fig.1.14. It is consist of a Zeiss LSM 510 confocal microscope (details can be found in section1.5) and a Becker & Hickl GmbH SPC-830 FLIM module. Two-photon excitation FLIM measurement can be carried out with a Chameleon laser running as the excitation source. The fluorescence light is diverted by a dichroic mirror directly behind the microscope lens and transferred into a photomultiplier tube (PMT) detector. A direct-detection setup is applied. Compared to confocal system, in which only photons from the focus plane will be counted, photons leaving the sample from a large area are collected and fed into the detector in a direct-detection system. Therefore the detection efficiency for scattered photons and for photons of background light increases. Any direct detection system with TCSPC has to be operated in absolute darkness.

1.6.2 Data analysis of FLIM experiments

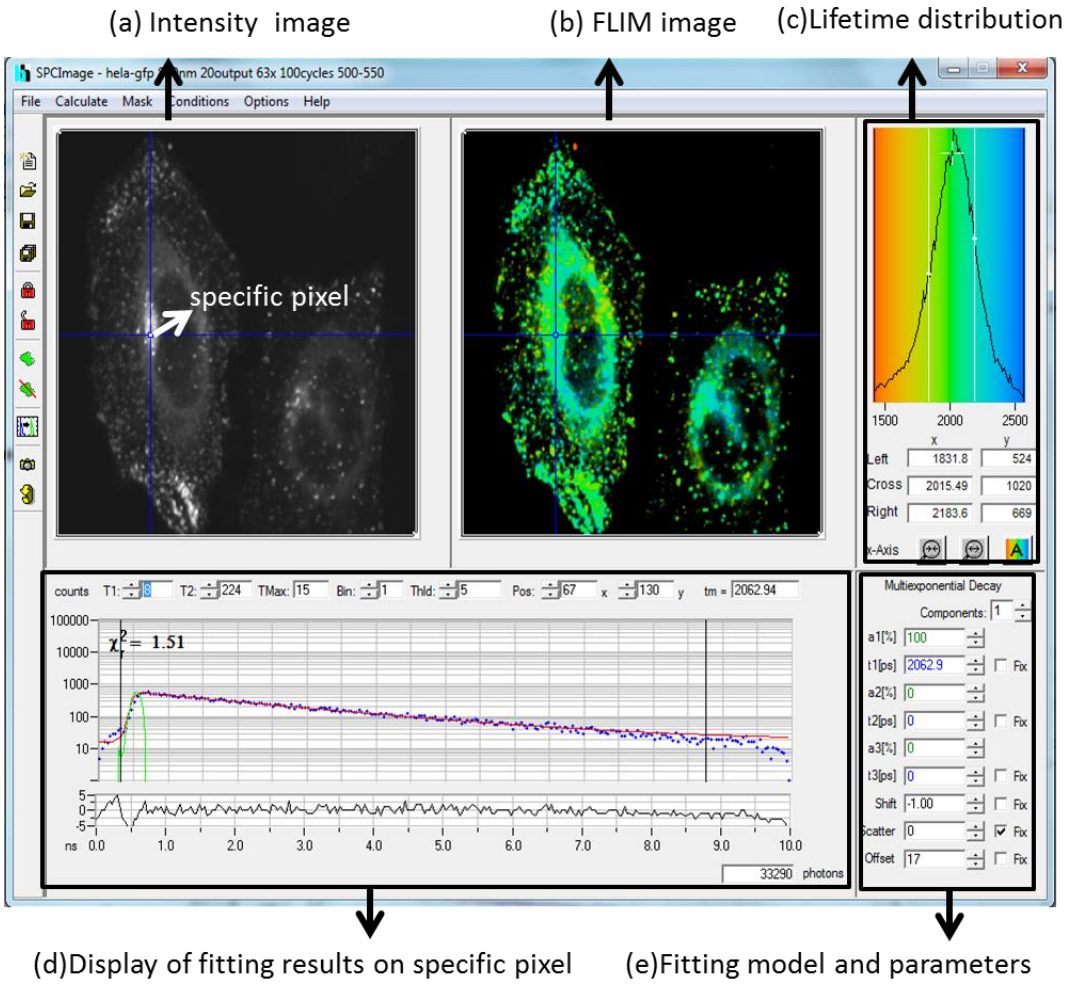

Fig.1.15 Example of data analysis on FLIM measurement.: (a) display of experimental intensity image; (b) FLIM results after applying a single-exponential decay fitting model on intensity image; (c) Lifetime distribution of FLIM result; (d) experimental decay curve and fitting results on specific pixel shown in intensity image, the blue dotted line representing the raw data, red solid curve for fitting result, and green line for system response; (e) selected fitting model and related fitting parameters.

The data analysis of FLIM experimental results is carried out by fitting the obtained raw data using a pre-set multi-exponential decay model that describes the physical process with certain fitting parameters. In our experiments, these parameters are usually the fluorescence decay times. The basic fitting process run by the FLIM software (SPCImage, provided by Becker & Hickl) is to minimize the chi-square χ_R^2 given by Equ.1.36 and 1.37 between experimental data and fitting curve. By displaying specific fitting parameters, such as the fluorescence lifetime in each pixel, one can achieve a final coded colour FLIM image. An example of fitted FLIM image of green fluorescence protein (GFP) (details will be discussed in Chapter 5) though this analysis process is shown in Fig.1.15. The 'FLIM image' displays the fluorescence lifetime of every single pixel in the 'intensity image'; the lifetime value is given by fitting the experimental decay curve (the blue dots at the bottom box) by a specific model (a single exponential model is applied in this case), the fitting curve is denoted by red solid line, and all fitting parameters is shown in the bottom right box. The lifetime distribution of all pixels is shown in the upper right box.

There are several important aspects of the fitting process:

1. The fitting models: The FLIM analysis software in our system uses a multi-exponential decay model (up to three components for current SPCImage, defined by Equ.1.27). Normally, a measured decay curve in one pixel is a sum of several single exponential decays, which can be caused by more than one emission molecule located in a single pixel, or when the fluorophores in a single pixel are in different photophyiscal states. One should select a proper model based on the practical physical process and experimental conditions, such as the signal to noise ratio (SNR): only data with a high SNR can be fitted by a reasonable multi-exponential model. A diagram showing a sum of two exponential decays and the final result can be found in Fig.1.16 (a).

2. The convolution process: as described in section 1.4.1, the experimental decay curve is a mathematical convolution of the system response and the fitting model function. The system response function is estimated by the FLIM data analysis

software by calculating the first derivative of the fluorescence rising part (the green curve in Fig.1.15). The parameter ‘shift’ which denotes the linear shift between the response function and experimental decay curve is also calculated by the software automatically. Fig.1.16 (b) depicts the impact from the convolution process to the final experimental curve.

3. The impact from scattering: the scattered light or second harmonic generation under two photon excitation will cause a peak at the starting part of the decay curve, but as this process is extremely fast compared to the system response it just adds a linear component to the decay trace. The ‘scatter’ parameter in Fig.1.15 (e) fitting box counts for this process. The impact from scattering can be found in Fig.1.16(c).

4. Contribution from dark noise: the detection system will count ambient light and detector noise during the experiment and produce a constant baseline, denoted as parameter ‘offset’ in Fig.1.15 fitting box. One should avoid the artificial generation of a long lifetime component caused by dark noise. The offset value can be generated by the software automatically based on experimental measurement: the photons in the time channels in front of the rising part can be considered as ‘offset’.

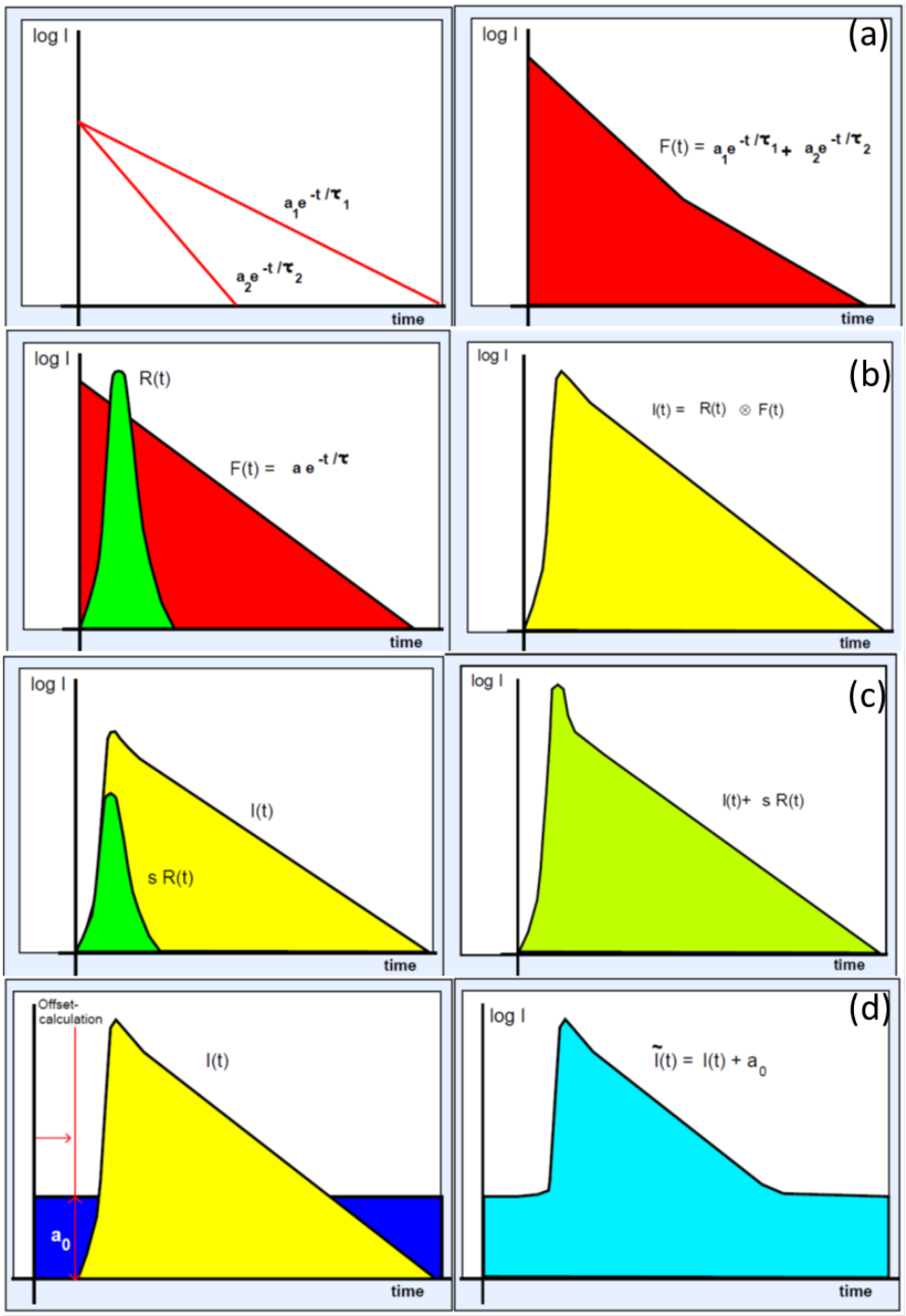

Fig.1.16 Illustration of the impact of different fitting parameters: (a) left: contribution from two single exponential decay; right: a two-exponential decay curve; (b) left: the system response and the intrinsic decay curve; right: result of the convolution process; (c) left: impact from scattering; right: total result considering scatter; (d) left: effect of dark counts; right: result after adding on dark photons.[64]

References

[1] X. Huang, S. Neretina, M. A. El-Sayed, “Gold nanorods: From Synthesis and Properties to Biological and Biomedical Applications”, Adv. Mater. 2009, 21, 4880-4910

[2] P. K. Jain, X. Huang, I. H. El-Sayed, M. A. El-Sayed, “Noble Metals on the Nanoscale: Optical and Photothermal Properties and Some Applications in Imaging, Sensing, Biology, and Medicine”, Accounts Chem. Res. 2008, 41, 1578-1586

[3] X. Huang, I. H. El-Sayed, W. Qian, M. A. El-Sayed, “Cancer cells assemble and align gold nanorods conjugated to antibodies to produce highly enhanced, sharp, and polarized surface Raman spectra: A potential cancer diagnostic marker”， Nano Lett. 2007, 7, 1591-1597

[4] E. Dulkeith, T. Niedereichholz, T. A. Klar, J. Feldmann, “Plasmon emission in photoexcited gold nanoparticles”, Phys. Rev. B 2004, 70, 205424

[5] K. Kumar, R. Richards-Kortum, “Optical Molecular Imaging Agents for Cancer Diagnostics and Therapeutics”, Nanomedicine 2006, 1, 23-30

[6] X. H. Huang, P. Jain, I. H. El-Sayed, M. A. El-Sayed, “Gold nanoparticles: interesting optical properties and recent applications in cancer diagnostics and therapy” Nanomedicine 2007，2，681-693

[7] M. Lippitz, M. A. van Dijk, M. Orrit, Nano “Third-Harmonic Generation from Single Gold Nanoparticles” Nano Lett. 2005, 5, 799-802

[8] M. Eghtedari, A. Oraevsky, J. A. Copland, N. A. Kotov, A. Conjusteau, M. Motamedi, “High Sensitivity of In Vivo Detection of Gold Nanorods Using a Laser Optoacoustic Imaging System”, Nano Lett. 2007, 7, 1914-1918

[9] D. Boyer, P. Tamarat, A. Maali, B. Lounis, M. Orrit, “Photothermal Imaging of Nanometer-Sized Metal Particles Among Scatterers”, Science 2002, 297, 1160-1163

[10] G. Lu, L. Hou, T. Zhang, W. Li, J. Liu, “Anisotropic Plasmonic Sensing of Individual or Coupled Gold Nanorods”, J. Phys. Chem. C 2011, 115, 22877-22885

[11] K. M. Mayer, F. Hao, S. Lee, P. Nordlander, J. H. Hafner, "A single molecule immunoassay by localized surface plasmon resonance", Nanotechnology 2010 21, 255503

[12] G. Wang, Z. Chen, L. Chen, "Mesoporous silica-coated gold nanorods: towards sensitive colorimetric sensing of ascorbic acid via target-induced silver overcoating", Nanoscale 2011, 3, 1756-1759

[13] J. Vera, Y. Bayazitoglu, Int. J. Heat Mass Tran. "A note on laser penetration in nanoshell deposited tissue", 2009, 52, 3402-3404

[14] A. M. Elliott, J. Schwartz, J. Wang, A. M. Shetty, C. Bourgoyne, D. P. O'Neal, J. D. Hazle, R. J. Stafford, "Quantitative comparison of delta P1 versus optical diffusion approximations for modeling near-infrared gold nanoshell heating", Medical Physics 2009, 36, 1351-1358

[15] P. Puvanakrishnan, J. Park, P. Diagaradjane, J. A. Scheartz, C. L. Coleman, K. L. Gill-Sharp, K. L. Sang, J. D. Payne, S. Krishanan, J. W. Tunnell, "Near-infrared narrow-band imaging of gold/silica nanoshells in tumors", J. Biomed. Opt. 2009, 14, 024044

[16] H. Wang, T. B. Huff, D. A. Zweifel, W. He, P. S. Low, A. Wei, J-X. Cheng, "In vitro and in vivo two-photon luminescence imaging of single gold nanorods", Proc. Natl. Acad. Sci. USA 2005, 102, 15752-15756

[17] A. Diaspro, "Confocal and two-photon microscopy Foundations Applications, and Advances", Wiley, 2001, Chapter 3, 43-44

[18] K. Imura, T. Nagahara, H. Okamoto, "Near-Field Two-Photon-Induced Photoluminescence from Single Gold Nanorods and Imaging of Plasmon Modes", J. Phys. Chem. B 2005, 109 (27), 13214-13220

[19] L. Vidgerman, B. P. Khanal, E. R. Zubarev, "Functional Gold Nanorods: Synthesis, Self-Assembly, and Sensing Applications", Adv. Mater. 2012, 24, 4811-4841

[20] T. Sen, S. Sadhu, A. Patra, "Surface energy transfer from rhodamine 6G to gold nanoparticles: A spectroscopic ruler", Appl. Phys. Lett. 2007, 91, 043104-3

[21] L. C. Kennedy, L. R. Bickford, N. A. Lewinski, A. J. Coughlin, Y. Hu, E. S. Day, J. L. West, R. A. Drezek, "A New Era for Cancer Treatment: Gold-Nanoparticle-Mediated Thermal Therapies", Small 2011, 7, 169-183

[22] T. B. Huff, L. Tong, Y. Zhao, M. N. Hansen, J. Cheng A. Wei, “Hyperthermic effects of gold nanorods on tumor cells”, Nanomedicine 2007, 2, 125-132

[23] P. Wust, B. Hildebrandt, G. Sreenivasa, B. Rau, J. Gellerman, H. Riess, R. Felix, P. M. Schlag, “Hyperthermia in combined treatment of cancer”, Lancet Oncol. 2002, 3, 487-497

[24] J. Perez-Juste, L. M. Liz-Marzan, S. Carnie, D. Y. C. Chan, P. Mulvaney, “Electric-Field-Directed Growth of Gold Nanorods in Aqueous Surfactant Solutions”, Adv. Funct. Mater. 2004, 14, 571-579

[25] C. J. Murphy, T. K. Sau, A. M. Gole, C. J. Orendorff, J. Gao, L. Gou, S. E. Hunyadi, T. Li, “Anisotropic Metal Nanoparticles: Synthesis, Assembly, and Optical Applications “, J. Phys. Chem. B. 2005, 109, 13875-13870

[26] T. B. Huff, M. N. Hansen, Y. Zhao, J. Cheng, A. Wei, “Controlling the Cellular Uptake of Gold Nanorods”, Langmuir, 2007, 23, 1596-1599

[27] X. Huang, I. H. El-Sayed, W. Qian, M. A. El-Sayed, “Cancer cells assemble and align gold nanorods conjugated to antibodies to produce highly enhanced, sharp, and polarized surface Raman spectra: A potential cancer diagnostic marker”, Nano Lett. 2007, 7, 1591-1597

[28] C.-C. Chen, Y.-P. Lin, C.-W. Wang, H.-C. Tzeng, C.-H. Wu, Y.-C. Chen, C.-P. Chen, L.-C. Chen, Y.-C. Wu, “DNA gold nanorods conjugates for remote control of localized gene expression by near infrared irradiation”, J. Am. Chem. Soc. 2006, 128, 3709-3715

[29] J. M. Romo-Herrera, R. A. Alvarez-Puebla, L. M. Liz-Marzán, “Controlled assembly of plasmonic colloidal nanoparticle clusters”, Nanoscale 2011, 3, 1304-1315

[30] S. Link, M. A. El-Sayed, “Shape and size dependence of radiative, non-radiative and photothermal properties of gold nanocrystals”, Int. Rev. Phys. Chem. 2000, 19(3), 409-453

[31] S. Link, M. B. Mohamed, M. A. El-Sayed, “Simulation of the Optical Absorption Spectra of Gold Nanorods as a Function of Their Aspect Ratio and the Effect of the Medium Dielectric Constant”, J. Phys. Chem. B 1999, 103, 3073-3077

[32] J. R. Lakowicz, “Principles of Fluorescence Spectroscopy”, Singapore: Springer Science +Business Media, LLC, 3rd ed., Chapter 1, 5-10

[33] W. Denk, D. W. Piston, W. W. Webb, “Two-photon molecular excitation in laser scanning microscopy, Handbook of Biological Confocal Microscopy”, Edited by Pawley J. New York: Plenum Press, 1995, 445-450

[34] W. Denk, K. Svboda, “Photon upmanship: why multiphoton imaging is more than a gimmick”, Neuron 1997, 18, 351-357

[35] C. Xu, W. W. Webb, “Multiphoton excitation of molecular fluorophores and nonlinear laser microscopy, Topics in Fluorescence Spectroscopy”, Volum 5: “Nonlinear and Two-photon Induced Fluorescence”, Edited by J. Lakowicz, New York: Plenum Press, 1997, 471-475

[36] R. M. Williams, D. W. Piston, W. W. Webb, “Two-photon molecular excitation provides intrinsic 3-dimensional resolution for laser based microscopy and microphotochemistry”, FASEBJ 1994, 8, 804-813

[37] J. B. Shear, “Multiphoton-excited fluorescence in bioanalytical chemistry”, Anal. Chem. 1999, 71, 598A-605A

[38] W. Becker, “The bh TCSPC Handbook Second Edition”, Becker & Hickl GmbH, 2006, 15-21

[39] J. R. Lakowicz “Principles of Fluorescence Spectroscopy”, Singapore: Springer Science +Business Media, LLC, 3rd ed., Chapter 4, 104-107

[40] W. Becker, “Advanced time-correlated single-photon counting techniques, Springer”, Berlin, Heidelberg, New York, 2005

[41] F. V. O’Connor, F. Phillips, “Time-correlated single photon counting”, Academics Press, London, 1984

[42] J. Yguerabide, “Nanosecond fluorescence spectroscopy of macromolecules”, Meth. Enzymol. 1974, 26, 498-578

[43] J. R. Lakowicz “Principles of Fluorescence Spectroscopy”, Singapore: Springer Science Business Media, LLC, 3rd ed., Chapter 4, 130-132

[44] D. Semwogerere, E. R. Weeks, “Confocal Microscopy, Encyclopedia of Biomaterials and Biomedical Engineering”, Taylor & Francis, 2005

[45] R. H. Webb, “Confocal optical microscopy”, Rep. Prog. Phys. 1996, 59, 427-471

[46] K. Suhling, P.M. W. French, D. Phillips, “Time-resolved fluorescence microscopy”, Photochem. Photobiol. Sci. 2005, 4, 13-22

[47] K. Carlsson, A. Liljeborg, R. M. Andersson and H. Brismar, “Confocal pH imaging of microscopic specimens using fluorescence lifetimes and phase fluorometry: influence of parameter choice on system performance”, J. Microsc., 2000, 199, 106-114

[48] K. Suhling, J. Siegel, D. Phillips, P. M.W. French, S. Lévêque-Fort, S. E. D. Webb and D. M. Davis, “Imaging the environment of green fluorescent protein”, Biophys. J. 2002, 83, 3589-3595

[49] R. Pepperkok, A. Squire, S. Geley and P. I. H. Bastiaens, “Simultaneous detection of multiple green fluorescent proteins in live cells by fluorescence lifetime imaging microscopy”, Curr. Biol. 1999, 9, 269-272

[50] J. R. Lakowicz, H. Szmacinski, K. Nowaczyk and W. J. Lederer, “Fluorescence lifetime imaging of intracellular calcium in COS cells using Quin-2”, Cell Calcium, 1994, 15, 7-27

[51] R. Sanders, H. C. Gerritsen, A. Draaijer, P. M. Houpt and Y. K. Levine, “Fluorescence Lifetime Imaging of Free Calcium in Single Cells”, Bioimaging, 1994, 2, 131

[52] H. J. Lin, P. Herman and J. R. Lakowicz, “Fluorescence lifetimeresolved pH imaging of living cells”, Cytometry 2003, 52, 77-89

[53] M. A. Haidekker, T. Ling, M. Anglo, H. Y. Stevens, J. A. Frangos, E. A. Theodorakis, “New fluorescent probes for the measurement of cell membrane viscosity”, Chem. Biol. 2001, 8, 123-131

[54] S. Jakobs, V. Subramaniam, A. Schonle, T. M. Jovin and S.W. Hell, “EGFP and DsRed expressing cultures of Escherichia coli imaged byconfocal, two-photon and fluorescence lifetime microscopy”, FEBS Lett. 2000, 479, 131-135

[55] R. Swaminathan, C. P. Hoang and A. S. Verkman, “Photobleaching recovery and anisotropy decay of green fluorescent protein GFPS65T in solution and cells: Cytoplasmic viscosity probed by green fluorescent protein translational and rotational diffusion”, Biophys. J. 1997, 72, 1900-1907

[56] S. T. Hess, E.D. Sheets, A.Wagenknecht-Wiesner, A. A. Heikal, "Quantitative Analysis of the Fluorescence Properties of Intrinsically Fluorescent Proteins in Living Cells", Biophys. J. 2003, 85, 2566-2580

[57] H. C. Gerritsen, R. Sanders, A. Draaijer, C. Ince and Y. K. Levine, "Fluorescence Lifetime Imaging of Oxygen in Living Cells", J. Fluoresc. 1997, 7, 11-15

[58] W. B. Amos, "Instruments for fluorescence imaging, in Protein localization by fluorescence microscopy". A practical approach, Oxford University Press, Oxford, 2000, 67

[59] C. J. R. Sheppard, "Scanning confocal microscopy, in Encyclopedia of Optical Engineering, Marcel Dekker", New York, 2003, 22

[60] P. T. C. So, C. Y. Dong, B. R. Masters and K. M. Berland, "Two-Photon Excitation Fluorescence Microscopy", Annu. Rev. Biomed. Eng. 2000, 2, 399-429

[61] K. König, "Multiphoton microscopy in life sciences", J. Microsc. 2000, 200, 83-104

[62] S. E. D. Webb, Y. Gu, S. Lévěque-Fort, J. Siegel, M. J. Cole, K. Dowling, R. Jones, P. M. W. French, M. A. A. Neil, R. Jǔskaitis, L. O. D. Sucharov, T. Wilson and M. J. Lever, "A wide-field time-domain fluorescence lifetime imaging microscope with optical sectioning", Rev. Sci. Instrum. 2002, 73, 1898-1907

[63] W. Becker, The bh TCSPC Handbook Second Edition, 2006, 167-169

[64] "SPCImage 2.8 Data Analysis Software for Fluorescence Lifetime Imaging Microscopy", Becker & Hickl GmbH, 2006, 2-6

Chapter 2

Characterization of Optical Properties of Gold Nanorods

2.1 Introduction

The surface plasmon oscillation is the coherent excitation of free electrons within the conduction band, leading to an in-phase oscillation. In the case of surface plasmon resonance (SPR), plasmons propagate in the directions along the metal-dielectric interface, for distances on the order of tens to hundreds of microns, and decay in the perpendicular direction with 1/e decay lengths on the order of 200nm.

There have been varieties of applications related to SPR, including surface-enhanced spectroscopy,[1-7] biological and chemical sensing,[8-16] and lithographic fabrication,[17-20] etc. With progress in fabrication and manipulation of metallic materials, especially on the nanoscale, localized surface plasmon resonance (LSPR) has attracted much attention.

For the case of localized surface plasmons, an incident electromagnetic (EM) wave interacts with particles much smaller than the incident wavelength, leading to a charge density oscillation confined to metallic nanostructures. Excitation of LSPR by EM field, such as light, where resonance occurs, provide strong light scattering in the appearance of intense surface plasmon absorption bands and enhancement of the local EM field.[20].

Many applications can be achieved by introducing LSPR, especially in spectroscopy research, such as near-field scanning optical microscopy,[21-23] surface-enhanced Raman spectroscopy (SERS),[24-26] multiphoton-induced luminescence,[27-29] radiative quenching or enhancement [30-34] and spaser.[35-37] Gold nanorods (GNRs) are potential candidate for examining all these SPR effects.

The surface plasmon bands of GNRs split into two parts: transverse and longitudinal band. The longitudinal one resonates in the near infra-red (NIR) region, where the absorption of water and biological tissue is minimized, making them useful in

biological research. Moreover, this longitudinal plasmon band can be tuned by changing the size, shape of nanorods and the dielectric environment.[38] In this chapter the synthesis of gold nanorods and a study on their optical properties are reviewed in details.

2.2 Synthesis of GNRs with different surface plasmon bands

Gold nanorods were synthesized using the seeded growth method (Murphy et al. 2005). Typically, 2.5ml $HAuCl_4x3H_2O$ (0.001M) and 0.6ml ice-cold $NaBH_4$ (0.01M) were added into 7.5ml cetyltrimethylammonium bromide (CTAB) (0.12M) to prepare the seeds solution. The growth solution were synthesized by adding 0.15M benzyldimethylhexadecylammonium chloride (BDAC), 50ml $HAuCl_4x3H_2O$ (0.001M), 3ml silver nitrate ($AgNO_3$) (0.004M) and 700µl Ascorbic Acid (0.778M) to 50ml CTAB solution (0.1M). Then 80µl seed solution (2 hours after preparation) was injected into growth solution to grow gold nanorods.

Sample NO.	1	2	3	4	5
CTAB	0.12M/L	0.12M/L	0.12M/L	0.2M/L	0.2M/L
BDAC	0.15M/L	0.15M/L	0.15M/L	0.25M/L	0.25M/L
$AgNO_3$	4ml	3ml	2ml	2ml	2ml
Absorption peak (longitudinal mode)	700nm	750nm	800nm	900nm	1050nm

Table 2.1. Detailed recipes for synthesising gold nanorods with different longitudinal surface plasmon peaks.

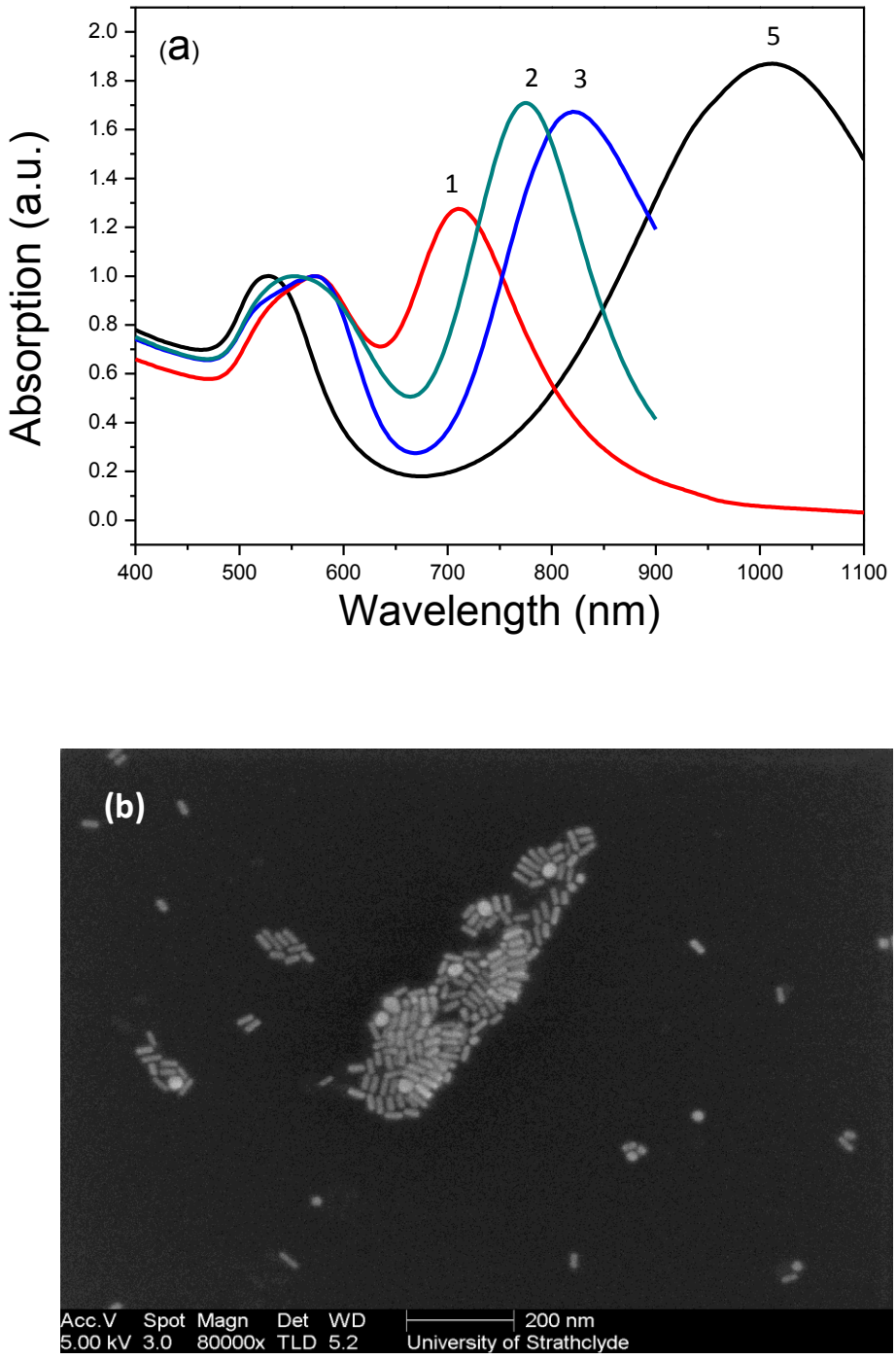

Fig.2.1. (a) Extinction spectrum of nanorod samples 1, 2, 3 and 5 in Table.1 with longitudinal band from 700nm to 1050nm, normalized at transverse band; (b) SEM image of Sample No.3.

Gold nanorods thus formed have a longitudinal plasmon mode centred at around 750nm. By varying the concentration of CTAB, BDAC and $AgNO_3$, a series of gold nanorods with different sizes and shapes can be synthesized, which are characterized using UV-VIS absorption spectroscopy and electron microscopic imaging. Table2.1 lists the relative concentrations to synthesize gold nanorods and their longitudinal mode. The longitudinal surface plasmon of different samples and SEM image of Sample No.3 is shown in Fig.2.1.

2.3 Two-photon luminescence (TPL) from GNRs

The photon induced luminescence from gold was first reported by Mooradian.[40] The photoemission is thought to arise from the direct transitions between electrons in the conduction band below the Fermi level and holes in the d bands. But the single photon luminescence efficiency is very low, around 10^{-10}. Luminescence of noble metal materials did not attract much attention until Boyd reported multiphoton-induced luminescence on roughened noble metal surfaces, which can induce luminescence several orders of magnitudes stronger than single photon emission.[41] This amplification of luminescence is believed due to a resonant coupling with localized surface plasmons,[42] which has broad applications in fluorescence research. In addition to enhanced luminescence intensity, multi-photon excitation provides unique advantages compared to single photon excitation. Multi-photon process has non-linear dependence on incidence power, which will provide better on-axis spatial resolution. Longer excitation wavelength also provides deeper penetration depth in biological tissue. For GNR luminescence research, two-photon excitation with near-infrared band is commonly applied, a energy window through which damage to biological system and tissue auto-fluorescence can be minimized.

Data shown in Fig.2.2 and 2.3 were obtained by our home built two-photon TCSPC unit. A quartz cuvette filled with a gold nanorod solution (OD around 1.0) was placed in the sample holder, and a Ti:Sapphire laser tuned to 800nm was utilized as the excitation source. A beam splitter was placed in the laser beam path. The

transmitted beam goes through the sample cuvette while the reflected beam reaches a laser power meter. The number of photon counts from the TCSPC detector was recorded as the luminescence intensity and the read-out from the laser power meter was used as the incidence power.

All gold nanorod solutions show strong luminescence under NIR excitation. The nonlinear nature of the TPL signal was confirmed by measuring the dependence of the luminescence intensity as a function of excitation power on all samples. A typical result is shown in Fig.2.2, where data was collected from nanorods with a longitudinal band at around 800nm (blue curve in Fig.2.1 (a)) under 800nm excitation and the incidence power increases from 5 to 20mW. The dependence of luminescence intensity on incidence laser power was found close to quadratic, suggesting a non-linear, and two-photon excitation process.

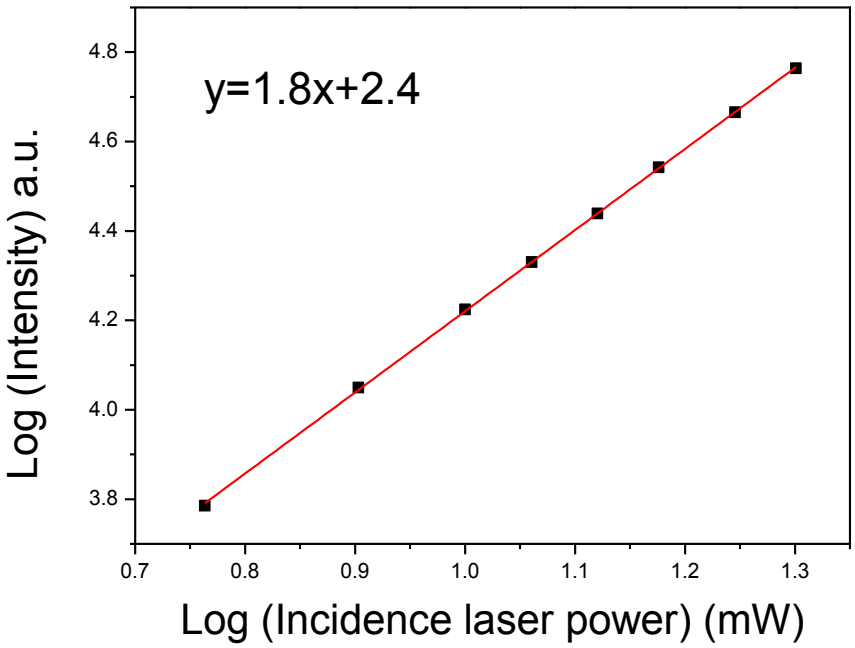

Fig.2.2 Fluorescence intensity dependence on incidence laser power (in log scale).

2.4 Surface plasmon effect

To examine the effect of surface plasmon band structure on luminescence properties of GNRs, we have carried out excitation luminescence spectroscopy experiments and made a direct comparison of luminescence from GNRs and nanospheres (GNSs). By using the same TCSPC measure unit mentioned in section 2.3, a gold nanorods solution was excited by Ti:Sapphire laser in the range from 720nm to 850nm., an effort has been made to maintain the excitation power to be identical at various excitation wavelengths. Photon counts from the TSCPC detector were recorded as luminescence intensity. To directly compare the difference in luminescence intensity, the optical density from extinction spectrum of GNRs and GNSs solution were adjusted to be roughly the same.

Fig.2.3(a) displays the TPL intensity (black squares) from nanorods excited under constant laser power but different wavelength varying from 720nm to 850nm, together with the extinction spectrum (solid line). The excitation spectrum overlaps well with the longitudinal plasmon band, indicating that the TPL intensity is governed by the local field enhancement from the plasmon resonance. A slightly blue shift between the excitation profile and the absorption spectrum was observable, possibly due to a slight descent in detector efficiency approaching to IR band. A similar excitation spectrum result was also observed by Wang et al.[43] They measured the relative TPL efficiency of GNRs of various aspect ratios ranging from 1.3 to 4.3 (meaning longitudinal modes from 540nm to 820nm) at 815nm excitation. The result shows that GNRs with longitudinal mode most close to the excitation wavelength (in their experiment, the one with longitudinal band at 820nm) have the greatest TPL efficiency. The enhanced absorption by surface plasmons is thought to be the main contribution to the enhanced TPL efficiency, which increases the pumping rate of electron-hole pairs.[43]

Furthermore, the TPL intensity from gold nanorods and nanospheres were compared in Fig.2.3 (b). The difference in absorption spectrum can be clearly identified in the inset of Fig.2.3 (b), where nanorods have a significant longitudinal band in the NIR region. With excitation at 800nm (marked by the solid line in the absorption

spectrum), under same excitation power, TPL intensity from nanorods shows a significant enhancement than that from nanospheres, which suggests that TPL from gold nanorods is mainly governed by the longitudinal surface plasmon band.

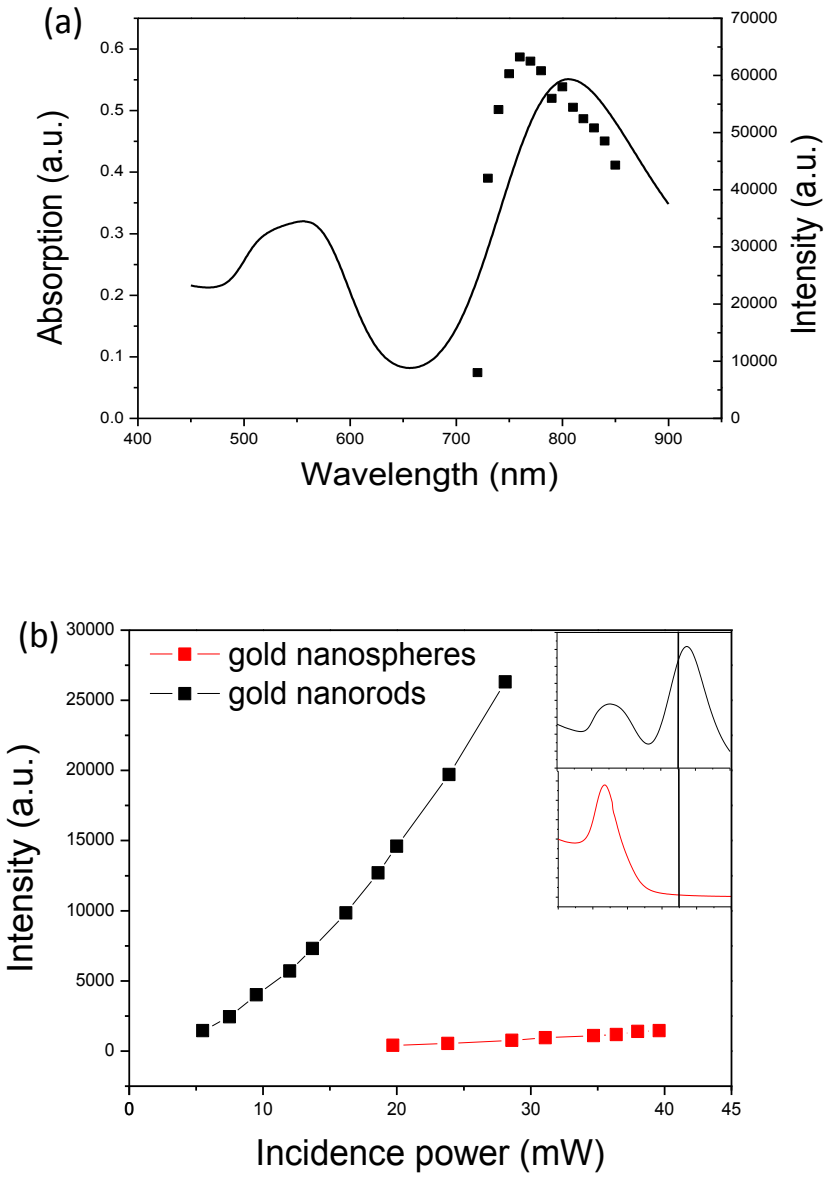

Fig.2.3 (a) TPL excitation spectrum (solid squares) compared with absorption of gold nanorods (solid line); (b) comparison of fluorescence intensity from gold nanorods (black squares) and nanospheres (red squares) excited at 800nm, inset: normalized absorption spectrum of nanorods (black line) and nanospheres (red line), the vertical black line indicates the excitation wavelength.

2.5 Polarization dependence

The polarization dependence measurements were carried out using Zeiss LSM 510 confocal fluorescence microscope, of which full details can be found in experimental chapter. GNRs (longitudinal surface plasmon band centred around 750nm) were dropped onto microscope glass slides for imaging. Ti:Sapphire laser tuning at 750nm was used as excitation source and an emission longpass 505nm filter was applied to remove excitation light. A polarizer was placed on the beam path of laser to change the incidence excitation polarization.

The intensity of TPL from gold nanorods is dependent on polarization of the incidence beam. TPL enhancement is maximized when the incident field is parallel to the longitudinal dipolar plasmon resonance along the long axis of the nanorod. This polarization dependence property makes it possible to identify single nanoparticles from particle clusters, as the latter provides similar TPL intensity under different excitation polarization while single particle does not. The polarization dependence behaviour on incidence excitation is shown in Figure 4, in which GNRs were excited under perpendicular incidence excitation polarizations. As shown in rectangular boxes, luminescence from single nanorod can be identified where luminescence vanishes when the incidence polarization is changed. Spots showing average luminescence intensity under both excitation orientations are considered to be nanorods clusters.

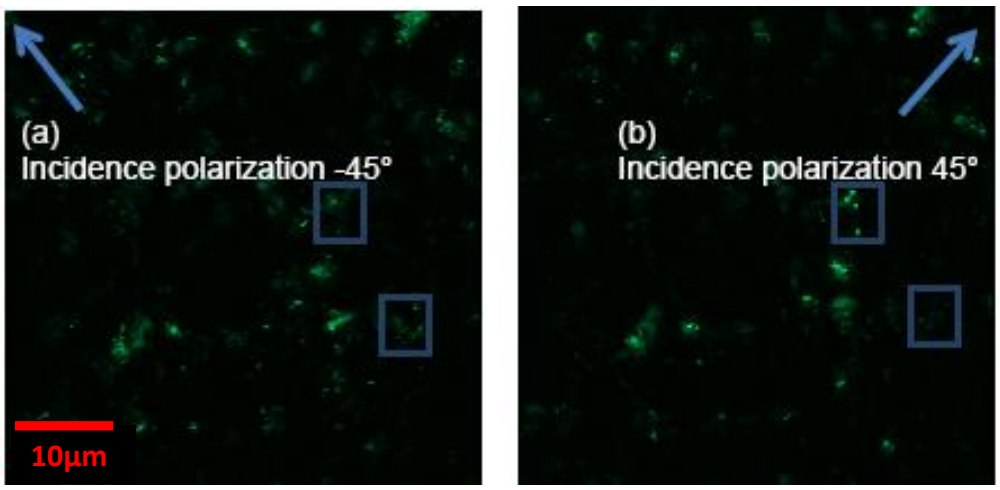

Fig.2.4. TPL images under perpendicular excitation polarizations.

Quantitative measurement by Wang et al. reveals that the TPL intensity, *I*, follows the relationship $I=I_{in}^{2}cos^{4}\theta$, where I_{in} is the incidence laser power and θ represents the angle between the incidence beam polarization and the long axis of gold nanorods. [29] The TPL from a single nanorod has the same polarization dependence as the two-photon fluorescence from a single fluorescent molecule, in accord with the dipolar nature of the LSP of gold nanorods.[29, 44] However, the TPL emission from gold nanorods is depolarized, different from plasmon-resonant scattering processes, which retain the polarization of the incident beam. Furthermore, the TPL emission spectrum appears to be very broad and is likely to be produced directly by electron–hole recombination rather than through intermediate particle plasmons in the single-photon luminescence of gold nanoparticles.

Therefore, the plasmon-enhanced TPL from nanorods is essentially due to a greater two-photon absorption cross section.[29, 44] On the other hand, for larger nanorods at sub-micro meter scale, near-field study by Imura et al. reveals a $cos^{2}\theta$ dependence of TPL intensity on incidence polarization. This relationship was explained by sequential one photon excitation processes: an electron in the sp conduction band is excited by the first photon from below the Fermi surface to above it via an intraband transition, resulting in a charge-separated state within the conduction band. A second photon excites an electron from the d band to the sp band, transferring the hole to the d band. Eventually, an electron-hole recombination emits luminescence. The first transition is maximized along the longitudinal surface plasmon orientation but the polarization information is rapidly lost after excitation, whereas the second transition is polarization insensitive. Therefore, the photoluminescence polarization follows a $cos^{2}\theta$ relationship, and does not depend on plasmon enhanced absorption as is the case of the smaller NRs. These observations are not in conflict because the submicron NRs used in the near-field study do not have the appropriate aspect ratio to support a dipolar plasmon resonance at NIR frequencies.[44-47].

2.6 GNR TPL lifetime

Fluorescence lifetime is the average time a fluorophore molecule spends in the excited state prior to return to the ground state. It is a critical parameter describing a fluorescence process, as it determines the time available for the fluorophore to interact with or diffuse in its environment. Time-resolved research on fluorescence decay time can provide information on fluorescence dynamics, surrounding environment and interactions of fluorophores with other particles. The lifetime decay curve of TPL from GNRs was measured with GNRs solution under 800nm excitation using a home-built time-correlated single photon counting (TSCPC) system. The lifetime is found to be around 100ps but is much longer than those achieved in pump-probe and up-conversion research, where the lifetime of excited electrons in gold nanorods is found to be less than several picoseconds [48, 49]. This is probably due to the limit of time resolution caused by the instrumental response function of the TCSPC system, which is also around 100 ps. Our measurements can give the upper limit of the decay time of TPL process. This result is confirmed by FLIM measurement on GNRs samples disposed on glass slides.

2.7 Two photon luminescence of size-selected gold nanorods

The optical properties of metal nanoparticles depend not only on size but also on shape, which is why the anisotropy of gold nanorods is so important. Most of the work published to date has used gold nanorods synthesized via a seed mediated growth process, as a greater level of control is assumed. The nanorods are typically prepared using the surfactant CTAB to produce an average length in the range of a few tens of nanometres. These nanorods are relatively large, and the prospect of producing size-selected nanorods on the scale of 10 nm is attractive, since the local-field enhancement would be even greater. To date, however, seed mediated growth suffers from some (seemingly) insurmountable challenges at such small sizes.

In this section, the investigation of the formation of size selected gold nanoparticles and their thermodynamically stable shapes will be presented. Luminescence was studied using fluorescence lifetime imaging microscopy and compared with colloidal gold nanorods. Compared to colloidal nanoparticles synthesized through a chemical process, nanoparticles produced using this method have a well-controlled size (5% resolution) which is tuneable from a few atoms up to hundreds of thousands of atoms (corresponding to sub-nanometre to a few nanometres in dimension). This facilitates a study on the evolution of optical properties, from the molecular characteristics of small nanoparticles to the surface plasmon dominated behaviour of large nanoparticles. In addition to size-control, nanoparticles thus formed are free of surfactant, which allows for a study on the influence of surface chemical states on the optical behaviour. A size-selected cluster source in Nanoscale Physics Research Laboratory, Birmingham University, has been used to create nanoparticles consisting of a specific number of atoms, and with the desired dimension less than 10 nm.

The size-selected cluster source employs a novel mass-selection technique based on the time-of-flight principle that has been implemented into a radio frequency magnetron sputtering and gas condensation processes.[50, 51] This method has been described in detail elsewhere, and has the advantage of simultaneously identifying the size with atomic level precision (via mass spectrometry) and providing the required degree of selectivity. Gold particles used for TPL imaging study consist of 8860 and 15000 Au atoms.

Fig. 2.5(a) shows a luminescence intensity image, where the bright spots represent the emission from individual gold nanoparticles. We have analysed different imaging pixels and display a typical result in Fig. 2.5(b), in comparison with that from chemically synthesized gold nanorods and 40-6-diamidino-2-phenylindole (DAPI) under typical two-photon excitation processes and the same experimental conditions (plotted for reference). A near quadratic dependence of the signal intensity on the input power, nearly identical to colloidal gold nanorods and close to DAPI, Fig. 2.5 (c), suggests that the luminescence of nanoparticles from both synthetic sources originates primarily from a two-photon excitation process. Measurement in a cuvette confirmed the two-photon behaviour for colloidal gold nanorods, but we have

noticed that microscope measurements often provide a lower value, possibly due to saturation of the low-density luminescence site. These measurements confirm that our gold nanorods, produced using the size-selected cluster source, have a similar optical behaviour to those produced using the traditional seed-mediated growth methods, and will therefore be suitable for the same types of applications.

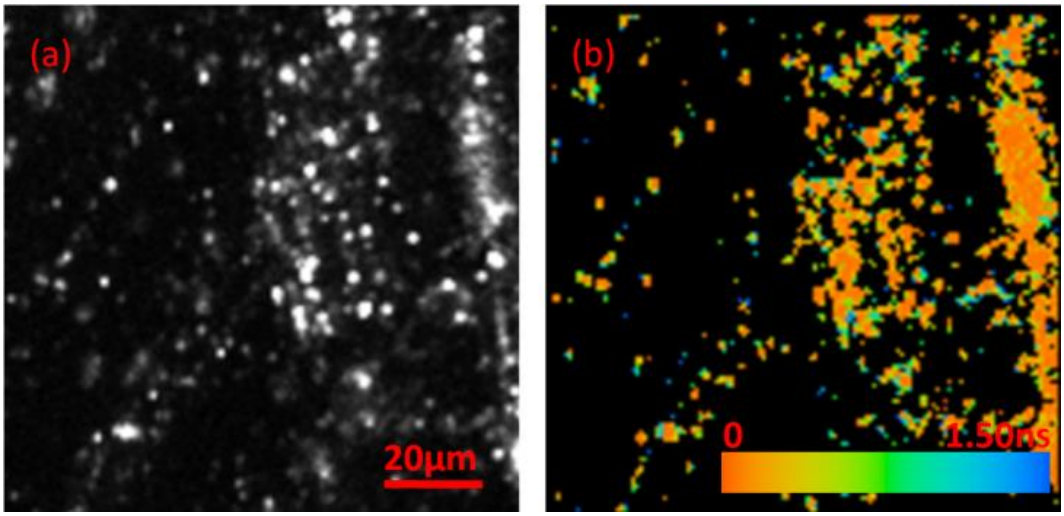

(c)

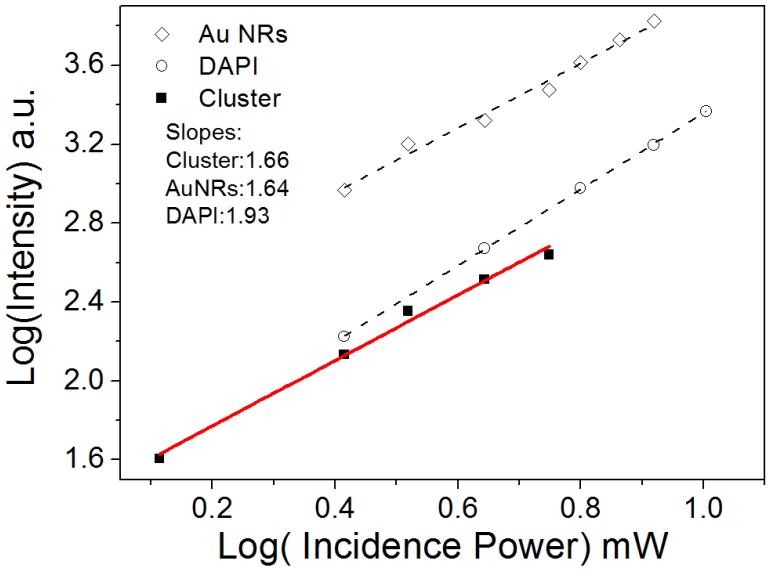

Fig.2.5 (a) Luminescence intensity and (b) lifetime images of gold nanoparticles (Au_{15000}); (c) Dependence of luminescence intensity on incidence laser power (in log scale).

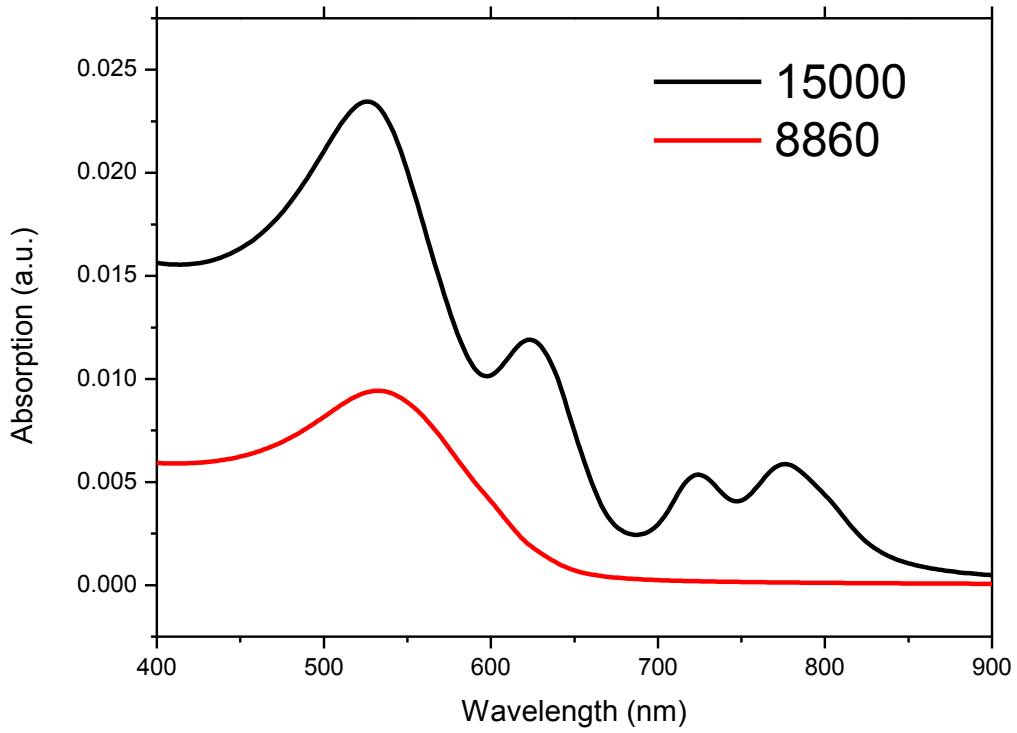

Fig.2.6 Calculated extinction spectra of Au15000 and Au8860 nanocluster ensembles.

The corresponding lifetime image, Fig. 2.5(b), with different colour codes representing different lifetime scales, also correlates well with its intensity counterpart. The luminescence lifetime of each pixel is obtained by applying a single or multi-exponential fit; in this case a single exponential model was used. The densely packed orange spots in Fig. 2.5(b) have a decay time shorter than the time resolution of 100 ps, which is the same as observed from CTAB stabilized gold nanorods under the same experimental conditions. Moreover, the sample in the absence of gold nanorods showed no fluorescence with a decay time faster than the 100 ps as displayed by the gold nanorods. These results confirm that our gas-cluster source nanorods have comparable optical properties to seed-mediated nanorods. The two-photon luminescence of seed-mediated gold nanorods is dominated by surface plasmon resonance. With the decrease of size, the surface plasmon resonance becomes broadened and weak due to electron-surface scattering and size dependent extinction cross-section. Small nanoparticles, with a size below 2 nm, no longer

possess plasmon resonance, but have molecule-like luminescence features with longer lifetimes. Because the absorption is too weak to be readily measurable, and to examine the possible influence of a surface plasmon, we calculated the extinction spectrum of our gas-cluster source nanorods using Mie theory. The extinction spectrum of Au15000, Fig. 2.6, shows a broad surface plasmon absorption ranging over 460–800 nm, overlapped with the excitation at 750 nm.

The nonlinear property of the luminescence was studied by measuring the luminescence intensity as a function of excitation power ranging from 1.2 to 10.2 mW and shown to be two-photon in origin.

Occasional bluish patches/pixels in Fig. 2.5(b) with lifetimes longer than nanoseconds are noticeable. They can be easily distinguished from the emissions from gold nanoparticles due to the significant difference in the lifetimes under two-photon excitation, and probably due to contaminants. In addition, these contamination spots show strong luminescence under single photon excitation, while signals from gold nanoparticles are below the detection limit. Luminescence is also observed from gold nanoparticles with 8860 atoms.

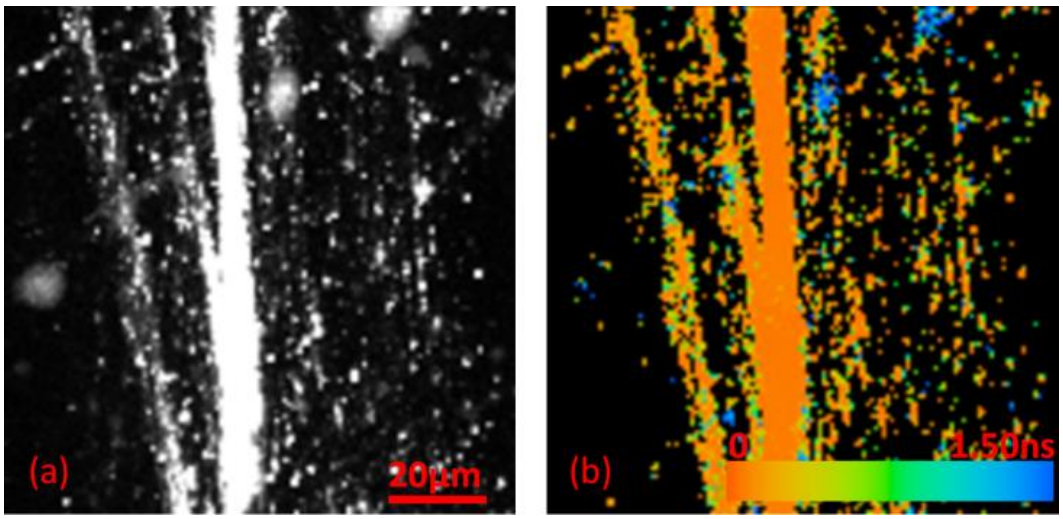

Fig.2.7 (a) Luminescence intensity and (b) lifetime images showing gold nanoparticles (Au_{15000}) assembled along trenches on a glass slide.

A keen eye will notice from both intensity and lifetime images that the fluorescent gold nanoparticles are not always uniformly distributed, Fig. 2.5. Fig. 2.7 shows intensity and lifetime images taken from an area of the surface decorated with numerous trenches. Bright lines on both images indicate aggregation of nanoparticles in these trenches, whereas the relatively dark areas between the trenches suggest a low coverage of nanoparticles. This is a result of nanoparticle diffusion after deposition at room temperature, and the nanoparticles being pinned at low energy defect sites. This distinction may seem trivial at first, but actually suggests the possibility of creating luminescent nanostructures through substrate surface patterning, which is another feature often attributed to seed-mediated nanoparticles.

References

[1] A. C. R. Pipino, G. C. Schatz, R. P. Van Duyne, “Surface-enhanced second-harmonic diffraction: Selective enhancement by spatial harmonics”, Phys. Rev. B 1994, 49, 8320-8330.

[2] P. Mulvaney, “Surface plasmon spectroscopy of nanosized metal particles”, Langmuir, 1996, 12, 788-800.

[3] T. R. Jensen, R. P. Van Duyne, S. A. Johnson, V. A. Maoni, “Surface-Enhanced Infrared Spectroscopy: A Comparison of Metal Island Films with Discrete and Nondiscrete Surface Plasmons”, Appl. Spectrosc. 2000, 54, 371-377.

[4] K. T. Shimizu, W. K. Woo, B. R. Fisher, H. J. Eisler, M. G. Bawendi, “Surface-Enhanced Emission from Single Semiconductor Nanocrystals”, Phys. Rev. Lett. 2002, 89, 117401.

[5] K. L. Haller, L. A. Bumm, R. I. Altkorn, E. J. Zeman, G. C. Schatz, R. P. Van Duyne, “Spatially resolved surface enhanced second harmonic generation: Theoretical and experimental evidence for electromagnetic enhancement in the near infrared on a laser microfabricated Pt surface”, J. Chem. Phys. 1989, 90, 1237-1252.

[6] A. M. Michaels, M. Nimal, L. E. Brus, “Surface enhanced Raman spectroscopy of individual rhodamine 6G molecules on large Ag nanocrystals”, J. Am. Chem. Soc., 1999, 121, 9932-9939.

[7] Y. Chen, J. P. Preece, R. E. Palmer, “Processing and Characterization of Gold Nanoparticles for Use in Plasmon Probe Spectroscopy and Microscopy of Biosystems”, Ann. N. Y. Acad. Sci. 2008, 1130, 201-206.

[8] A. J. Haes, L. Chang, W. L. Klein, R. P. Van Duyne, “Detection of a Biomarker for Alzheimer's Disease from Synthetic and Clinical Samples Using a Nanoscale Optical Biosensor”, J. Am. Chem. Soc. 2005, 127, 2264-2271.

[9] A. J. Haes, W. P. Hall, L. Chang, W. L. Klei, R. P. Van Duyne, “A Localized Surface Plasmon Resonance Biosensor: First Steps toward an Assay for Alzheimer's Disease”, Nano. Lett. 2004, 4, 1029-1034.

[10] A. D. McFarland, R. P. Van Duyne, " "Single Silver Nanoparticles as Real-Time Optical Sensors with Zeptomole Sensitivity", Nano. Lett. 2003, 3, 1057-1062.

[11] C. R. Yonzon, D. A. Stuart, X. Zhang, A. D. McFarland C. L. Haynes, R. P. Van Duyne, "Towards advanced chemical and biological nanosensors—An overview", Talanta 2005, 67, 438-448.

[12] L. S. Jung, C. T. Campbell, T. M. Chinowsky, M. N. Mar, S. S. Yee, "Quantitative Interpretation of the Response of Surface Plasmon Resonance Sensors to Adsorbed Films", Langmuir 1998, 14, 5636-5648.

[13] T. Endo, K. Kerman, N. Nagatani, Y. Takamura, E. Tamiya, "Label-Free Detection of Peptide Nucleic Acid−DNA Hybridization Using Localized Surface Plasmon Resonance Based Optical Biosensor", Anal. Chem. 2005, 77, 6976-6984.

[14] J. M. Brockman, B. P. Nelson, R. M. Corn, "Surface Plasmon Resonance Imaging Measurements of Ultrathin Organic Films", Annu. Rev. Phys. Chem. 2000, 51, 41-63.

[15] A. J. Haes, D. A. Stuart. S. M.Nie, R. P. Van Duyne, "Using solution-phase nanoparticles, surface-confined nanoparticle arrays and single nanoparticles as biological sensing platforms", J. Fluoresc. 2004, 14, 335-367.

[16] E. A. Smith. R. M. Corn, "Surface Plasmon Resonance Imaging as a Tool to Monitor Biomolecular Interactions in an Array Based Format", Appl. Spectrosc. 2003, 57, 320A-322A.

[17] W. Srituravanich, N. Fang, C. Sun, Q. Luo, X. Zhang, "Plasmonic Nanolithography", Nano Lett. 2004, 4, 1085-1088.

[18] P. G. Kik, S. A. Maier, H. A. Atwater, "Surface plasmons for nanofabrication", SPIE, Proc. 2004, 5347, 215-223.

[19] A. Sundaramurthy, P. J. Schuck, N. R. Conley, D. P. Fromm, G. S.Kino, W. E. Moerner, "Toward Nanometer-Scale Optical Photolithography: Utilizing the Near-Field of Bowtie Optical Nanoantennas", Nano. Lett. 2006, 6, 355-360.

[20] A. W. Katherine, R. P.Van Duyne, "Localized Surface Plasmon Resonance Spectroscopy and Sensing", Annu. Rev. Phys. Chem. 2007, 58, 267-297.

[21] U. Ch. Fisher, D. W. Pohl, “Observation of Single-Particle Plasmons by Near-Field Optical Microscopy”, Phys. Rev. Lett. 1989, 62, 458.

[22] A. Garc á-Etxarri, I. Romero, F. J. Garc á de Abajo, R. Hillenbrand, J. Aipurua, “Influence of the tip in near-field imaging of nanoparticle plasmon modes: Weak and strong coupling regimes”, Phys. Rev. B 2009, 79, 125439.

[23] T. Kitazawa, S. Miyanishi, Y. Murakami, K. Kojima, A. Takahashi, “Refraction of surface plasmon-polaritons at Au-Al boundaries observed scanning near-field optical microscopy” Phys. Rev. B 2008, 77, 193404.

[24] S. Nie, S. R. Emory, “Probing Single Molecules and Single Nanoparticles by Surface-Enhanced Raman Scattering”, Science, 1997, 275, 1102-1106.

[25] C. I. Haynes, C. R. Yonzon, X. J. Zhang, R. P. Can Duyne, “Surface-enhanced Raman sensors: early history and the development of sensors for quantitative biowarfare agent and glucose detection”; Raman Spectrosc. 2005, 36, 471-84.

[26] C. R. Yonzon,C, I. Haynes. X. Zhang, J. T. Walsh, R. P. Van Duyne, “Glucose Biosensor Based on Surface-Enhanced Raman Scattering: Improved Partition Layer, Temporal Stability, Reversibility, and Resistance to Serum Protein Interference”, Anal. Chem. 2004, 76, 78-85.

[27] T. B. Huff, L. Tong, Y. Zhao, M. N. Hansen, J-X. Cheng, A. Wei, Nanomedicine, “Hyperthermic effects of gold nanorods on tumor cells”, 2007, 2, 125-132.

[28] A. Bouhelier, R. Bachelot, G. Lerondel, S. Kostcheev, P. Royer, G. P. Wiederrecht, “Surface Plasmon Characteristics of Tunable Photoluminescence in Single Gold Nanorods”, Phys. Rev. Lett. 2005, 95, 267405.

[29] H. Wang, T. B. Huff, D. A. Zweifel, W. He, P. S. Low, A. Wei, J-X. Cheng, “*In vitro* and *in vivo* two-photon luminescence imaging of single gold nanorods”; Proc. Natl. Acad. Sci. 2005, 102, 15752-15756.

[30] T. Sen. S. Sadhu, A. Patra, “Surface energy transfer from rhodamine 6G to gold nanoparticles: A spectroscopic ruler”, Appl. Phys. Lett. 2007, 91, 043104.

[31] T. L. Jennings, M. P. Singh,G. F. Strouse, “Fluorescent Lifetime Quenching near d = 1.5 nm Gold Nanoparticles: Probing NSET Validity”’, J. Am. Chem. Soc. 2006, 128, 5462-5467.

[32] X. Li, J. Qian, L. Jiang, S. He, “Fluorescence quenching of quantum dots by gold nanorods and its application to DNA detection”, Appl. Phys. Lett. 2009, 94, 063111.

[33] J. Zhang, Y. Fu, M. H. Chowdhury, J. R. Lakowicz, “Enhanced Förster Resonance Energy Transfer on Single Metal Particle. 2. Dependence on Donor−Acceptor Separation Distance, Particle Size, and Distance from Metal Surface”, J. Phys. Chem. C 2007, 111, 11784-11792.

[34] J. Zhang, J. R. Lakowicz, “Metal-enhanced fluorescence of an organic fluorophore using gold particles”, Opt. Express 2007, 15, 2598-2606.

[35] M. I. Stockman, “Spasers explained”, Nature Photon. 2008, 2, 327-329.

[36] N. I. Zheludev, S. L. Prosvirnin, N. Papasimakis, V. A. Fedotov, “Lasing spaser”, Nature Photon., 2008, 2, 351-354.

[37] D. J. Bergman, M. L. Stockman, “Surface Plasmon Amplification by Stimulated Emission of Radiation: Quantum Generation of Coherent Surface Plasmons in Nanosystems”, Phys. Rev. Lett. 2003, 90, 027402.

[38] C. Bruda, X. Chen, R. Narayanan, M. A. El-Sayed, “Chemistry and Properties of Nanocrystals of Different Shapes”, Chem. Rev. 2005, 105, 1025-1102.

[39] C. J. Murphy, A. M. Gole, J. W. Stone, P. N. Sisco, A. M. Alkilany, E. C. Goldsmith, S. C. Baxter, “Gold Nanoparticles in Biology: Beyond Toxicity to Cellular Imaging”, Acc. Chem. Res. 2008, 41, 1721-1730.

[40] A. Mooradian, “Photoluminescence of Metals”, Phys. Rev. Lett. 1969, 22, 185-187.

[41] G. T. Boyd, Z. H. Yu, Y. R. Shen, “Photoinduced luminescence from the noble metals and its enhancement on roughened surfaces”, Phys. Rev. B, 1986, 33(12), 7923-7936.

[42] G. T. Boyd, T. Rasing, J. R. R. Leite, Y. R. Shen, “Local-field enhancement on rough surfaces of metals, semimetals, and semiconductors with the use of optical second-harmonic generation”, Phys. Rev. B, 1984, 30(2), 519-526.

[43] D-S. Wang, F-Y. Hsu, C-W. Lin, “Surface plasmon effects on two photon luminescence of gold nanorods”, Opt. Express, 2009, 17, 11350-11359.

[44] L. Tong, Q. Wei, A. Wei, J-X. Cheng, “Gold Nanorods as Contrast Agents for Biological Imaging: Optical Properties, Surface Conjugation and Photothermal Effects”, Photochem. Photobiol., 2009, 85, 21-32.

[45] K. Imura, T. Nagahara, H. Okamoto, “Near-Field Two-Photon-Induced Photoluminescence from Single Gold Nanorods and Imaging of Plasmon Modes”, J. Phys. Chem. B, 2005, 109, 13214-13220.

[46] M. A. El-Sayed, “Some Interesting Properties of Metals Confined in Time and Nanometer Space of Different Shapes”; Acc. Chem. Res., 2001, 34, 257-264.

[47] C. Noguez, “Surface Plasmons on Metal Nanoparticles: The Influence of Shape and Physical Environment”, J. Phys. Chem. C, 2007, 111, 3806-3819.

[48] O. P. Varnavski, M. B. Mohamed, M. A. El-Sayed, “Relative Enhancement of Ultrafast Emission in Gold Nanorods “, J. Phys. Chem. B 2003, 107, 3101-3104.

[49] P. Biagioni, M. Celebrano, G. Grancini, D.; Brida, S. Mátéfi-Tempfli, L. Duò, B. Hecht, G. Cerullo, M. Finazzi, “Dependence of the two-photon photoluminescence yield of gold nanostructures on the laser pulse duration”, Phys. Rev. B, 2009, 80, 045411.

[50] W. Cui, J. Li, Y. Zhang, H. Rong, W. Lu, L. Jiang, “Effects of aggregation and the surface properties of gold nanoparticles on cytotoxicity and cell growth”, Nanomedicine, 2012 8, 46–53

[51] Y. Hao, X. Yang, S. Song M. Huang, c. He, J. Chen, “Exploring the cell uptake mechanism of phospholipid and polyethylene glycol coated gold nanoparticles”, Nanotechnology, 2012, 23, 045103

Chapter 3 Gold nanorods for fluorescence lifetime imaging in biology

3.1 Introduction

Gold nanorods are of great interest for optical imaging due to their remarkable absorption and scattering in the visible and near-infrared (NIR) regions enhanced by surface plasmon resonance (SPR).[1,2] Especially, the NIR band absorption between 700 and 900 nm, a spectral window which permits photons to penetrate biological tissues with relatively high transmission, induces two-photon luminescence with strong intensity.[3,4] Two-Photon luminescence (TPL) from gold nanorods has been found to be sensitive to the polarization of the incident excitation.[4,5] All these properties make gold nanorods attractive probes for in vitro and in vivo imaging.[4,6,7] But so far, most related work has utilized traditional microscopy methods, such as confocal microscopy and near-field optical microscopy imaging.[8-12]

In contrast with traditional imaging methods based on fluorescence intensity, fluorescence lifetime imaging microscopy (FLIM) provides contrast according to the fluorescence decay time, the term fluorescence being more usually associated with aromatic dye molecules. Here we have an inorganic system for which the term luminescence is more usually applied. Lifetime imaging can be integrated with confocal microscopy, two-photon excitation microscopy, and other microscope systems. The luminescence (or fluorescence) decay time is the average time a fluorophore remains in the excited state after excitation. It doesn't change upon intensity variations and therefore lifetime measurements are not dependent on the local concentration of fluorophores, bleaching, the optical path of the microscope, the local excitation light intensity, or on the local luminescence detection efficiency. Also, the fluorescence decay time for aromatic molecules usually usefully depends on the intrinsic characteristics of the fluorophore and local environment - the local

viscosity, pH, or refractive index,[13-15] as well as interactions with other molecules, such as collisional or energy transfer quenching.[16,17] Thus, as well as being able to distinguish spectrally overlapping fluorophores,[18**]** imaging of the fluorescence lifetime can be used to probe the surroundings and dynamical processes of a fluorophore[19,20]. Unlike electron microscopy, fluorescence/luminescence techniques can be used in situ.

In this chapter, we use FLIM to visualize gold nanorods uptaken by Madin-Darby canine kidney (MDCK) cells. A very short luminescence decay time of TPL from gold nanorods is observed. Compared with the lifetime of 4-6-diamidino-2-phenylindole (DAPI), which is more than 2ns, lifetime imaging shows good contrast. Furthermore, besides emission, the lifetime could be an alternative identification of gold nanorods in biological imaging.

3.2 Experimental methods

Gold nanorods were synthesized by the seeded growth method. [21] Detailed synthesis process and recipe can be found in Chapter 2. The absorption spectrum shows a longitudinal plasmon mode centred at around 750nm and a weak transverse plasmon mode at 550nm.

Gold nanorods dispersions were centrifuged to remove the excess CTAB and re-dispersed in deionized water twice (14000rpm, 5 mins per cycle) with a final optical density about 1.0 at 750nm. MDCK cells were treated with 100 μl of gold nanorods solution and incubated for 3 hours under standard cell culture conditions at 37 ℃ and 5% CO_2. The cells were washed thoroughly with phosphate buffered saline (PBS) to remove excess nanorods and fixed with 3.7% paraformaldehyde. After staining with 4'-6-Diamidino-2-phenylindole (DAPI), the sample was dispersed on a glass slide and covered with a coverslip for imaging.

FLIM was performed by using a confocal microscope (LSM 510, Carl Zeiss) equipped with a time-correlated single photon counting (TCSPC) module (SPC-830, Becker & Hickl GmbH). A femtosecond Ti:Sapphire laser (Chameleon, Coherent) was tuned at 750nm to generate TPL from gold nanorods as well as DAPI. The laser pulse has a repetition rate of 80 MHz and a duration of less than 200fs. Emission was collected by a 63x water-immersion objective (N.A.=1.0) and a bandpass filter with a transmission window from 535nm to 590nm.

3.3 Results and discussion

The TPL image of gold nanorods dispersed on a glass slide is shown in Fig.3.1 (a). Bright spots are due to the TPL from nanorods, while large bright islands correspond to nanorods clusters. Strong TPL from separated nanorods can be well identified, suggesting potential application in cell imaging. Fig.3.1 (b) and (c) correspond to nuclei stained by DAPI (Emission maximizes at around 460nm and does not shift much under two photon excitation [22]), while bright spots are due to TPL from gold nanorods. Compared with cell reference sample (Fig.3.1 (b)), it is clear that there was nanorods taken up by MDCK cells, and nanorods showed a stable and strong luminescence in cell environment. Fig.3.1 (d) shows the spatial intensity distribution of the region marked by red rectangle in Fig.3.1 (c), where emission from gold nanorods, represented by sharp peaks, has intensity several times stronger than that from DAPI.

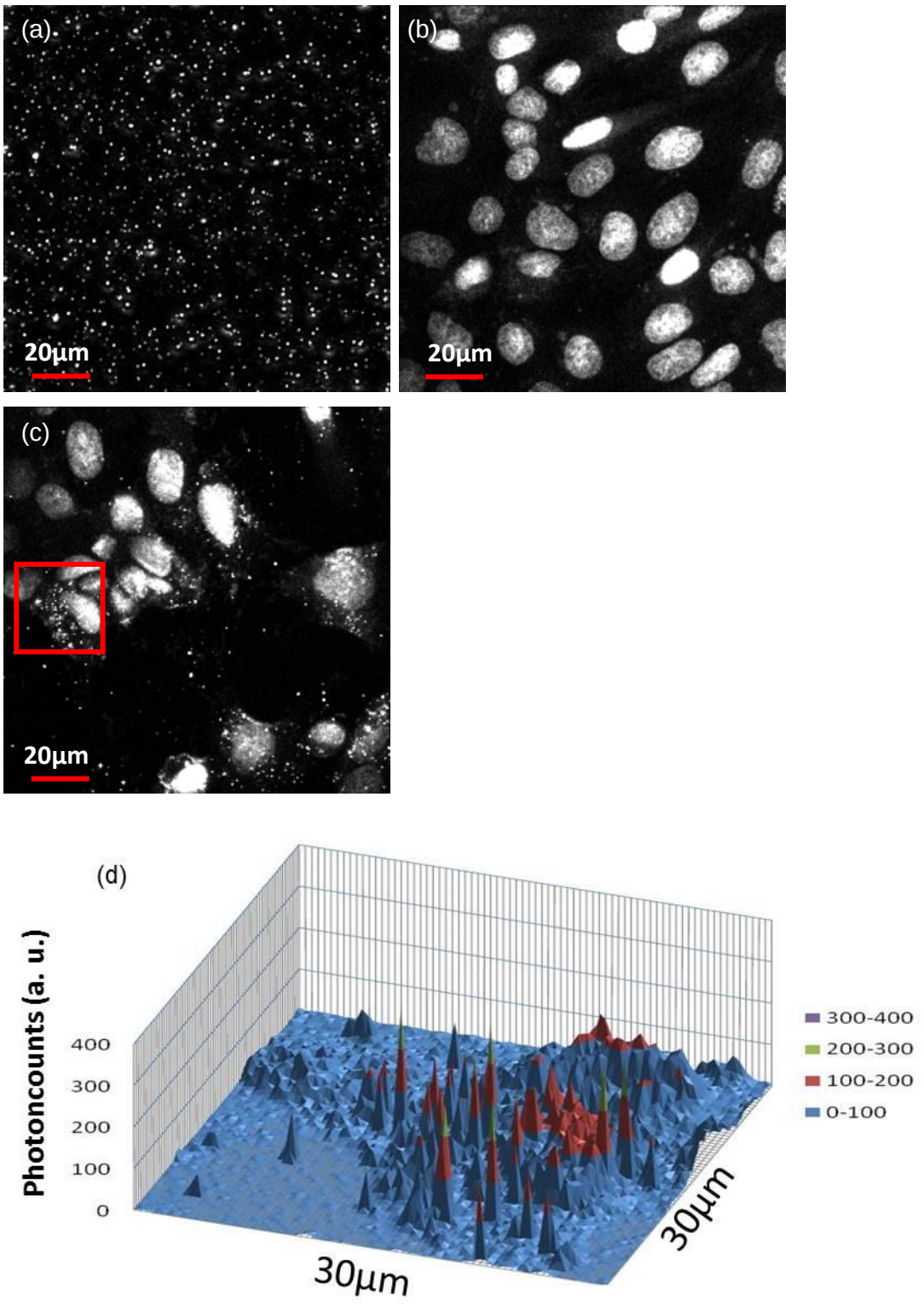

Fig.3.1 Two-photon fluorescence image of gold nanorods in cell culture. (a) gold nanorods solution on glass slides; (b) reference cell sample; (c) Cells incubated with

gold nanorods; (d) comparison of two-photon luminescence from gold nanorods and DAPI.

Results of confocal and FLIM imaging from gold nanoparticles and MDCK cells are presented in Figure 3.2. Similar to Fig.3.1, The elliptical shapes in Fig.3.2 (a) correspond to nuclei, and bright spots are TPL from gold nanorods. Internalization of CTAB stabilized gold nanorods in cells has been reported before, and studied using 3-D stack confocal microscopy[8, 9]. Fig.3.2 (b) is a FLIM image from the same sample area as in Fig. 3.2(a), with different coded colors representing different lifetime scale. The luminescence lifetime of each pixel is obtained by applying a single or multi-exponential fit; in this case a single exponential model was used. The fluorescence lifetime of DAPI is found to be longer than 2 ns, and fitted well by a single exponential model. This value is in accordance with published data on FLIM analysis of DAPI.[12]While the TPL decay time of gold nanorods is shorter than 100ps, and this result is confirmed by FLIM study of pure gold nanorods on a glass slide as well as time resolved luminescence measurement of gold nanorods in a cuvette using the same excitation and time-correlated single-photon counting (TCSPC) [23] (not shown here). To avoid photo bleaching or damages to the biological sample, excitation power and accusation time in FLIM experiments cannot be set to be too high. Therefore, number of accumulated photons will be less than that of a solution phase TCSPC setup. The peak value of a decay curve in a FLIM result should be at least 100 photoncounts to get a reliable single exponential fit, 1,000 photons for a two-exponential and 10,000 for a three-exponential decay model. This threshold number can be decreased if any component of a multi-exponential model is known. Our results meet the required photoncounts for a reliable fit. Furthermore, due to the huge time gap between the two decay components, the fit result will be even more reliable.

.

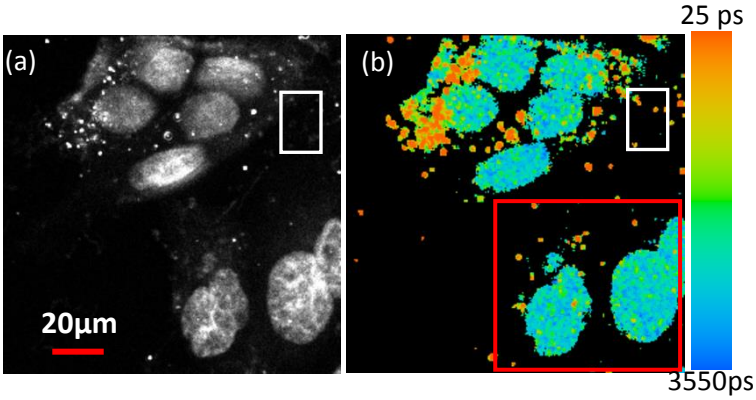
(a)
(b)
20μm
25 ps
3550ps

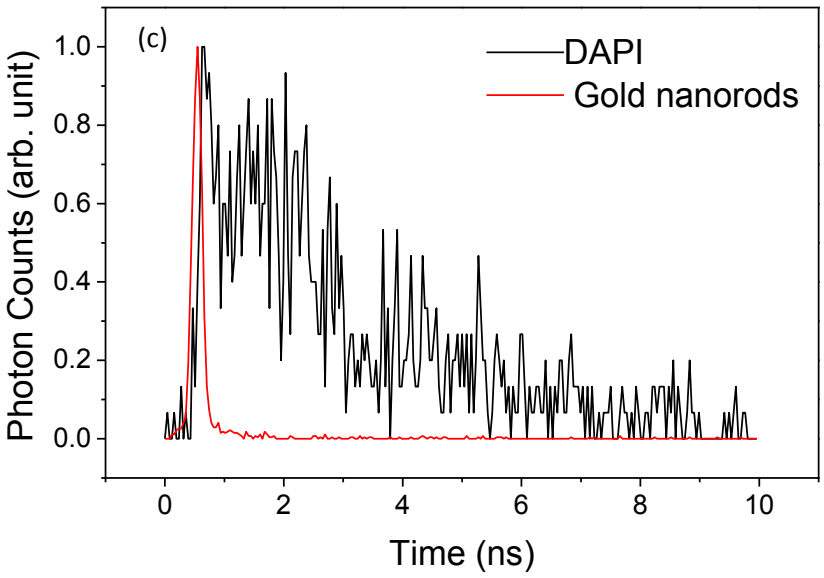
(c)
DAPI
Gold nanorods
Photon Counts (arb. unit)
Time (ns)
0.0
0.2
0.4
0.6
0.8
1.0
0
2
4
6
8
10

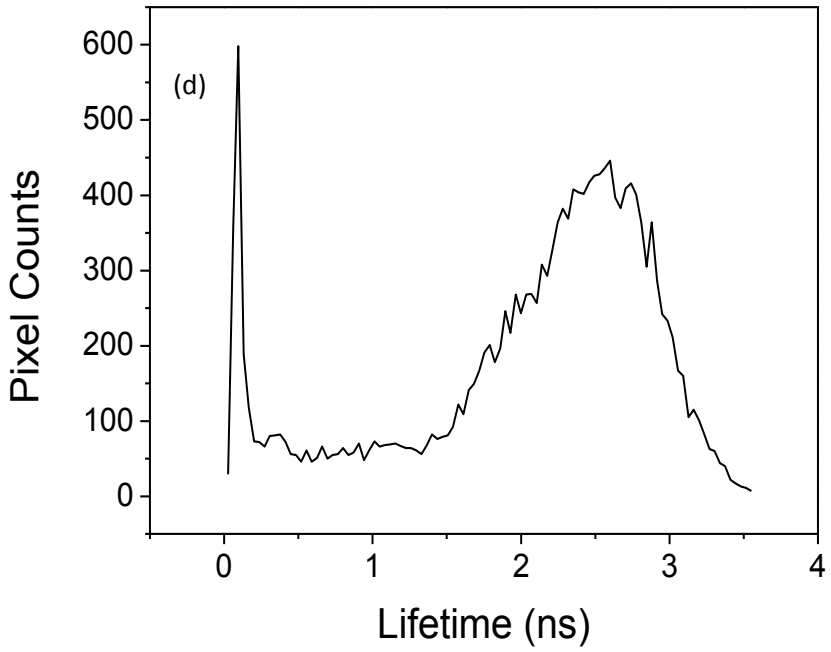
(d)
Pixel Counts
Lifetime (ns)
0
100
200
300
400
500
600
0
1
2
3
4

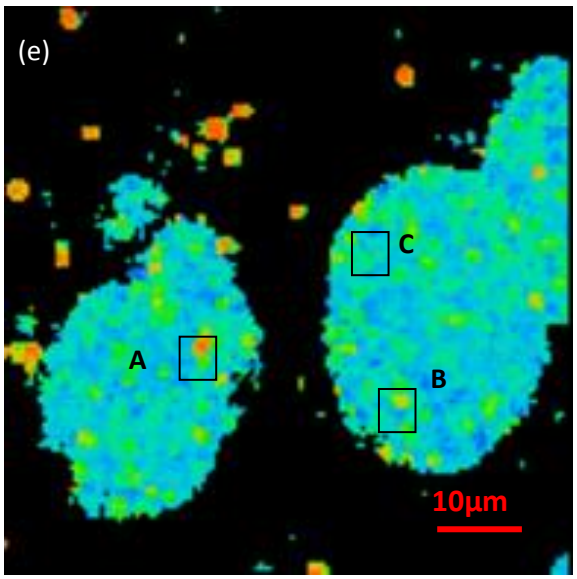

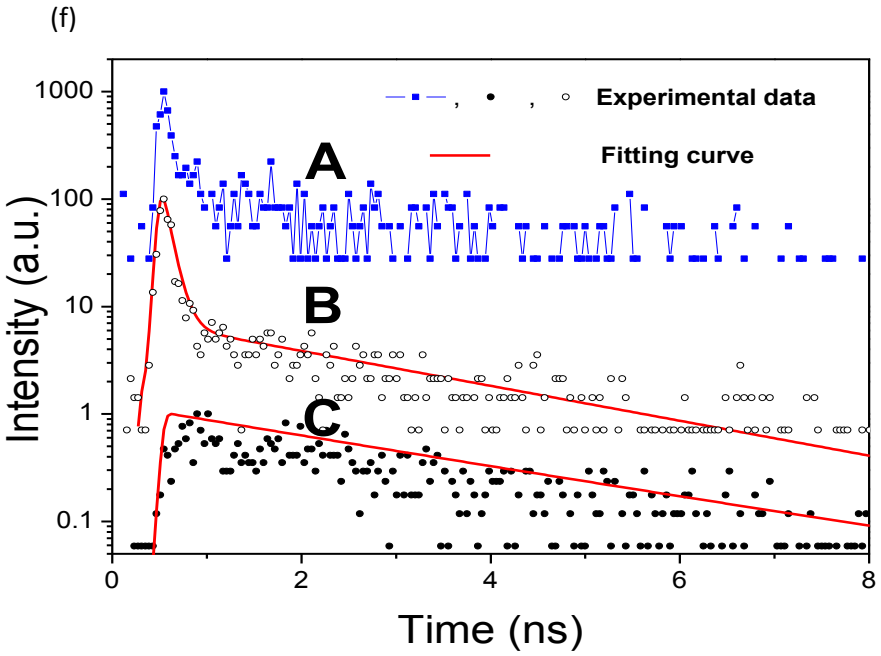

Fig.3.2 (a) Intensity image of reference MDCK cells; (b) lifetime image of gold nanorods in MDCK cells; (c) Typical TPL decay curves of DAPI and gold nanorods; (d) Histogram of lifetime of every single pixel in the FLIM image; (e) Enlarged lifetime image corresponding to red rectangular area in (b); (f) decay curves and fittings derived from region A, B and C in (e). Scanning area: 133 μm x 133 μm for (a), 67 μm x 67 μm for (e).

Nevertheless, the contrast in lifetime scale can be clearly seen in Fig.3.2 (b), which gives the typical line shapes of fluorescence decay curves of DAPI (black) and gold nanorods (red) as shown in Fig.3.2(c). The luminescence lifetime distribution of all the pixels is shown in Fig.3.2 (d), where two peaks can be identified, one at around 100ps corresponding to gold nanorods and the other to DAPI.

The FLIM image is in good accord with the intensity image, but is superior in contrast to the latter, which is caused by the huge gap between the decay time from gold nanorods and DAPI. As the lifetime of gold nanorods is much shorter than that of commonly used fluorescent molecules and other quantum particles, the lifetime can be a useful identification parameter in bio-imaging. Moreover, FLIM provides details which are lost when using traditional imaging due to the low luminescence intensity, because lifetime measurement does not depend upon the fluorophore concentration. For example, detailed features from gold nanorods in the rectangular region in the FLIM image, Fig.3.2 (b), are apparent but not visible in the intensity image, Fig.3.2 (a).

FLIM can also provide more information based on luminescence lifetime analysis. Fig.3.2 (e) amplifies the red rectangular region in Fig.3.2 (b). In the nuclei areas, orange dots and yellow areas are clearly visible surrounded by blue areas (DAPI). Three typical regions are labelled as A, B and C. Corresponding decay curves of these three regions derived from the FLIM image are shown in Fig.3.2 (f) together with mono-exponential (C) or bi-exponential (B) fittings. Typically, DAPI has a long lifetime in the range from 1.5ns to 3.5ns, such as that found in region C. In contrast, decay curve in region A is in the system response level, similar to that from separated gold nanorods, indicating a lifetime shorter than 100ps. Decay curve from region B, which can be well fitted by a bi-exponential model with one component around 100ps and the other 3ns, are considered to be an overlay of the emissions of nanorods and DAPI. Thus FLIM image reveals the existence of gold nanorods in these orange-yellow areas, indicating the uptaken of gold nanorods by MDCK cells.

3.4 Conclusion

In summary, we have studied gold nanorods as luminescence label in MDCK cells by FLIM, which provides a better contrast ratio and more detailed features than with intensity imaging. The luminescence lifetime of gold nanorods is found to be less than 100ps, much shorter than most dye molecules, suggesting the possibility of distinguishing gold nanorods from extrinsic and endogenous fluorophores in biological systems. Thus, the characteristic lifetime together with polarization of TPL from gold nanorods can be a promising imaging contrast agent for use in luminescence microscopy in biology.

References

1. S. Link, M. A. El-Sayed, "Shape and size dependence of radiative, non-radiative and photothermal properties of gold nanocrystals", Int. Rev. in Phys. Chem. 2000, 19 (3), 409- 453
2. M. B. Mohamed, V. Volkov, S. Link, M. A. El-Sayed, "The 'lightning' gold nanorods: fluorescence enhancement of over a million compared to the gold metal", Chem. Phys. Lett. 2000, 317**,** 517–523
3. R. A. Farrer, F. L. Butterfield, V. W. Chen, J. T. Fourkas, "Highly Efficient Multiphoton-Absorption-Induced Luminescence from Gold Nanoparticles", Nano Lett., 2005, 5 (6) 1139-1142
4. H. Wang, T. B. Huff, D. A. Zweifel, W. He, P. S. Low, A. Wei, J. Cheng, "In vitro and in vivo two-photon luminescence imaging of single gold nanorods"; Proc. Natl Acad. Sci. USA 2005, 102(44), 15752–15756
5. K. Imura, T. Nagahara, H.mi Okamoto, "Near-Field Two-Photon-Induced Photoluminescence from Single Gold Nanorods and Imaging of Plasmon Modes", J. Phys. Chem. B 2005, 109 (27), 13214-13220
6. X. H. Huang, I. H. El-Sayed, W. Qian, M. A. El-Sayed, "Cancer Cell Imaging and Photothermal Therapy in the Near-Infrared Region by Using Gold Nanorods", J Am. Chem. Soc. 2006, 128 **(**6), 2115-2120
7. H. Ding, K.-T. Yong, I. Roy, H. E. Pudavar, W. C. Law, E. J. Bergey, P. N. Prasad, "Gold Nanorods Coated with Multilayer Polyelectrolyte as Contrast Agents for Multimodal Imaging", *J. Phys. Chem. C* 2007, *111* (34), 12552–12557
8. T. B. Huff, M. N. Hansen, Y. Zhao, J. Cheng, A. Wei, "Controlling the Cellular Uptake of Gold Nanorods", Langmuir 2007, 23, 1596-1599
9. T. B. Huff, M. N. Hansen, Y. Zhao, J. Cheng, A. Wei, "Hyperthermic effects of gold nanorods on tumor cells" Nanomedicine 2007, 2, 125–132
10. N. J. Durr, T. Larson, D. K. Smith, B. A. Korgel, K. Sokolov, A. Ben-Yakar "Two-Photon Luminescence Imaging of Cancer Cells Using Molecularly

Targeted Gold Nanorods", Nano Lett. 2007, 7 (4), 941-945

11. K. Imura, T. Nagahara, H. Okamoto, "Imaging of Surface Plasmon and Ultrafast Dynamics in Gold Nanorods by Near-Field Microscopy", J. Phys. Chem. B, 2004, 108, 16344-16347
12. L. Tong, Q. Wei, A. Wei, J. Cheng, "Gold Nanorods as Contrast Agents for Biological Imaging: Optical Properties, Surface Conjugation and Photothermal Effects", Photochem. Photobiol. 2009, 85, 21-32
13. S. T. Hess, E. D. Sheets, A. Wagenknecht-Wiesner, A. A. Heikal, "Quantitative analysis of the fluorescence properties of intrinsically fluorescent proteins in living cells", Biophys. J. 2003, 85, 2566–2580
14. B. Wilhelmi, Chem. "Influence of solvent viscosity on excited-state lifetime and fluorescence quantum yield of dye molecules", Phys. 1982, 66, 351–355
15. K. Suhling, J. Siegel, P. M. P. Lanigan, S. Leveque-Fort, S. E. D. Webb, D. Phillips, D. M. Davis, P. M. W. French, "Time-resolved fluorescence anisotropy imaging applied to live cells", Opt. Lett. 2004, 29, 584-586.
16. J. R. Lakowicz, "Principles of Fluorescence Spectroscopy", Kluwer Academic–Plenum Publishers, New York, 2nd Ed. 1999
17. B. Valeur, "Molecular Fluorescence", Wiley-VCH, New York, 2002
18. A. Rück, CH. Hülshoff, I. Kinzler, W. Becker, R. Steiner, "SLIM: A new method for molecular imaging", Micros. Res. and Tech. 2007, 70, 485–492
19. T. Ng, A. Squire, G. Hansra, F. Bornancin, C. Prevostel, A. Hanby, W. Harris, D. Barnes, S. Schmidt, H.Mellor, P. I. Bastiaens, P. J.Parker, "Imaging Protein Kinase Cα Activation in Cells", Science, 1999, 283, 2085-2089
20. M. Peter, S. M. Ameer-Beg, "Imaging molecular interactions by multiphoton FLIM", Biol. Cell 2004, 96, 231–236
21. J. Murphy, T. K. Sau, A. M. Gole, C. J. Orendorff, J. Gao, L. Gou, S. E. Hunyadi, T. Li, "Anisotropic Metal Nanoparticles: Synthesis, Assembly, and Optical Applications", J. Phys. Chem. B. 2005, 109, 13857-13870
22. F. Bestvater, E. Spiess, G. Stobrawa, M. Hacker, T. Feurer, T. Porwol, U. Berchner-Pfannschmidt, C. Wotzlaw, H. Acker, "Two-photon fluorescence absorption and emission spectra of dyes relevant for cell imaging", J. of Micros. 2002, 208, 108–115

23. A. Volkmer, D. A. Hatrick, D. J. S. Birch, “Time-resolved nonlinear fluorescence spectroscopy using femtosecond multiphoton excitation and single-photon timing detection”, Meas. Sci. Technol. 1997, 8, 1339-1349

Chapter 4

Two-photon excited surface plasmon enhanced energy transfer between DAPI and gold nanoparticles: opportunities in intra-cellular imaging and sensing

4.1 Introduction

Energy transfer is one of the fundamental processes governing light-harvesting in biological systems and energy conversion in electronic devices such as organic solar cells or light-emitting diodes. Förster resonance energy transfer (FRET), which occurs between donors and acceptors in close proximity, is referred to as the 'spectroscopic ruler' and has been applied to a broad range of research, including distance distributions,[1, 2] metabolic sensing,[3] protein and cell function.[4-6] FRET theory assumes a (point)-dipole-dipole interaction between a donor and an acceptor and derives an expression for the energy transfer rate $k_T(r)$ defined as,

$$k_\tau(r) = \frac{1}{\tau_D}\left(\frac{R_0}{r}\right)^6 \tag{4.1}$$

where τ_D is the intrinsic fluorescence lifetime of the donor, R_0 is the Förster distance at which the energy transfer rate equals the donor decay rate in the absence of acceptor and r is the distance between donor and acceptor.[7,8] The effective range of FRET is reported to be typically less than 80Å, as limited by the nature of the dipole-dipole mechanism. However, this constraint in the length scale of detection can be extended dramatically when metallic particles act as acceptors since the distance dependence now scales at less than the 6^{th} power. A surface energy transfer

(SET) model has been proposed to described the energy transfer from a dye to metal,[9] where the transfer rate goes as d^4 given by Equation (2)

$$k_\tau(r) = \frac{1}{\tau_D}\left(\frac{d_0}{d}\right)^4 \tag{4.2}$$

Here, τ_D is the lifetime of donor and d is the separation between donor and acceptor; d_0 is the separation at which the transfer rate equals to unity. The 4th order distance dependence compared to a 6th order relationship in FRET model is due to the coupling of electronic dipole of the donor to the free electron dipoles on the metal surface, relaxing the dependence of the vector projection. Therefore, SET can be extend the spectrum ruler range compared to FRET, and the effective energy transfer distance between donor and acceptor particle can be as much as twice compared to FRET model.[10, 11]

In addition to extending the upper range limit, gold nanoparticles are in many ways superior to organic dye molecules in energy transfer application as they are photostable, low toxicity and can also be easily conjugated to biological structures. This is especially true for gold nanorods (GNRs), where their strong two-photon luminescence (TPL) arising from surface plasmon resonance, makes them excellent fluorescence probes in biological imaging.[12-16] Two-photon excitation has advantages over one-photon excitation because of higher spatial resolution, deeper penetration and less photo-damage due to near infrared (NIR) excitation. It thus has special appeal for intracellular measurement. Previously we demonstrated that by incorporating GNRs in cells their fast fluorescence decay time of GNRs could be used to good effect in FLIM.[17]

In this chapter we report another important aspect of GNRs, namely the study of energy transfer between 4'-6-Diamidino-2-phenylindole (DAPI), a commonly used DNA dye,[18,19] and GNRs in comparison with gold nanospheres (GNSs) under two-photon excitation. Solution phase studies reveal the energy transfer efficiency is higher in the presence of GNRs than GNSs. Further study on a cell culture environment confirms energy transfer between DAPI molecules and GNRs taken up

by MDCK cells. The study shows the possibility of exploiting both the TPL imaging and energy transfer process to trace gold nanoparticles and their interaction with biomolecules within cells.

4.2 Experimental methods

Gold nanorods and spheres were both synthesized by the seeded growth method.[20] Gold nanorods have a longitudinal plasmon mode centred at around 850nm, a transverse band at 525nm, while GNSs have single surface plasmon band at 535nm. For energy transfer studies, 2ml 4.3μM DAPI solution was mixed with 1ml GNRs (Sample 1), 1.4ml GNRs (Sample 2), 1ml GNSs (Sample 3), 1.4ml GNSs solution (Sample 4) and 2.8ml GNSs (Sample 5) solution. 150μl of each sample was placed in an imaging chamber for microscopy studies.

To prepare cell culture samples, gold nanorod dispersions were centrifuged to remove the excess CTAB and re-dispersed in deionized water twice (14000rpm, 5 mins per cycle) with a final optical density about 1.0. MDCK cells were treated with 100 μl of gold nanorod solution and incubated for 3 hours under standard cell culture conditions at 37℃ and 5% CO_2. The cells were washed thoroughly with phosphate buffered saline (PBS) to remove excess nanorods and fixed with 3.7% paraformaldehyde. After staining with 4'-6-Diamidino-2-phenylindole (DAPI), the sample was dispersed on a glass slide and covered with a coverslip for imaging.

FLIM imaging experiments were performed using a confocal microscope (LSM 510, Carl Zeiss) equipped with a time-correlated single photon counting (TCSPC) module (SPC-830, Becker & Hickl GmbH). A femtosecond Ti:Sapphire laser (Chameleon, Coherent) was tuned to 750nm. The laser pulse has a repetition rate of 80 MHz and duration less than 200fs. Emission was collected by a 60x water-immersion objective (N.A.=1.0) and a bandpass filter with a transmission window from 390nm to 465nm.

4.3 Results and discussion

4.3.1 Spectroscopic characterization of donor and acceptor particles

The spectrum overlapping between donors and acceptors are presented in Figure 4.1. Figure 4.1 (b) shows the absorption and emission spectrum of donor molecules. The emission band of DAPI centres around 475nm and the absorption peak lies close to 350nm. Figure 4.1 (c) depicts the absorption spectrum of GNRs and GNSs, with a surface plasmon peak at 530nm for GNSs and a transverse surface plasmon peak around 520nm for GNRs, and the overlapping of the emission spectrum of DAPI (taken with excitation at 305nm, intensity denoted with *I*)). It reveals that the emission spectrum of DAPI overlaps quite well with the absorption spectrum of the GNRs and GNSs solution. As the emission spectrum of DAPI follows the same structure under single and multi-photon excitation,[21] we use this spectrum to calculate the overall integral of donor and acceptor overlap.

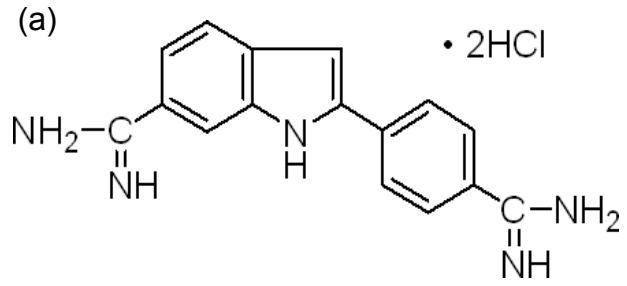

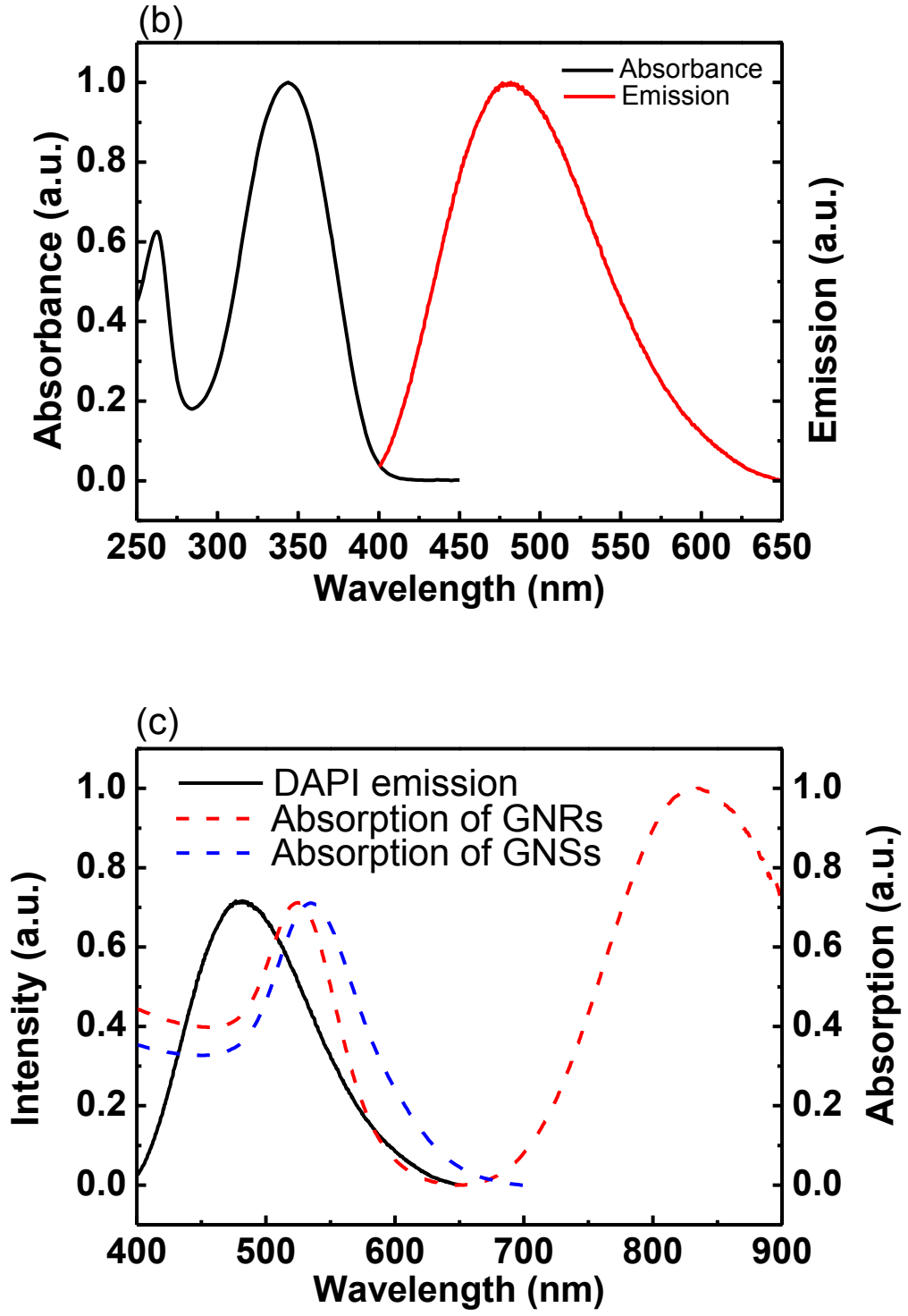

Fig.4.1. (a) Chemical structure of DPAI molecule (b) Absorption and emission spectrum of DAPI; (c) Emission spectrum of DAPI solution (solid line) and extinction spectrum of GNRs and GNSs (dashed lines, red for GNRs and blue for GNSs).

4.3.2 Decay time measurements of donor (DAPI) molecules

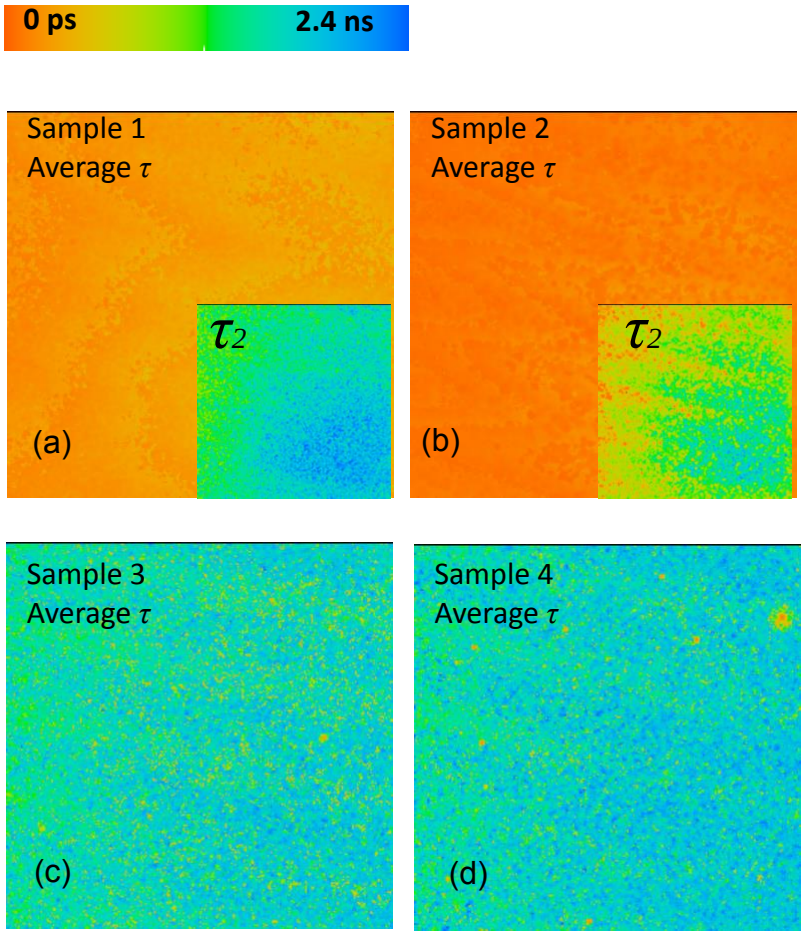

Fig. 4.2 (a), (b) Average lifetime images of sample 1 and 2 mixed with GNRs; inset displays the mapping of long lifetime component, τ_2, (details see text); (c), (d) Avrage lifetime images of sample 3 and 4 mixed with GNSs.

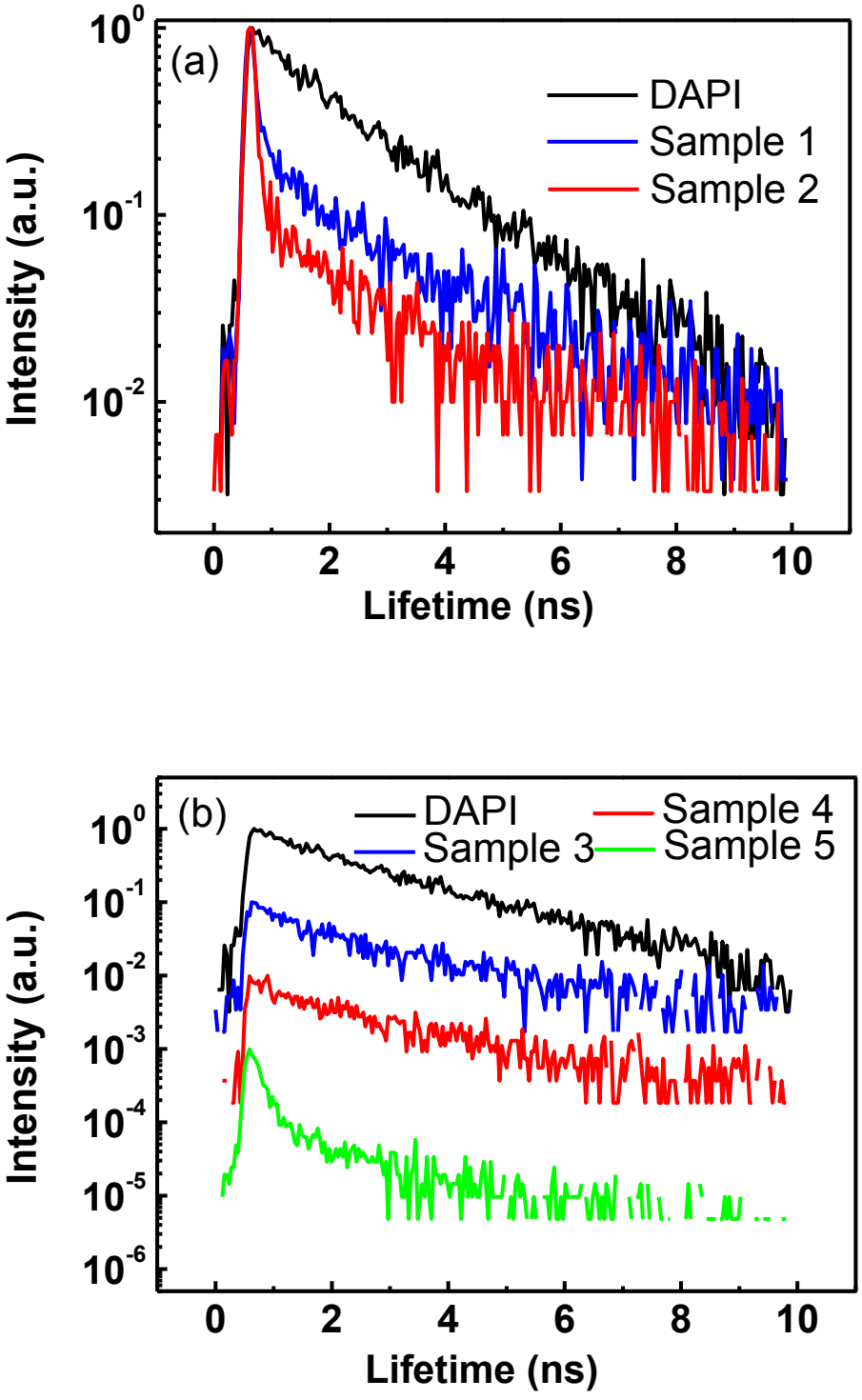

Fig.4.3. Normalized decay curves of DAPI solution (a) in the presence of GNRs and (b) GNSs, with DAPI solution in the absence of gold nanoparticles as reference. Decay curves were manually shifted vertically in (b) for comparison purpose.

150 μl of each mixture solution was placed in imaging chambers for the FLIM test, which are shown in Fig.4.2. With colour codes representing decay times form 0 (orange) to about 2.4ns (blue), significant differences between lifetimes of individual mixture samples can be seen. As both acceptor gold nanorods and donor molecules DAPI emit light under the excitation condition, and their emissions cannot be distinguished due to spectroscopic overlapping, a two-exponential decay model were applied to sample 1 and 2. The multi-exponential model is expressed in Equ.4.3, for two-exponential model, *n*=2. While for sample 3, 4 and 5, a single exponential model (*n*=1) was utilized because gold nanospheres do not emit light. The average lifetime, which can be expressed in Eqn.4.4, for sample 1 and 2 are shown in Fig 4.2 (a) and (b). As we are more interested in the donor lifetime, the long lifetime component τ_2, representing the contribution from DAPI, can be found in the insets of Fig4.2 (a) and (b).

$$I = \sum_{i=1}^{n} \alpha_i \exp(-t/\tau_i) \tag{4.3}$$

$$\tau_{ave} = \frac{\sum_{i=1}^{n} \alpha_i \, \tau_i}{\sum_{i=1}^{n} \alpha_i} \tag{4.4}$$

Fig 4.3 (a) displays typical decay curves of DAPI solution with and without GNRs extracted from FLIM results (dependence of fluorescence intensity *I* on time *t*). The photoluminescence decay of DAPI solution without GNRs can be fitted by a mono-exponential model with a decay time of 1.7 ns. A bi-exponential decay is observed for DAPI solution with GNRs, as expected because GNRs have two-photon luminescence under 750nm excitation. The average decay time is 290 ps (τ_1=100ps and τ_2=1.55ns) for S1, and 90 ps (τ_1=80ps and τ_2=800ps) for S2, respectively. The long lifetime component, τ_2, is related to the emission from DAPI, while the short

component, τ_1, limited by the system response time, is considered to be emission from GNRs and is consistent with our previous study.[17, 22] It suggests that at a relatively low concentration of GNRs (S1), τ_2 shows no significant decrease compared to pure DAPI solution. With further increase of GNRs concentration, as in S2, about 50% decrease of τ_2 (from 1.55ns to 800ps) has been observed. Furthermore, the contribution from GNRs, τ_1, to the total decay curve increased from around 85% to 95%, which indicates an enhancement of acceptor emission. These results confirm energy transfer from DAPI to GNRs. In contrast, no lifetime change was observed for DAPI solution with and without GNSs (S3 and S4 in Fig 4.3 (b)). All decay curves show a lifetime around 1.7ns. Only, on adding more GNSs (double the concentration of S4), the lifetime of DAPI decreases, S5 in Fig4.3 (b), where the long lifetime component decreases to less than 1ns.

4.3.3 Comparison of FRET and SET model

The concentration of GNRs and GNSs are estimated from the absorption spectrum using reported gold nanoparticle extinction coefficient.[23,24] They are comparable at $1.8\text{x}10^{-11}$ M for GNRs and $2.8\text{x}10^{-11}$ M for GNSs. Scanning Electron Microscope (SEM) study reveals that the sizes of these two nanoparticles are also comparable, with diameter of GNSs and long axis of GNRs both around 50nm.

The FRET transfer rate for a donor and acceptor separated with a distance *r* can be calculated as:

$$k_\tau(r) = \frac{Q_D \kappa^2}{\tau_D r^6}\left(\frac{9000(ln10)}{128\pi^5 N n^4}\right)\int_0^\infty F_D(\lambda)\,\varepsilon_A(\lambda)\lambda^4 d\lambda \qquad (4.5)$$

where Q_D is the quantum yield of the donor in the absence of acceptor, *n* is the refractive index of the medium, *N* is Avogadro's constant, *r* is the distance between the donor and acceptor, and τ_D is the lifetime of the donor in the absence of acceptor. The refractive index *(n)* is typically assumed to be 1.4 for aqueous solution. $F_D(\lambda)$ is the corrected fluorescence intensity of the donor in the wavelength range λ to $\lambda+\Delta\lambda$

with the total intensity (area under the curve) normalized to unity. ε_A is the extinction coefficient of the acceptor at λ, which is typically in units of $M^{-1}cm^{-1}$. The κ^2 term is relative orientation factor in space of the transition dipoles of the donor and acceptor.

The overlap integral $J(\lambda)$ expresses the degree of spectral overlap between the donor emission and the acceptor absorption, and is given by

$$J(\lambda) = \int_0^\infty F_D(\lambda)\,\varepsilon_A(\lambda)\lambda^4 d\lambda = \frac{\int_0^\infty F_D(\lambda)\,\varepsilon_A(\lambda)\lambda^4 d\lambda}{\int_0^\infty F_D(\lambda)\,d\lambda}$$

(4.6)

$F_D(\lambda)$ is dimensionless, and if ε_A is expressed in the units of $M^{-1}cm^{-1}$ and λ is in nanometers, then $J(\lambda)$ is in units of $M^{-1}cm^{-1}nm^4$. In calculating $J(\lambda)$, corrected emission spectrum, with which area under spectrum curve is normalized to unity, should be used.

At Förster distance R_0, half the donor molecules decay by energy transfer, with $k^T(r)=\tau_D^{-1}$, R^0 can be calculated using equation below,

$$R_0^6 = \frac{9000(ln10)Q_D\kappa^2}{128\pi^5 N n^4}\int_0^\infty F_D(\lambda)\,\varepsilon_A(\lambda)\lambda^4 d\lambda$$

(4.7)

From this expression, the Förster distance R_0 can be calculated by the spectral properties of the donor and acceptor, as well as the donor quantum yield. By combining know values and experimental constants, R_0 can be expressed as

$$R_0 = 0.21[\kappa^2 n^{-4} Q_D J(\lambda)]^{1/6}\ \mathring{A}$$

(4.8)

with wavelength is in the units of nm. In our experiments, replacing Q_D with quantum yield of DAPI Φ_{DAPI} , R_0 can be calculated by

$$R_0 = 0.21[\kappa^2 n^{-4} \Phi_{DAPI} J(\lambda)]^{1/6}\ \mathring{A}$$

(4.9)

where κ^2 is the orientation factor, Φ_{DAPI} is the quantum yield of DAPI, $J(\lambda)$ is the overlap integral between the absorption of GNRs and the emission of the DAPI, and n is the refractive index of the medium. The R_0 is calculated as 534Å using κ^2=2/3, n=1.4, Φ_{DAPI} =0.03, and $J(\lambda)$ =5.10x10^{22} M^{-1} cm^{-1} nm^4 for DAPI solution with GNRs. The calculated R_0 is far beyond the effective FRET distance, suggesting a transfer mechanism different from FRET dipole-dipole theory. On the other hand, the d_0 in SET, can be calculated from the following equation:

$$d_0 = \left(\frac{0.225c^3\Phi_{DAPI}}{\omega_{DAPI}^2\omega_F k_F}\right)^{1/4}$$

(4.10)

where c is the light speed, ω_{DAPI} the frequency of the donor electronic transition and the ω_F Fermi frequency, and k_F Fermi wave vector of the metal. With ω_{DAPI}=3.9x10^{15}s^{-1}, k_F =1.2x10^{8}cm, and ω_F=8.4x10^{15}s^{-1}, d_0 is calculated as 33 Å, which is smaller than calculated d_0 (around 80 Å) in previous research on SET from rhodamine 6G to gold nanoparticles,[25] probably due to the relatively low quantum yield of DAPI.

However, neither FRET nor the SET model can explain the difference between the transfer efficiency of GNRs and GNSs. In the FRET model, R_0 for rods and spheres should be comparable, as the absorption spectrum of these two nanoparticles show similar structure in the DAPI emission range. While in the SET model, d_0 are identical for GNRs and GNSs, as the parameters related to acceptor, i.e., ω_F and k_F, are derived from bulk gold. This large discrepancy is unlikely to be due to surface (size) effect,[26] as the sizes of the two nanoparticles are comparable and both are significantly larger than dye molecule. Enhanced FRET from donor molecules to acceptor molecules in the presence of metal nanoparticles has been reported.[27] Considering the difference of these two nanoparticles in their near infrared absorption, we propose that under two-photon excitation of DAPI, where incidence

light wavelength overlaps with the longitudinal surface plasmon band of GNRs, the enhanced local field as a result of surface plasmon resonance leads to the stronger energy transfer effect.

4.3.4 Applications in biological imaging

The potential for gold nanoparticle-dye energy transfer combinations was demonstrated in a FLIM study of GNRs internalized by MDCK cells. As shown in Fig 4.4 (a), with coded colours representing average lifetimes from 0.05ns to 3.5ns, emission from GNRs and DAPI can be easily distinguished. Blue elliptical shapes with average lifetime around 2.5ns are nuclei dyed with DAPI and orange spots around nuclei with average lifetime at the level of the system response time are emission from GNRs, which is in accordance with our previous report.[17, 22] Concentrating on detailed structures, lifetime decays from rectangular region labelled A and B are displayed in Fig 4.4(b). A decay curve of pure DAPI in cell culture is plotted as a reference, and can be fitted by single-exponential decay with a lifetime of 2.5ns. Both decay curves A and B can be fitted with a bi-exponential model, with a shorter component at the system response level due to GNRs and a longer component at the magnitude of ns due to DAPI. For decay curve A, the longer component is 2.5ns. A reduced lifetime component, 0.9ns, is found for decay curve B. The shortening of DAPI lifetime indicates energy transfer between DAPI and GNRs taken up by MDCK cells in the latter case. This result is consistent with that observed in the solution phase study.

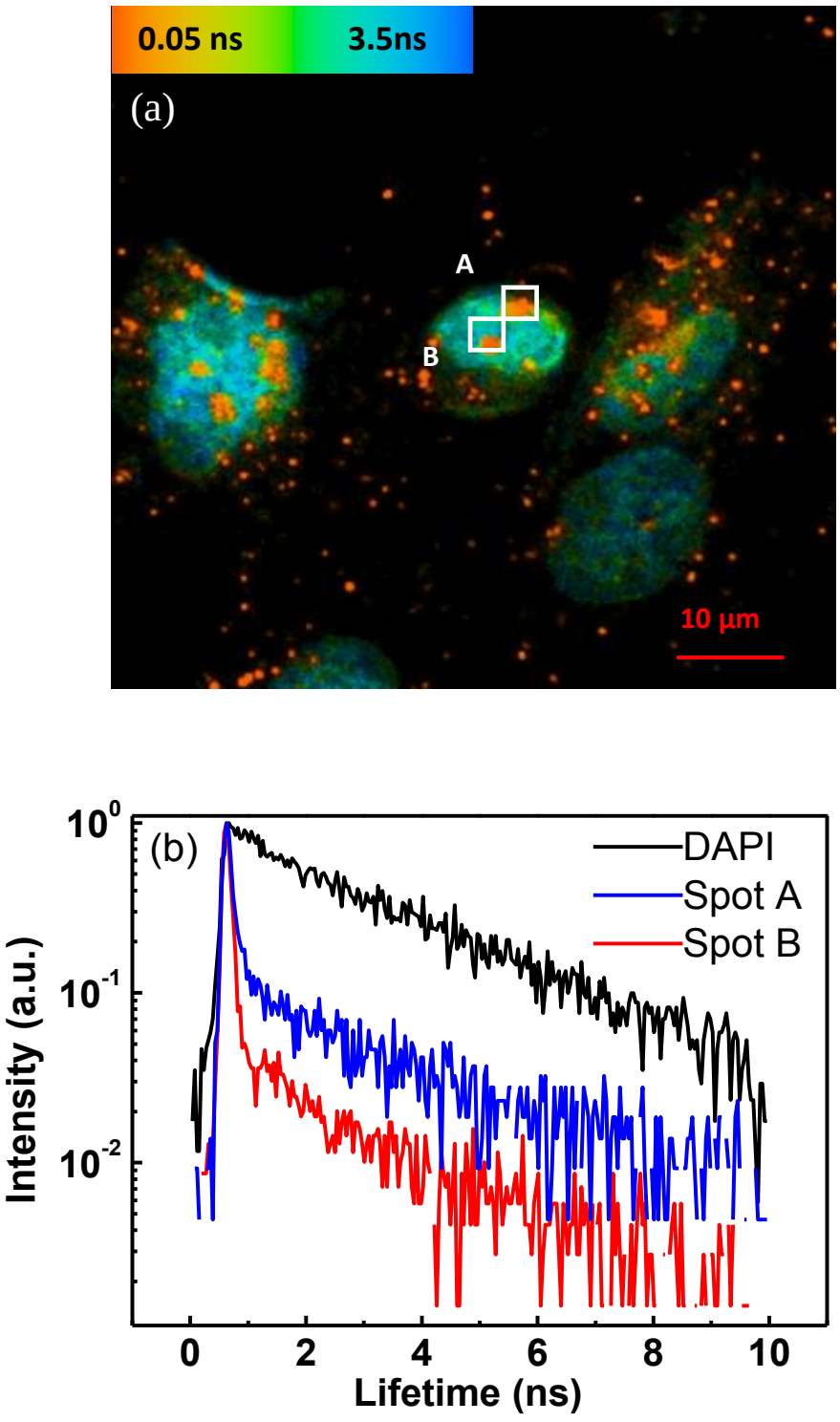

Fig 4.4. (a) FLIM image of GNRs incubated in MDCK cells. Images taken under 750nm excitation, emission collected with 535-590nm, scanning area 67µm x 67µm; (b) Normalized decay curves derived from region A and B in (a), with decay curve of DAPI as reference.

4. Conclusion

In summary, we have found enhanced energy transfer between DAPI and GNRs under two-photon excitation, which is consistent with the result from a FLIM study in cell culture. The energy transfer provides more detailed information in biological studies using GNRs as fluorescence probes, especially when combined with the advantages of two-photon excitation microscopy and more intense TPL from GNRs. GNRs would seem to have further potential, not only in FRET imaging, but also in ways that complement the growing application of other nanoparticles, such as quantum dots,[28] in fluorescence lifetime-based intra-cellular sensing of bio-analytes such as metal ions,[29] protein,[2] as well as nuclear targeting cancer therapy.[30]

References

[1] O. J. Rolinski, D. J. S. Birch, L. J. McCartney, J. C. Pickup, "A time-resolved near-infrared fluorescence assay for glucose: opportunities for trans-dermal sensing", J. Photochem. and Photobiol. B. 2000, 54, 26-34.

[2] J. C. Pickup, F. Hussain, N. D. Evans, O. J. Rolinski, D. J. S. Birch, "Fluorescence-based glucose sensors", Biosens. Bioelectron. 2005, 20, 2555-2565.

[3] T. Mizutani, T. Kondo, S. Darmanin, M. Tsuda, S. Tanaka, M. Tobiume, M. Asaka, Y. Ohba, "A Novel FRET-Based Biosensor for the Measurement of BCR-ABL Activity and Its Response to Drugs in Living Cells", Clin. Cancer Res. 2010, 16(15), 3964-3975.

[4] M. P. Lillo, B. K. Szpikowska, M. T. Mas, J. D. Sutin, J. M. Beechem, "Real-time measurement of multiple intramolecular distances during protein folding reactions: A multisite stopped-flow fluorescence energy-transfer study of yeast phosphoglycerate kinase", Biochemistry. 1997, 36, 11273– 1128.

[5] E. A. Jares-Erijman, T. M. Jovin, "FRET imaging", Nat. Biotechnol. 2003, 21, 1387-1395.

[6] A. Miyawaki, A. Sawano, T. Kogure, "Lighting up cells: labelling proteins with fluorophores", Nat. Cell Biol. Suppl. 2003, S1-7.

[7] T. Förster, "Zwischenmolekulare enegiewanderung und fluoreszenz", Ann. Physik. 1948, 437, 55-75.

[8] M. Y. Berezin, S. Achilefu, "Fluorescence Lifetime Measurements and Biological Imaging", Chem. Rev. 2010, 110, 2641-2684.

[9] C. S. Yun, A. Javier, T. Jennings, M. Fisher, S. Hira, S. Peterson, B. Hopkins, N. O. Reich, G. F. Strouse, "Nanometal Surface Energy Transfer in Optical Rulers, Breaking the FRET Barrier", J. Am. Chem. Soc.2005, 127, 3115-3119.

[10] J. Griffin, A. K. Singh, D> Senapati, P. Rhodes, K. Mitchell, B. Robinson, E. Yu, P. C. Ray, "Size- and Distance-Dependent Nanoparticle Surface-Energy Transfer (NSET) Method for Selective Sensing of Hepatitis C Virus RNA", Chem. Eur. J. 2009, 15, 342-351

[11] T. L. Jennings, J. C. Schlatterer, M. P. Singh, N. L. Greenbaum, G. F. Strouse, "NSET Molecular Beacon Analysis of Hammerhead RNA Substrate Binding and Catalysis", Nano Lett. 2006, 6, 1318-1324

[12] T. B. Huff, L. Tong, Y. Zhao, M. N. Hansen, A. Wei, "Hyperthermic effects of gold nanorods on tumor cells", Nanomedicine, 2007, 2(1), 125-132.

[13] H. Wang, T. B. Huff, D. A. Zweifel, W. He, P. S. Low, A. Wei, J-X. Cheng, "In vitro and in vivo two-photon luminescence imaging of single gold nanorods", Proc. Natl. Acad. Sci. 2005, 102, 44 15752-15756.

[14] X. H. Huang, S. Neretina, M. A. EL-Sayed, "Gold Nanorods: From Synthesis and Properties to Biological and Biomedical Applications", Adv. Mater. 2009, 21, 4880-4910.

[15] C. J. Murphy, A. M. Gole, J. W. Stone, P. N. Sisco, A. M. Alkilany, E. C. Goldsmith, S. C. Baxter, "Gold Nanoparticles in Biology: Beyond Toxicity to Cellular Imaging", Acc. Chem. Res. 2008, 41, 1721-1730

[16] N. J. Durr, T. Larson, D. K. Smith, B. A. Korgel, K. Sokolov, A. Ben-Yakar, "Two-Photon Luminescence Imaging of Cancer Cells Using Molecularly Targeted Gold Nanorods", Nano Lett. 2007, **7**, 941-945

[17] D. H. Williamson, D. J. Fennell, "Visualization of yeast mitochondrial DNA with the fluorescent stain "DAPI".", Methods Enzymol. 1979, 56, 728-733

[18] J. J. Kapuscinski, "DAPI - A DNA-Specific fluorescent probe", Biotech. Histochem. 1995, 70, 220 – 233

[19] J. Murphy, T. K. Sau, A. M . Gole, C. J. Orendorff, J. Gao, L. Gou, S. E. Hunyadi, T. Li, J. "Anisotropic Metal Nanoparticles: Synthesis, Assembly, and Optical Applications", Phys. Chem. B. 2005, 109, 13875-13879

[20] J. R. Lakowicz, I. Gryczynski, H. Malak, M. Schrader, P. Engelhardt, H. Kano, S. W. Hell, "Time-resolved fluorescence spectroscopy and imaging of DNA labeled with DAPI and hoechst 33342 using three-photon excitation", Biophys. J. 1997, 72, 567-578

[21] Y. Zhang, J. Yu, D. J. S. Birch, Y. Chen, "Gold nanorods for fluorescence lifetime imaging in biology", J. Biomed. Opt. 2010, 15, 020504-3

[22] A. Gulati, H. Liao, J. H. Hafner, "Monitoring Gold Nanorod Synthesis by Localized Surface Plasmon Resonance", J. Phys. Chem. B. 2006, 110, 22323-22327

[23] X. Liu, M. Atwater, J. Wang, Q, Huo, "Extinction coefficient of gold nanoparticles with different sizes and different capping ligands", Colloids Surf., B. 2007, 58, 3-7

[24] T. Sen, S. Sadhu, A. Patra, "Surface energy transfer from rhodamine 6G to gold nanoparticles: A spectroscopic ruler", Appl. Phys. Lett. 2007, 91, 043104-3

[25] X. Li, L. Qian, L. Jiang, S. He, "Fluorescence quenching of quantum dots by gold nanorods and its application to DNA detection", Appl. Phys. Lett. 2009, 94, 063111-3

[26] J. Zhang, Y. Fu, M. H. Chowdhury, J. R. Lakowicz, "Enhanced Förster Resonance Energy Transfer on Single Metal Particle. 2. Dependence on Donor−Acceptor Separation Distance, Particle Size, and Distance from Metal Surface", J. Phys. Chem. C. 2007, 111, 11784-11792

[27] J. Zhang, Y. Fu, M. H. Chowdhury, and J. R. Lakowicz, "Enhanced Forster resonance energy transfer on single metal particle. 2. Dependence on donor-acceptor separation distance, particle size, and distance from metal surface", J. Phys. Chem. C.111, 11784-11792.

[28] J. U. Sutter, D. J. S. Birch, and O. J. Rolinski, "The effect of intensity of excitation on CdSe/ZnS quantum dots: Opportunities in luminescence sensing", Appl. Phys. Lett. 2011, 98, 021108.

[29] O. J. Rolinski, D. J. S. Birch, "A fluorescence lifetime sensor for Cu(I) ions", Meas. Sci. Technol .1999, 10, 127-136

[30] B. Kang, M. A. Mackey, and M. A. El-sayed, J. Am. Chem. Soc. 132, 1517 (2010).

Chapter 5

Two photon excitation enhanced energy transfer and FLIM-FRET study on intracellular pathways of gold nanorods

5.1 Introduction

Interaction between metal nanoparticles and fluorophores, such as enhanced photoluminescence, luminescence quenching and the energy transfer effect, has been well utilized in both fundamental and applied research work.[1-10] Among all those interactions, the energy transfer effect depends critically on the separation between donor and acceptor molecules, and has been referred to as a molecular ruler. There have been substantive published reports on energy transfer effect based on gold nanoparticles,[6, 9-12] especially in the field of biological study such as bio-imaging and sensing, due to their noble physical properties and subtle cytotoxicity to biosystems.[13-17] For gold nanoparticles, especially nanorods, the particle shape is critical for their surface plasmon band structure, which affects the particle physical properties dramatically (details can be found in Chapter 1 and 2). In research related to biological imaging and sensing, two-photon induced luminescence (TPL) plays an important role, as TPL from gold nanorods is strong and stable compared to common fluorophores. Moreover, multi-photon excitation has advantages over single photon excitation, such as larger penetration depth and higher spatial resolution (details can be found in in Chapter 1). However, most publications so far have treated gold particles as metal surface in energy transfer study,[18-20] few reports have been focused on the contribution from particle shape, and excitation conditions.

In Chapter 4, we have demonstrated that in the mixed nanoparticle–DAPI system, compared to gold nanospheres, gold nanorods can enhance energy transfer effect due to their strong localized surface plasmon oscillation in near infrared range. In the first

part of this chapter, we will study the energy transfer considering different excitation conditions in hybrid Fluor405 dye and gold nanoparticles.

In the second part of this chapter, we will demonstrate an application of combined fluorescence resonant energy transfer (FRET)-fluorescence lifetime imaging microscopy (FLIM) technique in the study of cell uptake process of gold nanoparticles. As gold nanorods have been widely used in biological research, such as drug delivery, cancer therapy or in vivo and in vitro imaging and sensing, understanding the uptake mechanism of gold nanoparticles into cells plays an important role in all these applications. However this is not a straightforward task, because both the cell function mechanism and properties of nanoparticles affect cell uptake process.[21-29] There are a variety of nanoparticle pathways and mechanisms into cell membrane, and results between different publications are still inconsistent. [30-31] Furthermore, the properties of nanoparticles, such as the size, shape, surface charge and coating conditions, all affect the uptake process.[30,32-34] At last, nowadays there is no effective research methodology to trace nanoparticles in this dynamic process. For example TEM can provide high resolution image, but visualizes specimen at vacuum, therefore is not able to provide in situ, time lapse examination. Traditional fluorescence microscopy can be operated in vivo or in vitro, but is lack of high sensitivity and resolution.
In this chapter, we will study the uptake mechanism of gold nanorods using two-photon FLIM-FRET method.

5.2 Experimental methods

Gold nanorods used were provided by our colleagues, and synthesized by seeded growth method. Multi-layer coated nanoparticles were prepared following a layer by layer procedure: capped nanorods were centrifuged at 8500 rpm for 10 minutes, and were modified to O.D. 1.0; then nanorods solution was mixed with polystryrenesulfonate (PSS) solution (10mg/ml in NaCl) with volume 5:1 and stirred for 5 minutes; after centrifuged at 8500 rpm for 15 minutes to remove excess polymers, and the remaining PSS coated nanorods solution was modified to O.D. 1.0; then PSS coated particles were mixed with poly-(diallyldimehtylammonium chloride

(PDDAC) solution (10mg/ml in NaCl) with volume ratio 5:1 and stirred for another 5 minutes; excess polymers can be removed by centrifuge. Multi-layer PSS/PDDAC coated nanoparticles can be prepared by repeating the process described above. The detailed recipe can be found at ref [35].

Fluor405 dyes were purchased from Sigma-Aldrich, and the mixture solution with gold nanorods was prepared as:

sample 'F0-1': mixture solution of 500 µl gold nanorods and 150 µl F405dye;

sample 'F0-2': mixture solution of 500 µl gold nanorods and 300 µl F405dye.

Hela cell-lines were obtained from American Type Culture Collection. Cell culture medium was high-glucose (4.5 g/l) DMEM containing foetal calf serum (10%), L-glutamine (2.9mg/mL), antibiotic-antimycotic solution (GIBCO). Cells were routinely cultured at 37^{o}C under 5% CO_2. Cell light Endosomes-GFP BacMam 2.0 GFP earlyendosome marker was purchased from Invitrogen.

Spectroscopy studies were carried out using a JASCO V-660 absorption spectrometer and HORIBA Fluorolog-3 FL3-22 emission spectrometer. Fluorescence decay times were obtained using both HORIBA-IBH TCSPC lifetime measurement kit and B&H lifetime module. Fluorescence and FLIM images were taken with Zeiss LSM-510 confocal microscope and attached B&H module. Detailed configuration can be found in results section.

5.3 Results and discussion

5.3.1 Two-photon enhanced energy transfer effect

The absorption spectrum of gold nanoparticles, the 'acceptor' in the energy transfer system, and emission spectrum of pure 9.7mM Fluor405, the 'donor", together with sample F0-1 are shown in Fig.5.1. After have been mixed with gold nanorods, the emission spectrum structure of the Fluor405 dye is found to be slightly changed,

which is still not thoroughly understood. This emission reshaping may origin from an environmental change of fluorophores when they are covalently bonded to gold particle surface, which has been found in semiconductor quantum dots-metal particle hybrid system.[38] We have compared the emission spectrum of Fluor405 mixed with multi-layer polymer coated gold particles, a similar spectrum structure as pure dye solution has been detected.

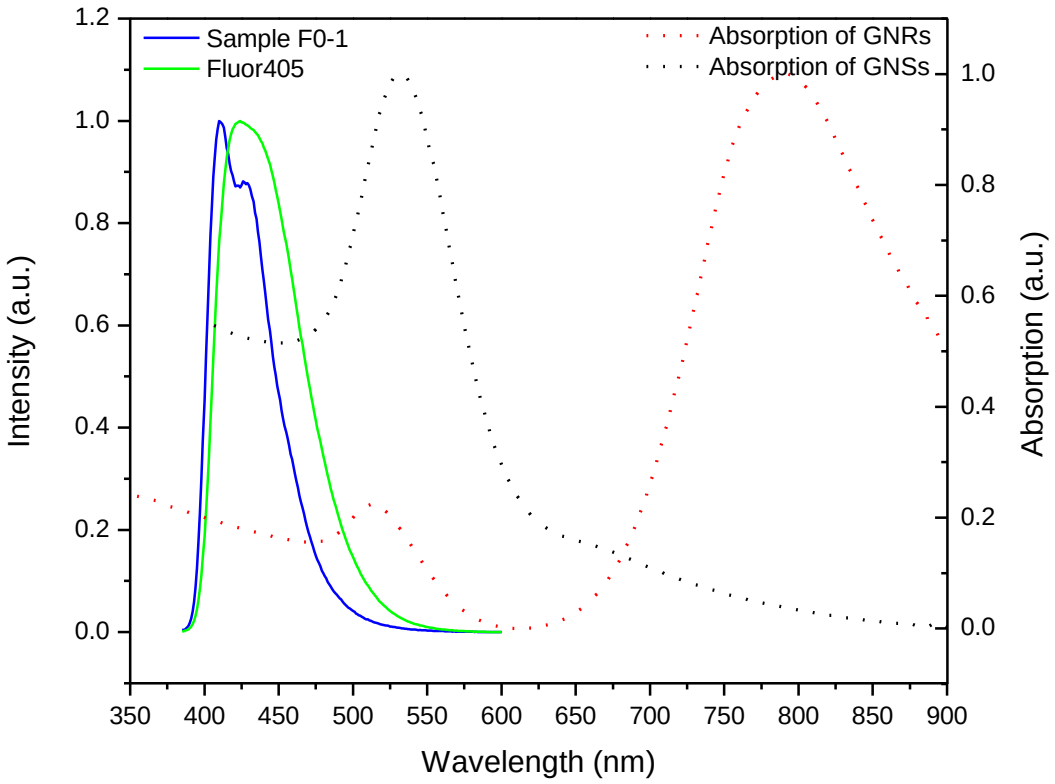

Fig.5.1 Emission spectrum of pure Fluor405 dyes and mixture solution with gold nanorods (solid lines); Absorption spectrum of gold nanorods (GNRs) and gold nanospheres (GNSs) (dotted lines). All spectra have been normalized for comparison purpose.

The single-photon excited fluorescence lifetime of the mixture solution and Fluor405 dyes can be seen in Fig.5.2. The y-axis stands for photon counts, or luminescence intensity, in arbitrary unit, and the x-axis shows time in ns. All samples were excited by 374nm laser, and emission light was collected with a longpass 405nm filter. The decay times of mixture solutions are found to be decreased compared to that of pure reference dye solution. After fitting all decay curves with multi-exponential model (see Chapter 1-1.2.1 for details),

$$I = I_0 \sum_{i=1}^{n} B_i \exp(-t/T_i) \tag{5.1}$$

the difference between samples can be demonstrated in a quantitative manner. In this case, for F0-1 and F0-2 n=3, and for F405 n=2. The fitting results can be found in Table.5.1.

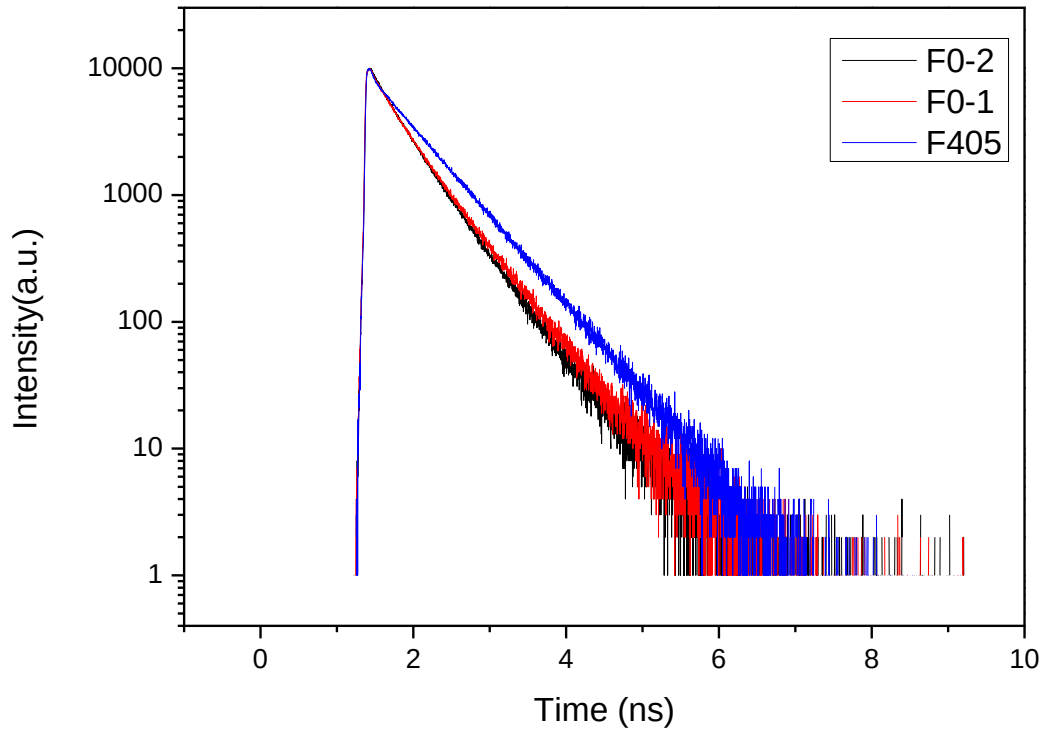

Fig.5.2 Single photon excitation fluorescence decay curves of Fluor405 dyes, sample F0-1 to F0-2.

	B1	B2	B3	T1	T2	T3	Chi-square
F0-1	23.2%	2.64%	74.16%	1.57±0.06ns	0.27±0.02ns	3.26±0.08ns	1.11
F0-2	32.5%	3.25%	64.25%	1.84±0.09ns	0.38±0.02ns	3.15±0.01ns	1.02
F405 control	4.76%	95.24%	N/A	0.27±0.05ns	3.60±0.03ns	N/A	1.03

Table5.1 Fitting results of mixture solution and pure Fluor405 dye under single photon excitation. A multi-exponential decay model described as equ.5. 1 was applied. For F0-1 and F0-2 n=3 and for F405 control n=2.

For the two-photon excitation lifetime measurement, all mixture solutions were placed in an imaging chamber and excited by a chameleon pulse laser operated at 810nm. The emission light was collected through a 390-465nm bandpass filter and the decay time was measured with B&H FLIM module operating at 'single' mode, which is used for classic lifetime measurement. The curve 'Prompt' is the decay curve from gold nanorods solution. The decay curve of Sample F0-1 is shown in Fig.3, denoted with 'Decay'. The oscillation in the decay curve, which was more apparent in the decay curves from pure gold nanorods solution, is believed due to the influence from luminescence of gold nanorods. Here we use signal from gold nanorods as prompt to fit decay curves to get reasonable results, as the lifetime of two-photon luminescence from gold nanorods is quite short (within the system response level, reported in early chapter as well and confirmed here in this system). As shown if Fig.5.3, the fitting curve overlaps quite well with experimental result. The detailed fitting results are shown in Table.5.2.

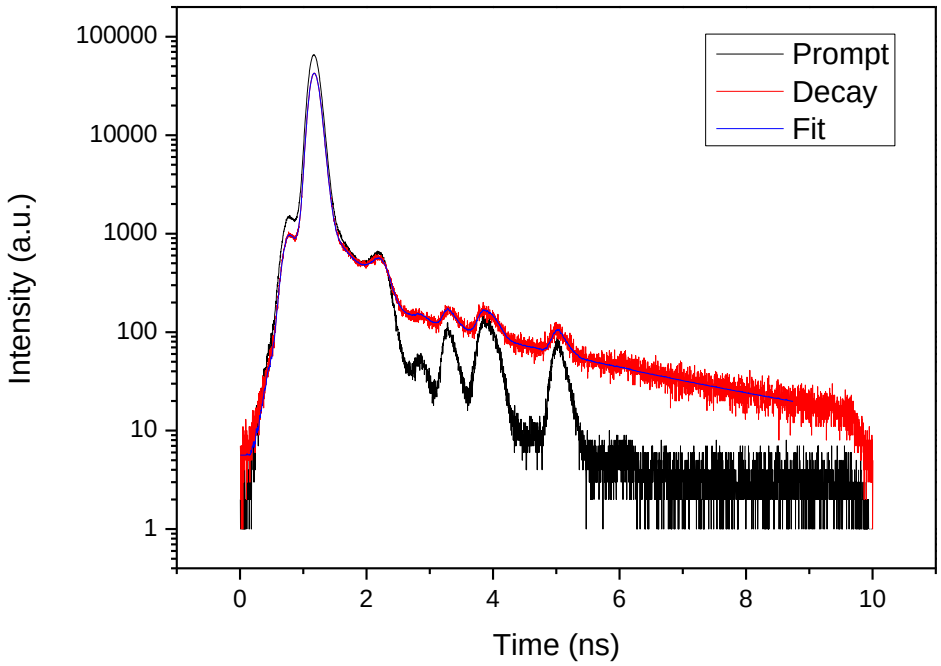

Fig.5.3 Decay curves of gold nanorods and Fluor405 mixture solution under two-photon excitation. Excited at 810nm, emission was collected with bandpass filter 390-465nm, sample F0-1.

	B1	B2	T1	T2	Chi-square
F0-1	4.88%	95.12%	2.81±0.02ns	0.0090±0.0002ns	1.09
F0-2	3.05%	96.94%	2.59±0.01ns	0.0062±0.0002ns	0.86
F405 control	100%	N/A	3.75±0.01ns	N/A	1.04

Table5.2 Fitting results of two-photon excitation data. A multi-exponential decay model described as equ.5. 1 was applied. For F0-1 and F0-2 n=2 and for F405 control n=1.

We have examined the interaction between gold nanoparticles and Fluor405 dyes in solution phase by monitoring the fluorescence lifetime change. The decay curves were fitted by equ.5.1, where n equals 2 for F0-1 and F0-2, 1 for F405 control. Comparison of decay times of different samples is shown in table 5.1 and table 5.2.. Under single photon excitation, decay time of F405 can be well fitted by a two-

exponential model, and the dominating long lifetime component is around 3.6ns. When mixed with gold nanorods, the longer component drops to 3.26 ns for sample F0-1 and 3.15ns for sample F0-2. Sample F0-1, which has a shorter distance between donor and acceptor than F0-2, is found to show less decrease in decay time. In the two-photon excitation experiments, the decay curves can be fitted by a two-exponential model, in which the shorter component is from gold nanorods and the longer one from Fluor405. Tabel.5.2 shows a more significant decrease in lifetime (from 3.85ns down to around 2.8 and 2.6ns), which may suggest an enhanced energy transfer process under two-photon excitation. Similar to what observed from hybrid system of DAPI and gold nanorods, this two-photon induced enhancement effect cannot be explained by Förster resonance energy transfer or surface energy transfer model, because both theories do not consider the effect from excitation conditions. It has been revealed that in the vicinity of metal particles or surfaces, the radiative dipole of donor fluorophores interacts with both the incidence and scattered electromagnetic field. Therefore we attribute the enhanced energy transfer under two-photon excitation to the effect arising from localized longitudinal surface plasmon oscillation, which resonates at the incidence wavelength and enhances the non-radiative energy transfer decay rate from the donor fluorophores to the nanoparticles.[39-42]

Moreover, no change in lifetime has been found in the mixture solution of gold nanospheres and Fluor405, no matter single or two-photon excitation， which is consistent with the result obtained from DAPI-gold nanorods system.

5.3.2 FLIM-FRET imaging: research on cell uptake mechanism of gold nanoparticles

The emission and absorption spectrum of GFP are shown in Fig.5.4, with emission peaking around 510nm and absorption around 488nm. Fig.5.5 (a) is a typical pseudo colour confocal image of Hela cells with earlyendosome labelled by GFP. The specimen was excited with 488nm Argon laser and the emission fluorescence was

collected with a long pass 505nm filter. Bright spots in the image are considered to be fluorescence from GFP. Fig.5.5 (b) shows the control sample where Hela cells were not treated with GFP and examined under the same imaging configuration as Fig.5.5 (a). Compared to labelled ones, no strong fluorescence signal but only weak cell self-emission can be seen in fig. 5.5 (b). In Fig.5.5 (c) and (d), the same region is examined under two-photon excitation. Fig.5.5 (c) is the TPL intensity image taken from the same sample as in Fig.5.5 (b) excited under 850nm femto-second laser and 500-550nm emission bandpass filter. Fig.5.5 (d) is the FLIM image of Fig.5.5 (c)，different colours in each image pixel varying from orange to blue demonstrate different fluorescence lifetimes ranging from 0 to 3ns. The fluorescence lifetime was obtained by fitting the experimental decay curves by a single exponential decay model, as shown in Fig.5.5 (e). Lifetime of GFP in cell culture is found to be around 2ns, as seen in the lifetime distribution in Fig.5.5 (f). This lifetime value is in consistent with published results.[43, 44] By comparing the images shown in Fig.5.5, we can confirm that Hela cells have been well stained by GFP. GFP emit strong and stable fluorescence under both single and two-photon excitation.

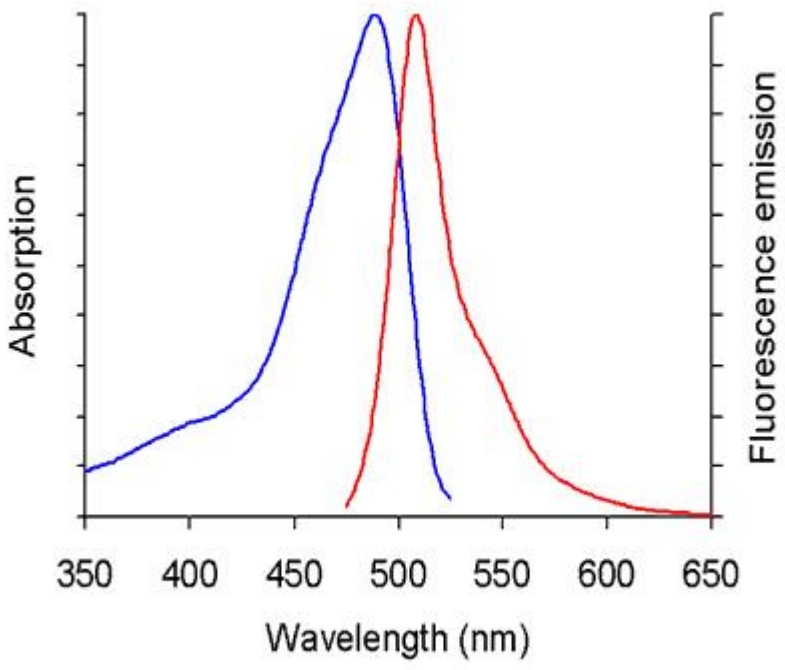

Fig.5.4 Absorption (blue solid line) and emission (red solid line) spectrum of GFP, from the manual book provided by Invitrogen.[45]

(a)

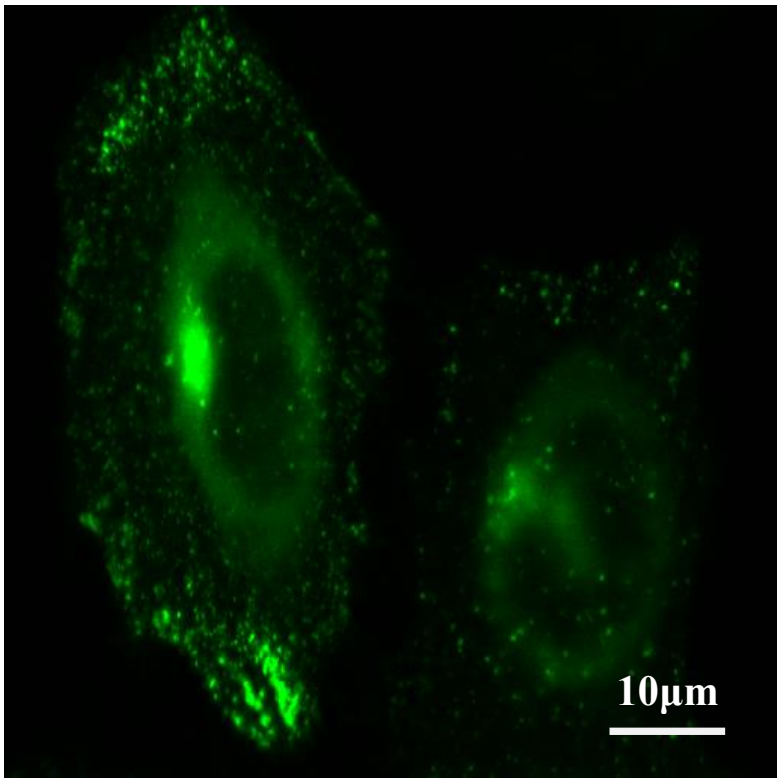

(b)

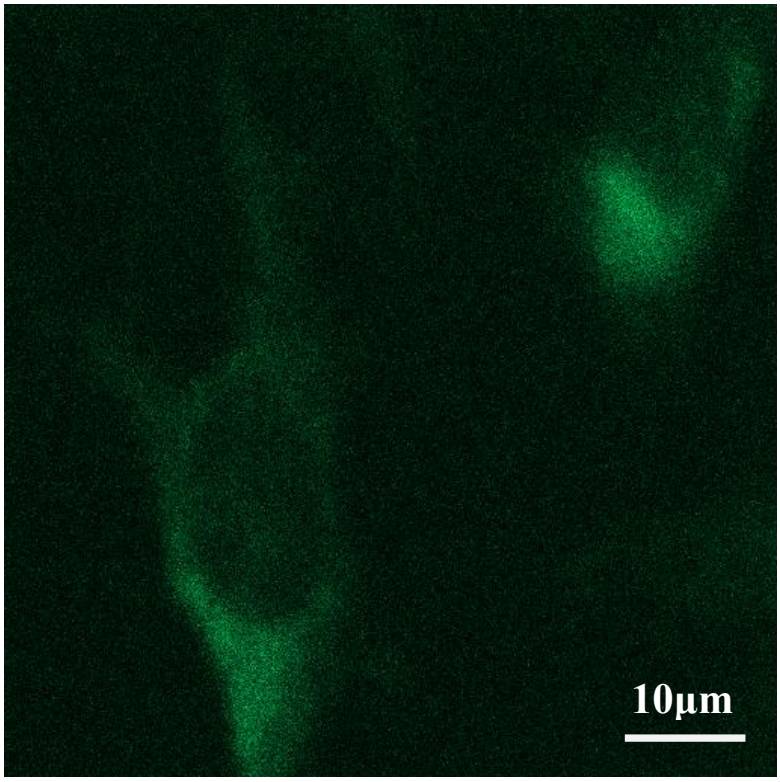

(c)

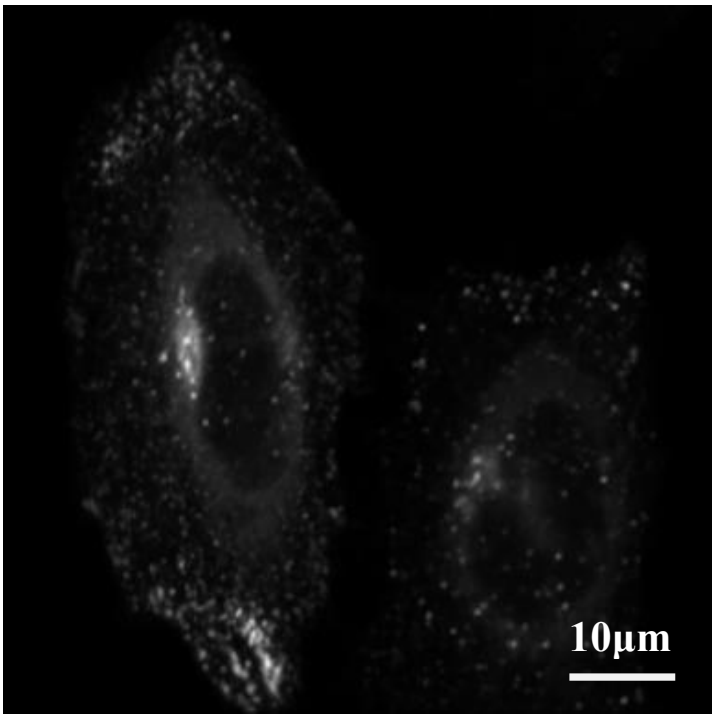

(d)

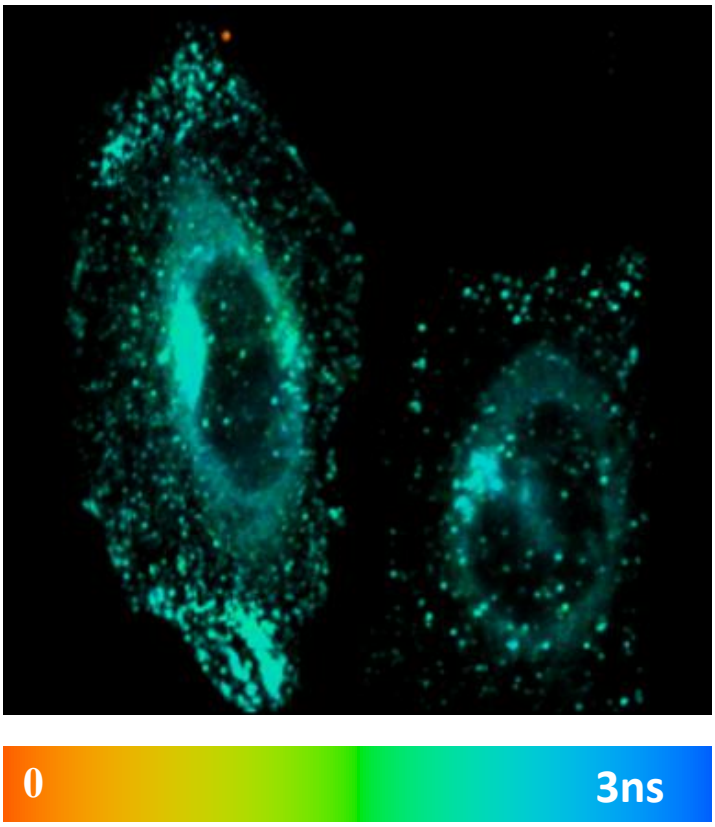

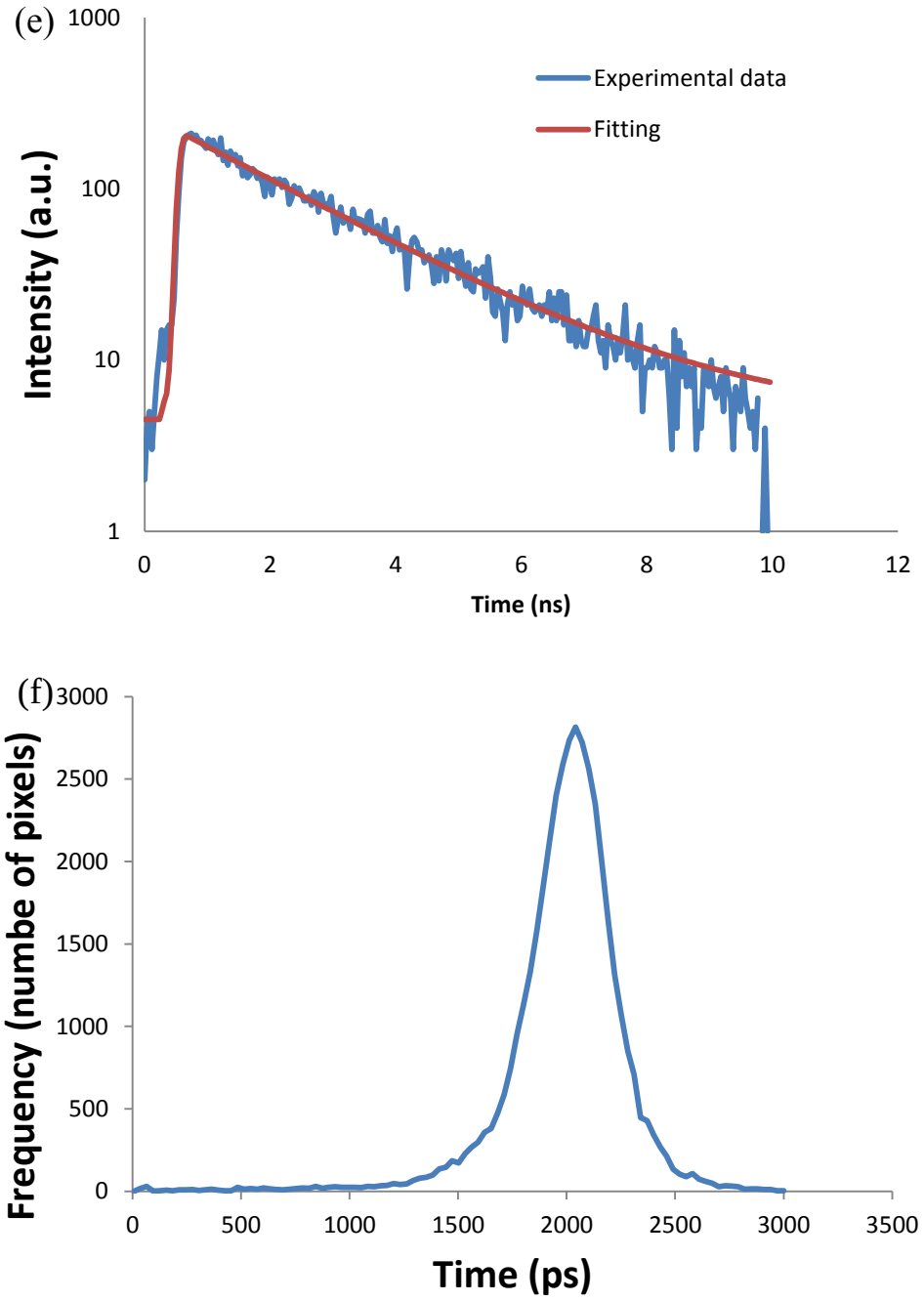

Fig.5.5 (a) Confocal fluorescence image of GFP stained Hela cells, excited under 488nm Argon laser, emission collected with longpass 505nm filter; (b) Hela cells without GFP labelling; (c), (d) Intensity and FLIM image of two-photon excited GFP stained Hela cells, excited under 850nm and emission collected with 500-550nm bandpass filter. For FLIM image, the lifetime ranges from 0 (orange) to 3ns (blue); (e) Typical decay curve of fluorescence from GFP in cell culture; (f) Distribution of fluorescence lifetimes displayed in (d).

To investigate the uptake process of gold nanorods by Hela cells, we have incubated the cell lines with gold nanorods at 5% volume concentration under 37℃ for different time periods, from 30 minutes to 1 hour. FLIM images are shown in Fig.5.6; from (a) to (c), the gold nanorods incubation time in Hela cells is 30minutes, 45 minutes, and 1 hour. All images have been fitted by a two-exponential model (equ.5.1, *n*=2)considering the luminescence from gold nanorods, and the coded colour represents the average lifetime

$$\tau_{ave} = \sum_i^n B_i T_i \qquad (5.2)$$

(descriptions of fitting model and average lifetime can be found in chapter 1 and 4). Due to the short decay time (in system response level) and strong luminescence of TPL from GNRs (contribution over 80%) in overlapping pixels where both emissions from GNRs and GFP were found, the average lifetime in these pixels is quite short, usually around several hundred pico seconds. Therefore brighter orange/yellow spots in cell region are considered to be signals from gold nanorods.

A few gold nanorods were found in cells after incubation of 30min and 45min, while significant amount of nanorods have been found in cells after 1 hr incubation, demonstrated by the increasing in number of the pixels displaying shorter lifetime luminescence. To investigate the influence of surface functionality of nanoparticle on cell uptaking, we treated Hela cells with multi-layer coated gold nanorods. The result of 4 layer coated nanorods with ending layer PDDAC is shown in Fig.5.6 (e). From the image result, a higher particle concentration internalized by Hela cells has been found, which may suggest polymer coated gold nanorods are easier to go through the cell membrane compared to CTAB capped ones. In contrast to intensity image, Fig.5.6 (d), which cannot clearly distinguish between luminescences from gold particles and GFP, FLIM provides a sensitive and convenient method for monitoring cell uptake process, with a potential for in vitro live cell monitoring.

(a)

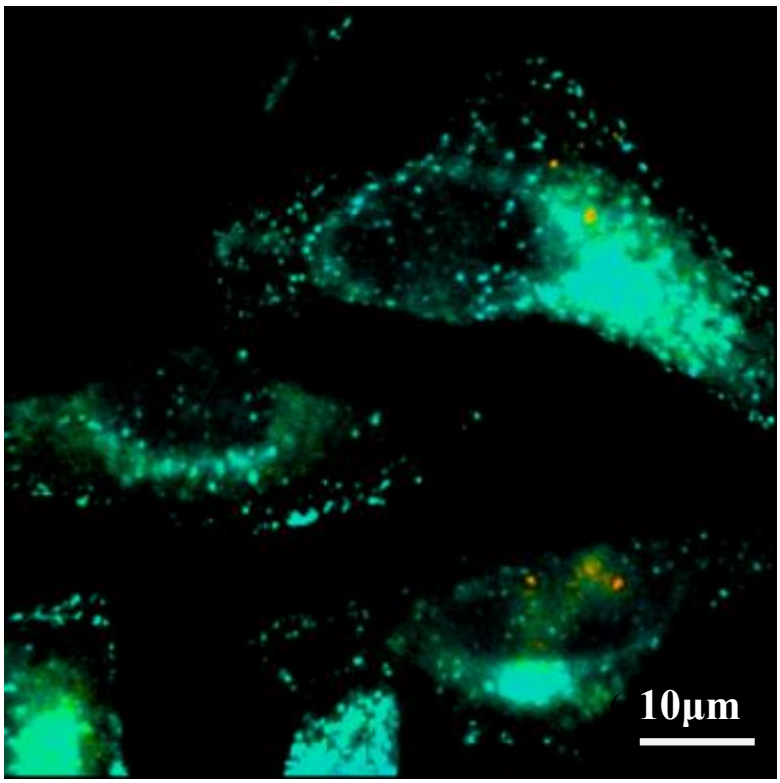

(b)

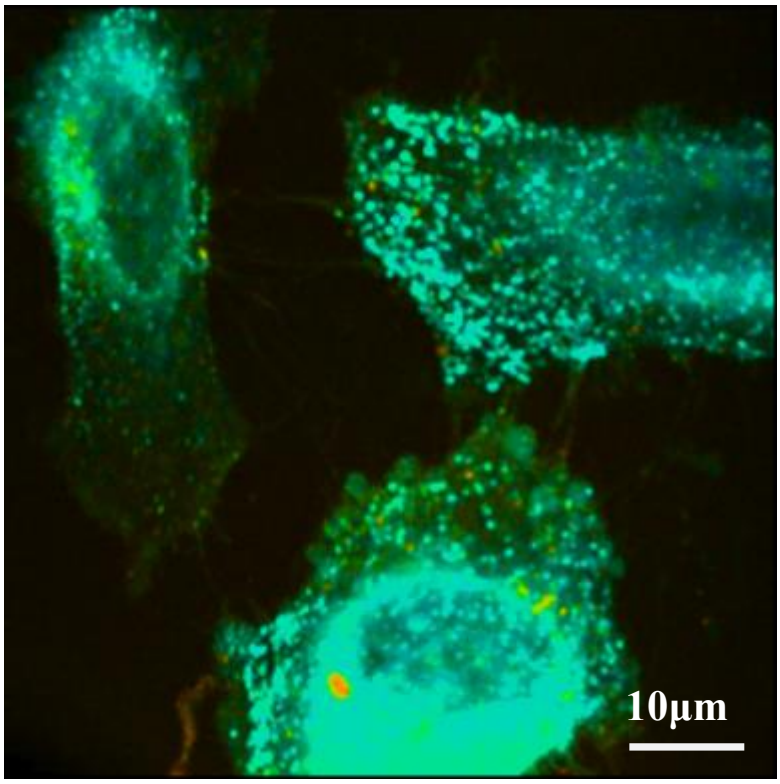

(c)

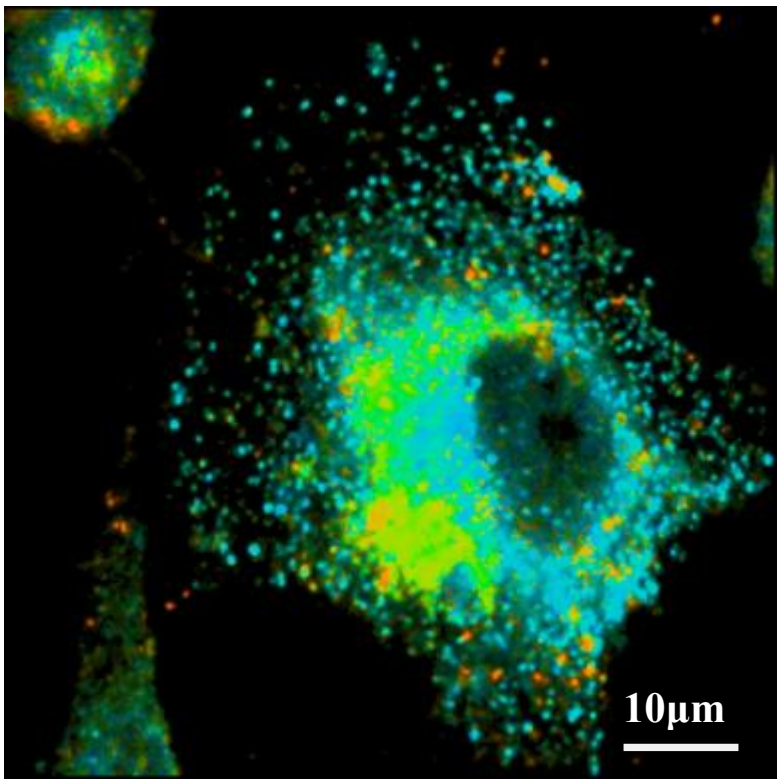

(d)

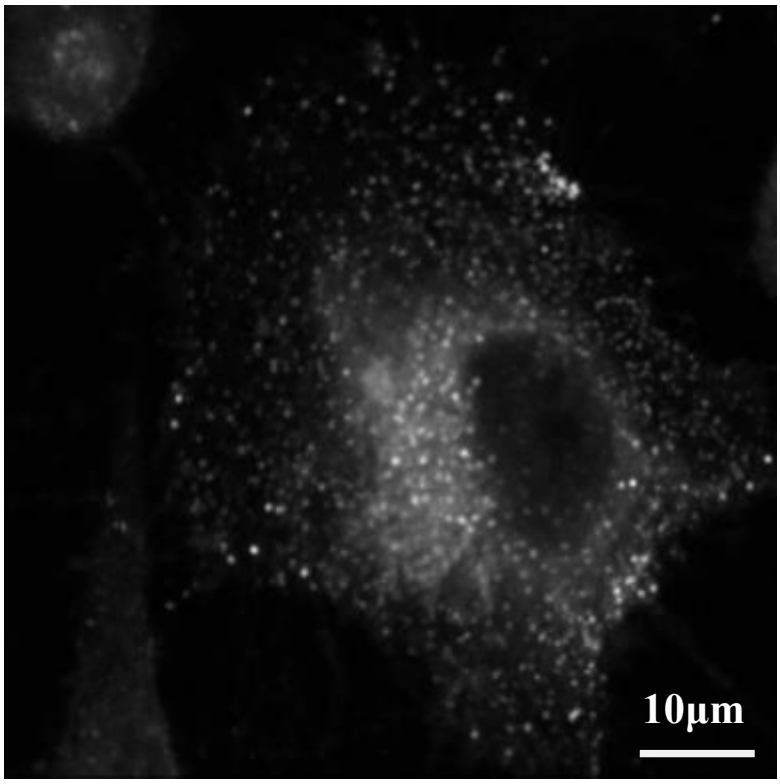

(e)

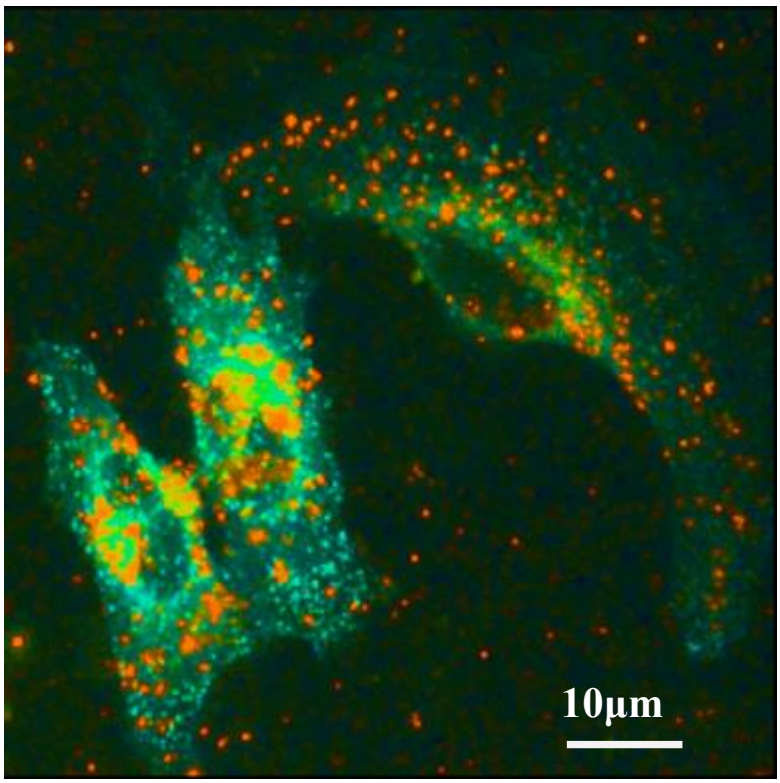

Fig.5.6 FLIM images of GFP-stained Hela cells incubated with CTAB capped gold nanorods for (a) 30 minutes, (b) 45 minutes, and (c) 1 hour; (d) intensity image of 1 hour sample; (e) incubated with multi-layer coated gold nanorods for 1 hour.

To study the interaction between gold particles and GFP labelled endosomes and in turn to confirm the endosome traffic pathway, a further analysis on FLIM results is essential. By examining the longer component, which is supposed to be the contribution from GFP at the overlapping areas, we can determine if there was energy transfer effect between GFP and gold nanoparticles when they were closer to each other. Short lifetimes of GFP (even down to around 1ns) do exist where gold nanorods were present, but as shown in Fig.5.5 (f), lifetime distribution of GFP in FLIM experiments ranges from 1.5ns to 2.5ns. To clarify whether the short lifetime is due to normal lifetime distribution or other mechanism, we used a statistical approach to compare the lifetime change. As shown in Fig.5.7, the longer component (lifetime of GFP) subtracted from 58 overlapping pixels in different FLIM images have been sorted in 100 ps interval from 1100 ps to 2400 ps. Compared to a symmetric lifetime distribution of GFP in Fig.5.5 (f), lifetime values of GFP in the

vicinity of gold nanorods form an asymmetric distribution, with a higher rate of shorter lifetime than the longer one and a long tail reaching 1.1ns , which suggests energy transfer process does exist between GFP and gold nanorods. Energy transfer only occurs when donor and acceptor fluorophores are in a near vicinity (within 8nm for Förster resonance energy transfer and double the distance for surface energy transfer), which indicates that gold nanorods are in a quite small separation with GFP, or GFP labelled earlyendosomes. This result can be an indirect proof showing that the cell uptake pathway of gold nanorods is probably through an endocytotic process. Furthermore, FLIM in combination with FRET can be a sensitive, high resolution and convenient way to study the cell uptake and intra cellular tracking of nanoparticles combining with fluorescent protein labeling techniques.

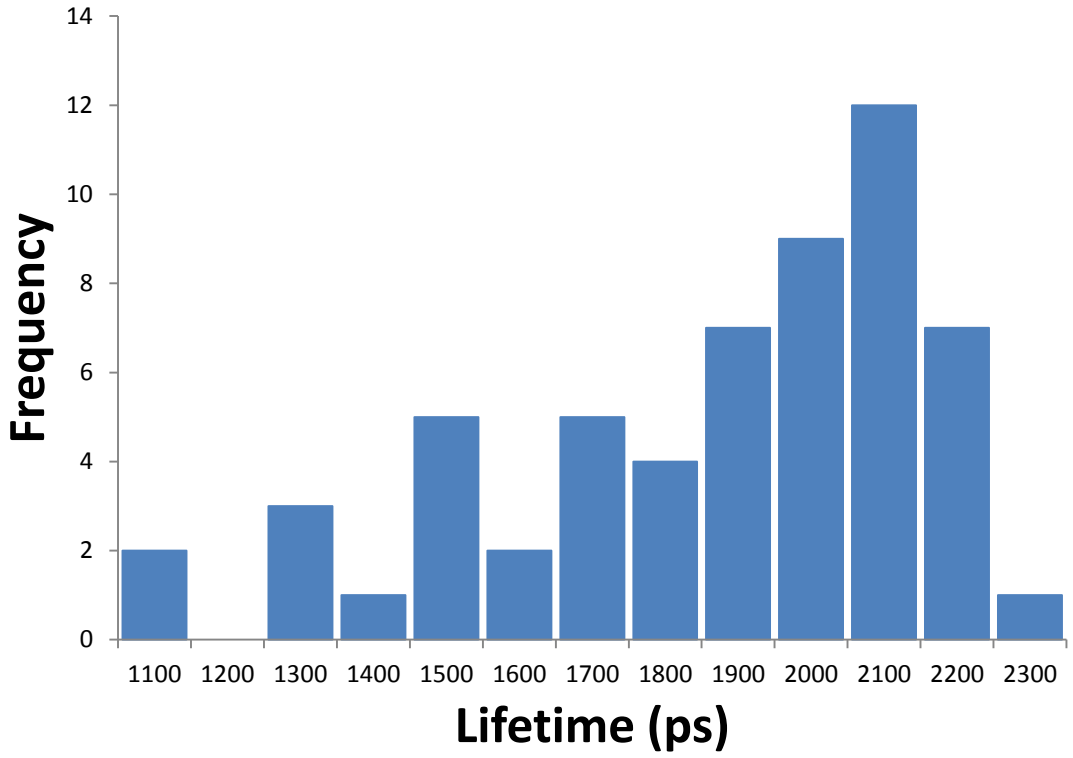

Fig.5.7 Lifetime distribution of GFP in overlapping areas.

5.4 Conclusion

In this chapter, we first investigated the influence of excitation conditions on the energy transfer process in fluorophores-gold nanoparticle hybrid systems. When mixing Fluor 405 dye with gold nanorods, an enhanced energy transfer has been detected under two-photon excitation, where the incidence excitation frequency resonates with the longitudinal surface plasmon band of gold nanorods and enhances the non-radiative energy transfer rate from donor to acceptor particles. Then the FLIM-FRET method has been used to study the intracellular pathways of gold nanorods. By staining the earlyendosomes of Hela cells with GFP, and monitoring the lifetime change of the fluorescent protein using FLIM, we have indirectly confirmed that the uptake of gold nanorods into cells is through an endocytic process. Moreover FLIM-FRET combined with gold nanoparticles can be a highly sensitive technique for in *vivo* and in *vitro* biological research.

References

[1] S. Eustis, M. A. El-Sayed, “Why gold nanoparticles are more precious than pretty gold: Noble metal surface plasmon resonance and its enhancement of the radiative and nonradiative properties of nanocrystals of different shapes”, Chem. Soc. Rev. 2006, 35, 209-217

[2] M. B. Mohamed, V. Volkov, S. Link, M. A. El-Sayed, “The 'lightning' gold nanorods: fluorescence enhancement of over a million compared to the gold metal”, Chem. Phys. Lett. 2000, 317, 517-523

[3] O. Kulakovich, N. Strekal, A. Yaroshevich, S. Maskevich, S. Gaponenko, I. Nabiev, U. Woggon, M. Artemyev, “Enhanced luminescence of CdSe quantum dots on gold colloids”, Nano Lett. 2002, 2, 1449-1452

[4] F. Tam, G. P. Goodrich, B. R. Johnson, N. J. Halas, “Plasmonic enhancement of molecular fluorescence”, Nano Lett. 2007, 7, 496-501

[5] B. Dubertret, M. Calame, A. J. Libchaber, “Single-mismatch detection using gold-quenched fluorescent oligonucleotides”, Nat. Biotechnol. 2001, 19, 365-370

[6] J. R. Lakowicz, “Radiative decay engineering 5: metal-enhanced fluorescence and plasmon emission”, Anal. Biochem. 2005, 337, 171-194

[7] E. Dulkeith, A. C. Morteani, T. Niedereichholz, T. A. Klar, J. Feldmann, S. A. Levi, F. C. J. M. van Veggel, D. N. Reinhoudt, M. Moller, D. I. Gittins, “Fluorescence quenching of dye molecules near gold nanoparticles: Radiative and nonradiative effects”, Phys. Rev. Lett. 2002, 89, 203002

[8] C. Sonnichsen, B. M. Reihard, J. Liphardt, A. P. Alivisatos, “Molecular ruler based on plasmon coupling of single gold and silver nanoparticles”, Nat. Biotechnol. 2005, 23, 741-745

[9] R. Sardar, A. M. Funston, P. Mulvaney, R. W. Murray, “Gold Nanoparticles: Past, Present, and Future”, Langmuir, 2009, 25, 13840-13851

[10] C. H. Fan, S. Wang, J. W. Hong, G.C. Bazan, K. W. Plaxco, A. J. Heeger, Beyond superquenching: “Hyper-efficient energy transfer from conjugated polymers to gold nanoparticles”, Proc. Natl. Acad. Sci. USA 2003, 100, 6297-

6301

[11] X. H. Huang, S. Neretina, M. A. El-Sayed, “Gold Nanorods: From Synthesis and Properties to Biological and Biomedical Applications”, Adv. Mater. 2009, 21, 4880-4910

[12] E. Oh, M. Y. Hong, D. Lee, S. H. Nam, H. C. Yoon, H. S. Kim, “Inhibition assay of biomolecules based on fluorescence resonance energy transfer (FRET) between quantum dots and gold nanoparticles”, J. Am. Chem. Soc. 2005, 127, 3270-3271

[13] A. M. Coto-Garcia, E. Sotelo-Gonzalez, M. Fernadez-Arguelles, R. Pereiro, J. M. Costa-Fernadez, A. Sanz-Medel, “Nanoparticles as fluorescent labels for optical imaging and sensing in genomics and proteomics”, Anal. Bioanal. Chem. 2011, 399, 29-42

[14] E. Hutter, D. Maysinger, “Gold Nanoparticles and Quantum Dots for Bioimaging”, Micros. Res. Techniq. 2011, 74, 592-604

[15] M. C. Daniel, D. Astruc, “Gold nanoparticles: Assembly, supramolecular chemistry, quantum-size-related properties, and applications toward biology, catalysis, and nanotechnology”, Chem. Rev. 2004, 104, 293-346

[16] A. J. Haes, R. P. Van Duyne, “A nanoscale optical biosensor: Sensitivity and selectivity of an approach based on the localized surface plasmon resonance spectroscopy of triangular silver nanoparticles”, J. Am. Chem. Soc. 2002, 124, 10596-10604

[17] P. K. Jain, X. H. Huang, I. H. El-Sayed, M. A. El-Sayed, “Noble Metals on the Nanoscale: Optical and Photothermal Properties and Some Applications in Imaging, Sensing, Biology, and Medicine”, Accounts Chem. Res. 2008, 41, 1578-1586

[18] T. Pons, I. L. Medintz, K. E. Sapsford, S. Higashiya, A. F. Grimes, D. S. English, H. Mattoussi, “On the quenching of semiconductor quantum dot photoluminescence by proximal gold nanoparticles”, Nano Lett. 2007, 7, 3157-3164

[19] T. L. Jennings, M. P. Singh, G. F. Strouse, “Fluorescent lifetime quenching near d=1.5 nm gold nanoparticles: Probing NSET validity”, J. Am. Chem. Soc. 2006, 128, 5462-5467

[20] T. Sen, S. Sadhu, A. Patra, “Surface energy transfer from rhodamine 6G to gold nanoparticles: A spectroscopic ruler”, Appl. Phys. Lett. 2007, 91, 043104

[21] A. E. Nel, L. Mädler, F. Velegol, T. Xia, E. M. V. Hoek, P. Somasundaran, F. Klaessig, V. Castranova, M. Thompson, “Understanding biophysicochemical interactions at the nano-bio interface”, Nat. Mater. 2009, 8, 543-557

[22] S. J. H. Soenen, M. D eCuyper, “Assessing iron oxide nanoparticle toxicity in vitro: current status and future prospects”, Nanomedicine, 2010, 5, 1261

[23] S. D. Conner, S. L. Schmid, “Regulated portals of entry into the cell”, Nature, 2003, 422 , 37-44

[24] M. E. Akerman, W. C. Chan, P. Laakkonen, S. N. Bhatia, E. Ruoslahti, “Biological Sciences - Applied Biological Sciences”, Proc. Natl. Acad. Sci. USA 2002, 99 , 12617

[25] J. Davda, V. Labhasetwar, “Characterization of nanoparticle uptake by endothelial cells”, Int. J. Pharm. 2002, 233 , 51-59

[26] T. Kato , T. Yashiro , Y. Murata , D. C. Herbert , K. Oshikawa, M. Bando, S. Ohn , Y. Sugiyama, “Evidence that exogenous substances can be phagocytized by alveolar epithelial cells and transported into blood capillaries”, Cell Tissue Res. 2003, 311 ,47-51

[27] A. T. Florence, N. Hussain, “Transcytosis of nanoparticle and dendrimer delivery systems: evolving vistas”, Adv. Drug Deliv. Rev. 2001, 50 , S69-S89

[28] F. Zhao, Y. Zhao, Y, Liu, X. Chang, C. Chen, Y. Zhao, “Cellular Uptake, Intracellular Trafficking, and Cytotoxicity of Nanomaterials”, Small, 2011, 7, 1322-1337

[29] A. Verma, F. Stellacci, “Effect of Surface Properties on Nanoparticle–Cell Interactions”, Small, 2010, 6 , 12-21

[30] Z. Liu, W. Cai, L. He, N. Nakayama, K. Chen, X. Sun, X. Chen, H. Dai, “In vivo biodistribution and highly efficient tumour targeting of carbon nanotubes in mice”, Nat. Nanotechnol. 2007, 2 , 47-52

[31] V. Mailänder, K. Landfester, “Interaction of Nanoparticles with Cells”, Biomacromolecules, 2009, 10, 2379-2400

[32] W. Jiang, B. Y. S. Kim, J. T. Rutka, W. C. W. Chan, “Nanoparticle-mediated cellular response is size-dependent”, Nat. Nanotechnol., 2008, 3 , 145

[33] B. D. Chithrani, W. C. W. Chan, “Elucidating the Mechanism of Cellular Uptake and Removal of Protein-Coated Gold Nanoparticles of Different Sizes and Shapes”, Nano Lett. 2007, 7 , 1542-1550

[34] S. J. H. Soenen , U. Himmelreich , N. Nuytten , T. R. Pisanic II, A. Ferrari, M. De Cuyper, “Intracellular Nanoparticle Coating Stability Determines Nanoparticle Diagnostics Efficacy and Cell Functionality”, Small, 2010, 6 , 2136-2145

[35] C. J. Orendorff, C. J. Murphy, “Quantitation of Metal Content in the Silver-Assisted Growth of Gold Nanorods”, J. Phys. Chem. B 2006, 110, 3990-3994

[36] N. Sui, V. Monnier, Y. Zakharko, Y. Chevolot, S. Alekseev, J. Bluet, V. Lysenk, E. Souteyrand,“Plasmon-controlled narrower and blue-shifted fluorescence emission in (Au@SiO2)SiC nanoh ybrids”, J. Nanopart. Res. 2012, 14, 1004

[37] D. Ratchford, F. Shafiei, S. Kim, S. K. Gray, X. Li, “Manipulating Coupling between a Single Semiconductor Quantum Dot and Single Gold Nanoparticle”, Nano Lett. 2011, 11, 1049-1054

[38] K.T. Shimizu, W. K. Woo, B. R. Fisher, H. J. Eisler, M.G. Bawendi, “Surface-Enhanced Emission from Single Semiconductor Nanocrystals”, Phys. Rev. Lett. 2002, 89, 117401

[39] R. Chance, A. Prock, R. Silbey, “Lifetime of an emitting molecule near a partially reflecting surface”, J. Chem. Phys. 1974, 60, 2744-2748

[40] J. Gersten, A. J. Nitzan, “Electromagnetic theory of enhanced Raman scattering by molecules adsorbed on rough surfaces”, Chem. Phys. 1980, 73 (7), 3023–3037

[41] K. Suhling, D. M. Davis, D. Phillips, J. Siegel, S. E. D. Webb, P. M. W. French, S. Lévěque-Fort, “Biomedical Topical Meeting, Miami Beach”, Florida, April 7, 2002

[42] B. Treanor, P. M. Lanigan, K. Suhling, T. Schreiber, I. Munro, M. A. Neil, D. Phillips, D. M. Davis, P. M. French, “Imaging fluorescence lifetime heterogeneity applied to GFP-tagged MHC protein at an immunological synapse”, J. Microsc. 2005, 217, 36-43

[43] Manual book for CellLight® Reagents *BacMam 2.0*, 2012, 3

Chapter 6

Effect of Size, Shape and Surface Modification on Cytotoxicity of Gold Nanoparticles to Human HEp-2 and Canine MDCK Cells

6.1 Introduction

Gold nanoparticles have been demonstrated to have extraordinary potential in bio-medical applications including biological imaging and sensing, drug and gene delivery, and thermal therapy.[1-11] Compared to gold nanospheres (GNSs), gold nanorods (GNRs) hold greater potential, especially in biological imaging and sensing due to their unique optical properties.[12-14] Cytotoxicity of gold nanoparticles, as the premise of any further biological study, is a key issue to be investigated. There have been intensive studies from different point of views focusing on the cytotoxicity of gold nanoparticles, which are complex and still under debating. Compared to GNSs, GNRs have been found to be toxic to cell culture, but almost non-toxic after coated with polymer molecules.[10, 15-27] This is because the cytotoxicity depends on the particle size, shape, surface charge and modification, agglomeration, as well as the mechanisms of cellular uptake and toxicity response.[28-30] Despite difference in particle shape, one primary concern about GNRs in biological research is cetyltrimethylammonium bromide (CTAB), the surfactant which is essential for nanorod growth in popularly used seed-growth GNRs synthesis method, but toxic to cell lines.[26, 31-33] CTAB is important in controlling the particle size and shape to achieve designed localized surface plasmon resonance bands for spectroscopic and microscopic applications in biological research.[34-36] As removal of CTAB will cause instability of GNRs, polymers, such as poly(acrylic acid) (PAA), and poly(diallyldimethylammonium chloride)-poly(4-styrenesulfonic acid) (PDADMAC-

PSS), and poly(ethyleneglycol) (PEG) et al, have been introduced to functionalize the GNRs surface.[31, 32, 37, 38]

Optical properties of gold nanoparticles critically depend on their size, shape and surface conditions. On the other hand, incubation time and particle concentration are key parameters in controlling the internalization process of nanoparticles into cells, as well as cell normal functions. This chapter presents a systematic investigation on the cytotoxicity of gold nanoparticles. GNRs synthesized via the same procedure but with 4 different aspect ratios, GNSs and polymer (polystryrenesulfonate (PSS) and poly (allylamine) hydrochloride (PAH)) coated GNRs have been applied to two cell lines with different exposure time and particle dosages. GNRs of aspect ratio of 3 are approximately 40nm long, which had excellent potential in biological imaging and sensing applications.[39-41] PSS and PAH have been used in multilayer membrane for long-term graft transplantation.[42] The layer-by-layer polyelectrolyte coating using PSS/PAH not only changes the surface condition of gold particles inducing changes in particle optical properties, but also plays important roles in functionalizing new types of bioimaging tools, such as SPASER (surface plasmon amplification by stimulated emission of radiation), a surface plasmon based nanolaser providing localized intensive excitation.[43-45] The dosage levels and incubation time selected for 3-(4,5-Dimethylthiazol-2-yl)-2,5-diphenyltetrazolium bromide MTT assay analysis was based on the previous imaging study.[39, 41] In addition to reveal the intrinsic cytotoxicity of gold nanoparticles, this study also provide insights on managing the cytotoxicity of gold nanoparticles in further biological research.

In this chapter, the cytotoxicity of gold nanoparticles will be studied by MTT and microscopy methods, effects from particle size, shape, surfactants, incubation time and dosage as well as the toxicity mechanism will all be examined.

6.2 Experimental Methods

GNRs were synthesized by the seeded growth method [46] and GNSs were prepared by Turkevich method. [47] Further coating on GNRs was proceeded via electrostatic layer-by-layer growth using PSS and PAH. Single layer of PSS and double layers of PSS/PAH coating were carried out following a process described by Omura et al. (denoted as PSS-GNRs and PAH-PSS-GNRs).[45] As the surface plasmon band of GNRs critically depends on the environmental refractive index, polymer coating onto particle surface will cause a significant change in absorption spectrum peak position, as shown in Fig.6.1 (a). All particles were centrifuged to remove the excess CTAB/polymers and re-dispersed in deionised water with a final concentration around 10^{-10}M.

MDCK (ATCC CCL-34 ^{TM}) and HEp-2 (ATCC CCL-23) cell-lines were obtained from American Type Culture Collection. Cell culture medium was high-glucose (4.5 g/l) DMEM containing foetal calf serum (10%), L-glutamine (2.9mg/mL), antibiotic-antimycotic solution (GIBCO). Cells were routinely cultured at 37^{o}C under 5% CO_2.

MTT assay was carried out in the following procedure. Briefly, both MDCK and HEp-2 cells were seeded at 1 x 10^4 cells per well in 96-well plates. After 24 hrs of incubation (37^{o}C, 5% CO_2), a series of concentrations of GNRs (in water) was added in each well. The cells were further incubated to appropriate time intervals. At appropriate time intervals, 20 μl of MTT (3-(4,5-Dimethylthiazol-2-yl)-2,5-diphenyltetrazolium bromide, 4 mg/ml in PBS) was added to each well and incubated for up to 4 hrs at 37^{o}C, 5% CO_2. After careful removal of the media, 150 μl of DMSO was added into each well to solubilise the purple crystals. After being incubated at 37^{o}C for 10 min, optical density at 540nm (OD_{540nm}) was measured with a plate reader (LabSystems Genesis). The MTT will mark only live cells and give absorption at 540nm, therefore, value of $OD540_{nm}$ can be seen as a degree of cell survival after have been treated with toxic substance, or the "cell viability".

For fluorescent microscopic observation of apoptosis, cells were seeded onto cover slides at 1 x 10^5 cells per slide in 24-well plates and cultured for 24 h at 37^{o}C under 5% CO_2. After exposure to GNRs for 5 hrs, the spent medium was discarded and cells were incubated for 1 hr in fresh media containing sulforhodaminyl-L-

valylalanylaspartyl fluoromethyl ketone (SR-VA-DFMK) according to manufacturer's instructions (Immunochemistry Technologies). Cells were washed with PBS, and fixed with 3.7% paraformaldehyde (in PBS) for 10 min at 37℃. The coverslips were mounted onto microscope slides with Prolong Gold antifade reagent containing 4',6'-diamidino-2-phenylindole (DAPI) (Invitrogen). Images were captured using a confocal microscope LSM 510 (Carl Zeiss).

6.3 Results and Discussion

6.3.1 Characterization of gold nanoparticles

Fig. 6.1(a) displays absorption spectra taken from GNRs, PSS-GNRs and PAH-PSS-GNRs. Absorption of three GNRs of different aspect ratios, 3(GNRs-1), 4.5(GNRs-2) and 5(GNRs-3), are shown in Fig.6.1(b), where a typical SEM image of GNR-1 is displayed in Fig.6.1(c). Fig.6.2 shows the MTT assay results on HEp-2 cells incubated for 1 hr with different types of gold nanoparticles. The dosage is calculated as the volume percentage of cell medium, for gold particles, concentration of 1% is approximately 10^{-12}M. Contribution in absorption from gold nanoparticles in MTT assay has been subtracted taking account the absorption coefficient of different gold nanoparticles at 540nm and number of nanoparticles in cell culture.

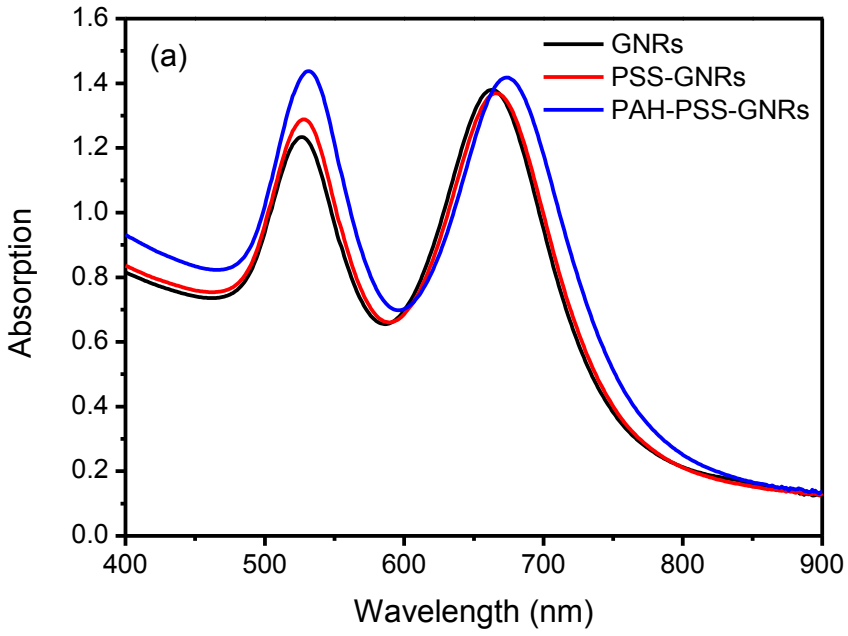

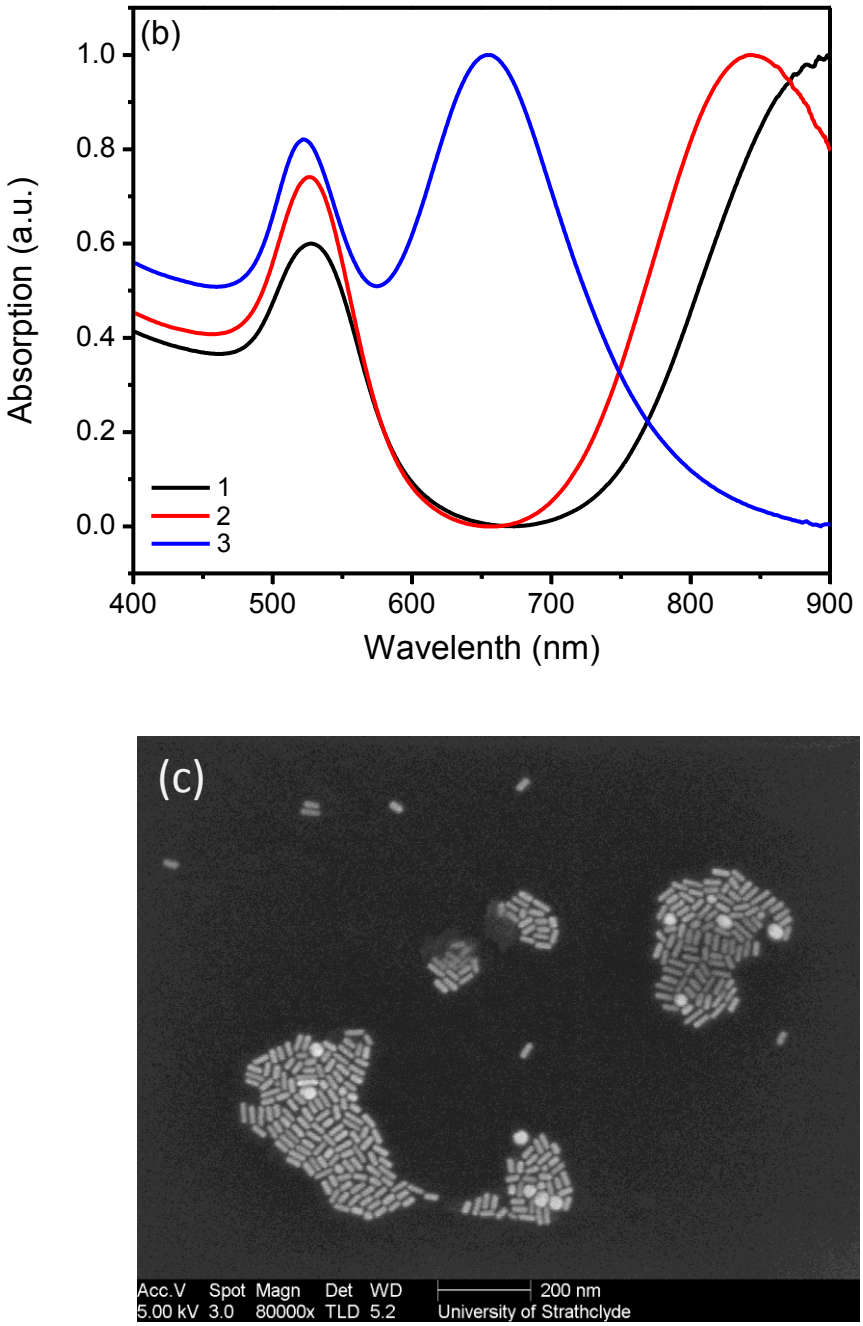

Fig.6.1**.** (a) Absorption spectrum of GNRs and polymer coated GNRs; (b) Absorption spectrum of GNR-1 (black), GNR-2 (red), and GNR-3 (blue); (c) Scanning electron microscopic image of GNR-1.

6.3.2 Cytotoxicity of different gold nanoparticles

Based on results displayed in Fig.6.2, cytotoxicity of different samples can be compared, where higher value of cell viability indicates higher number of cell survival, or lower cytotoxicity. GNRs have shown much higher toxicity compared to GNSs. The (Citrate stabilized) GNSs showed no significant cytotoxicity under all dosage levels used, while for CTAB capped GNRs, high cytotoxicity was found especially at large dosages. It cannot be simply explained as shape effect, as GNSs and GNRs have different surfactants and surface charge states. To elucidate the effects from capped CTAB, polymer coated GNRs have been compared with CTAB capped GNRs. Fig.6.2 shows that both PSS-GNRs and PAH-PSS-GNRs are less toxic than GNRs, which becomes more apparent at higher dosages.

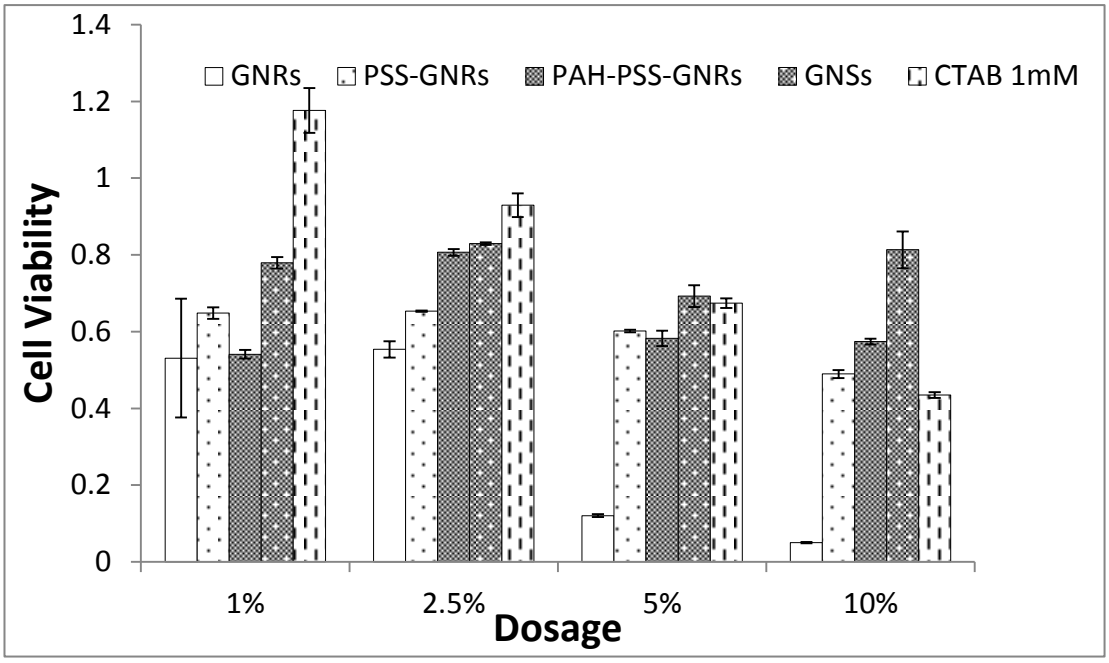

Fig.6.2**.** Cytotoxicity of different types of gold particles and free CTAB based on MTT assay outlined above.

6.3.3 Effect of CTAB

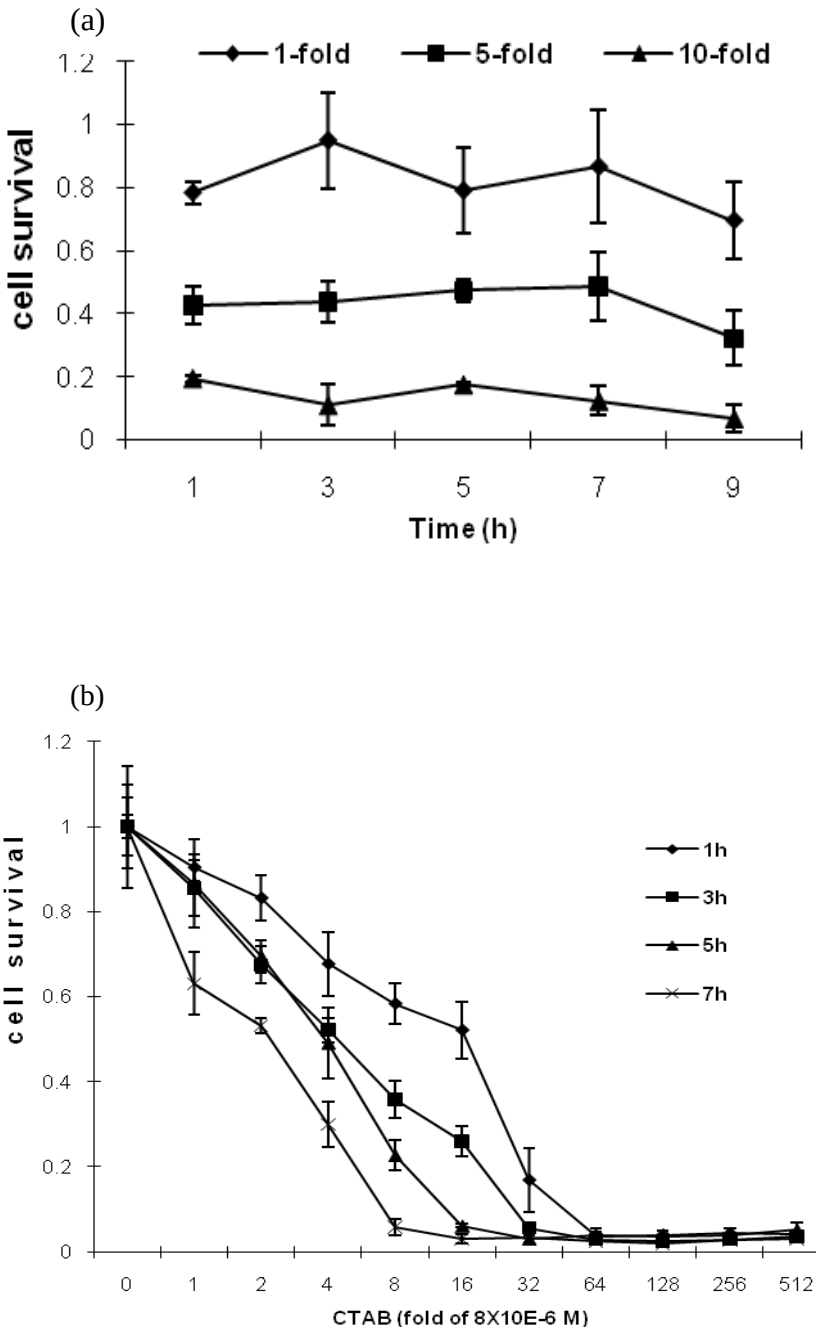

Fig.6.3 Time lapse cytotoxicity of GNRs (a) and free CTAB (b) to HEp-2, 1h, 3h, 5h and 7h indicate different incubation times and 1 fold of $8x10^{-6}$M CTAB is comparable to the 1% concentration in the form of volume concentration in Fig.6.2.

Experiments and data processing in section 6.3.3, 6.3.5 and sample preparation in section 6.3.6 were performed by our collaborators, Ms Dan Xu and Dr. Jun Yu. The above observation is in line with the previous finding that CTAB is the major reason for cytotoxicity.[31, 32] Nevertheless, the cause of the cytotoxicity, either the free CTAB in solution or surfactant ones, is still debatable. To bring insights into this issue, toxicity of free CTAB to Hep2 was examined. Fig.6.2 shows that free CTAB solution is less toxic than CTAB capped GNRs. We thus propose that the toxicity of GNRs is mainly related to the surface CTAB on GNRs rather than free form in the solution based on three facts. Firstly, as polymer-coated GNRs were centrifuged under the same condition as GNRs, concentration of free CTAB in the solution can be considered at a similar level. Therefore the different cytotoxic properties should be originated from different surface conditions. Secondly, 1mM of CTAB used here is 1% of the concentration used for GNRs synthesis and considered to be the upper limit of remaining CTAB in GNRs solution after centrifuge. This is because GNRs solution was diluted roughly 10 times after each centrifugation and concentration of free CTAB is below 1/100 of the original concentration after two times of centrifugations. Fig.6.2 shows that 1mM CTAB has only moderate cytotoxicity, much lower than GNRs, implying that toxicity of GNRs is not mainly due to free CTAB. This result is consistent with that of the time-lapse toxicity shown in Fig.6.3 (b), as cell survival of samples treated with 1mM CTAB solution from 1% to 10% of medium volume (actual concentration $1x10^{-5}$ M to $1x10^{-4}$M) decreased from more than 90% to around 60%. At last, time-lapse toxicity study reveals different cytotoxic behaviour between GRNs and free CTAB. Fig.6.3(a) shows that cell survival value reaches a stable number in the first hour, and further incubation only results in slight reduction in cell survival up to 9 hrs. While by incubating a series of concentrations of free CTAB solution to the cells for 1, 3, 5 and 7 hours, a dependence on both concentration and incubation time was observed in Fig.6.3(b).

6.3.4 Effect of particle surfactants

Additional polymer coating of GNRs not only prevents direct interaction of CTAB with cell membrane, but also modifies the surface charge state. Previous work

suggests that cationic gold particles are moderately toxic, whereas anionic ones are relatively non-toxic.[25, 48] This phenomenon can be explained as the cell membrane is negatively charged in which case cationic particles are prone to adsorb. Furthermore, it has also been reported that cationic particles are more likely follow a direct diffusion pathway while anionic GNPs are internalized by endocytosis.[25, 49] In this work, negatively charged PSS-GNRs perform less toxic on all dosages, and no significant difference was observed between PSS-GNRs and positively charged PAH-PSS-GNRs. Considering both PAH-PSS-GNRs and GNRs have positive surface charge, the discrepancy in cytotoxicity between CTAB capped and polymer coated GNRs should be related to the surface CTAB on GNRs. With GNRs sizing around 50nm, surface modification and interaction with membrane functional parts may play a more important role than surface charge property.

6.3.5 Effect of particle shape

To study the influence of size and shape on the cytotoxicity, GNRs of different aspect ratios were examined. It is found that all three types of GNRs exhibited cytotoxicity to both MDCK and HEp-2 cells in a dose-dependent manner as shown in Fig.6.4(a) and (b), but no significant difference were found between GNRs. The viability of the cells decreased as the concentrations of GNRs increased. However, the two cell-lines had significant difference in susceptibility to GNR-1 and GNR-2 at 2-fold of 10^{-12} M (Student T-test, $p < 0.1$ in both cases): viability of HEp-2 cells dropped below 60% whereas MDCK cells remained above 90% in both cases. Based on gold particle concentration and cell counts, we estimated that at 10^{-12} M GNRs concentration, the particle cell ratio is approximately 300 GNRs per cell, which reduced cell viability by ~20% in all cases and may be used as an upper limit reference for cellular research.

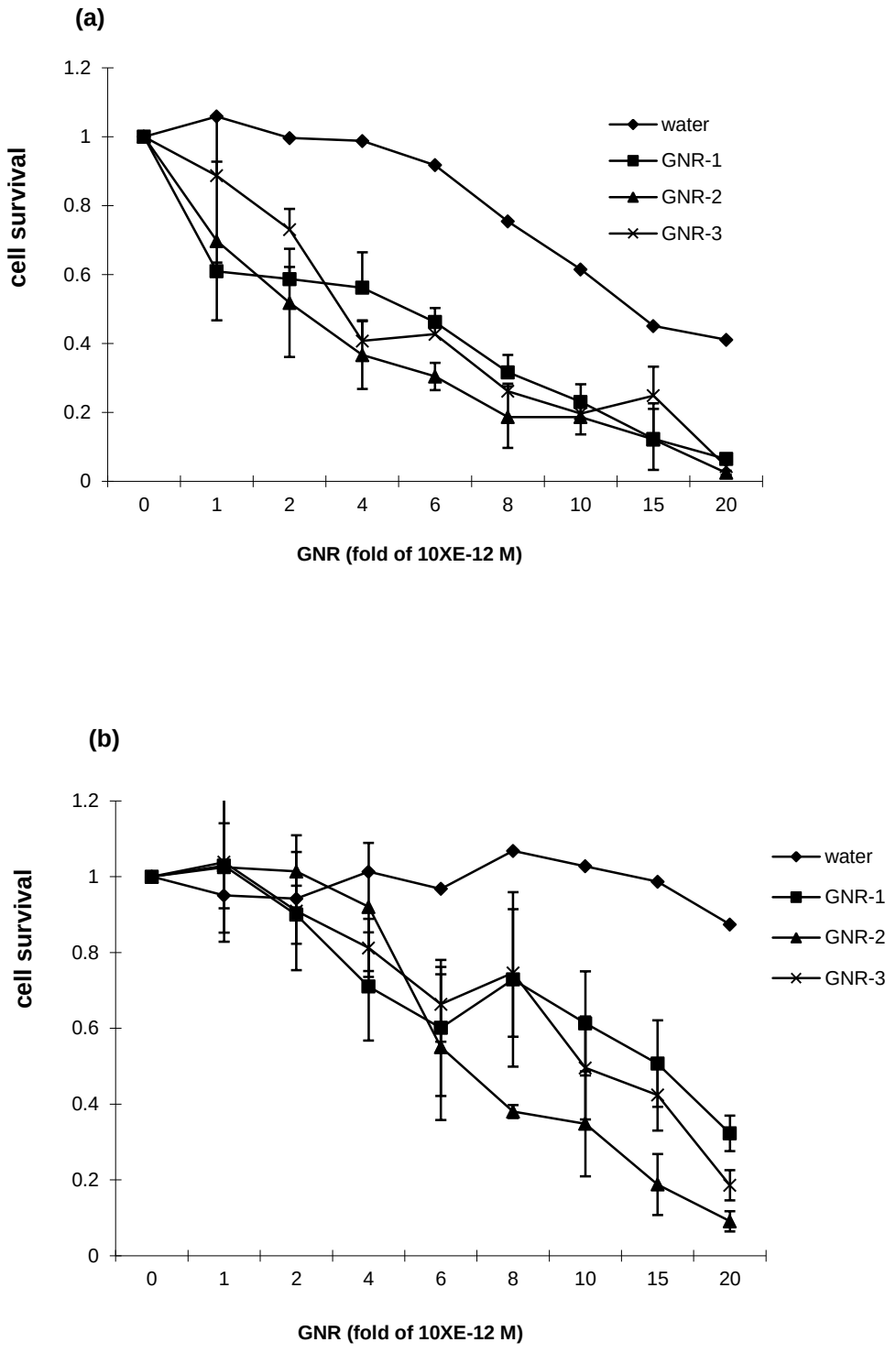

Fig.6.4 MTT assay for HEp-2 (a) and MDCK (b) cells.

6.3.6 Apoptosis study

Generally, there are two mechanisms accounting for cytotoxicity: necrosis and apoptosis although there are overlapping properties towards late stages of the events [50]. Necrosis is usually caused by extreme adverse factors such as fast-acting poisons and strong physical or chemical stress to large sections of tissues， while apoptosis is a programmed cell death mechanism, or to say a ‘suicide’ death form. Apoptosis is triggered to eliminate excess, improper or cells with genetic damage, and is mediated by a group of proteins called caspases, which become activated when cells receive ‘danger’ signals, and in turn they collectively responsible for initiation and execution of the process.[51, 52] To detect apoptosis, cells were stained with SR-VAD-FMK, which detect all activated caspases. The activation of caspases can be quantitatively correlated with the intensity of the fluorescence. All three types of GNRs were confirmed to induce the activation of caspases in both cell lines with different capacity as is shown in Fig.6.5. In general, the accumulation of activated caspases depends on the dosage of GNRs, which is in accordance with the MTT assay. Even at low dosage, activated caspases were detected in HEp-2 cells. The signal intensity increased with the rising dosage, and in the cases of treatment with high dose (10 fold of 10^{-12} M), all cells were all stained strongly and many cells were detached at this stage. All these results suggest GNRs have triggered apoptotic process. For MDCK cells, figures not shown here, a similar trend has been observed, while the stain was relatively weaker compared to Hep-2 cells, and did not increase as drastically as HEp-2 cells when higher concentrations of GNRs applied, which is in accordance with the MTT assay results.

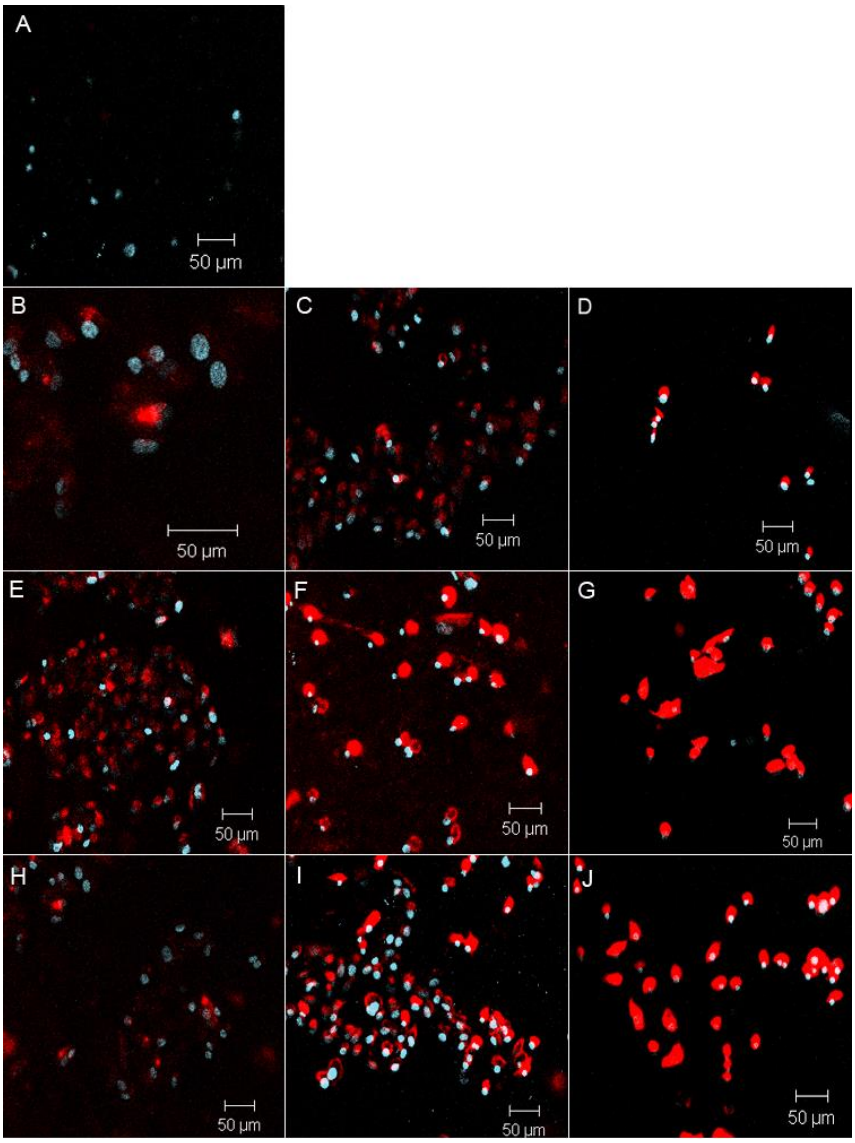

Fig.6.5 Confocal microscopy on HEp-2 cells for activated caspases (in red) and nuclei (in-blue). All images were taken 5 hrs after GNR treatment. A, Negative control (untreated cells); B, C, and D, respectively, were cells treated with GNR-1 at the concentration of 1-, 5- and 10-fold of 10^{-12} M of stock solution. Similarly, E, F, and G were cells treated with GNR-2, and H, I, J were cells treated with GNR-3, respectively, at the concentrations of 1-, 5-, and 10-fold of the 10^{-12} M solutions.

6.4 Conclusion

In conclusion, GNRs show relative higher cytotoxicity compared to GNSs and PSS/PAH coated GNRs to HEp-2 cells, which is mainly related to the CATB on particle surface rather than the free ones in solution. Furthermore, dosage rather than time scale is more important in GNRs induced cytotoxicity. The majority of cell death occurs within one hour of incubation via GNRs induced apoptosis processes. Change in the aspect ratio up to 5 has little influence on GNRs' cytotoxicity. Additional polymer (PSS/PAH) coating can significantly improve cell survival, which seems not due to the change of surface charge properties but isolation of CTAB from cell membrane by additional layer(s) of barrier.

References

[1] P. K. Jain, I. H. El-Sayed, M. A. El-Sayed,“Au nanoparticles target cancer”, Nano Today, 2007, 2, 18-29

[2] X. Liu, Q. Dai, L. Austin, J. Coutts, G. Knowles, J. Zou, H. Chen, Q. Huo, “A one-step homogeneous immunoassay for cancer biomarker detection using gold nanoparticle probes coupled with dynamic light scattering”, J. Am. Chem. Soc., 2008, 130, 2780-2782

[3] C. Yu, J. Irudayaraj, “Multiplex biosensor using gold nanorods”, . Anal. Chem. 2006, 79,572-579

[4] A. K. Salem, P. C. Searson, K. W. Leong, “Multifunctional nanorods for gene delivery”,. Nat. Mater. 2003, 2, 668-671

[5] C. C. Chen, Y. Lin, C. W. Wang, H. C. Tzeng, C. H. Wu, Y. C. Chen, C. P. Chen, L. C. Chen, Y. C. Wu, “DNA-gold nanorod conjugates for remote control of localized gene expression by near infrared irradiation”, J. Am. Chem. Soc. 2006, 128, 3709-3715

[6] N. Durr, T. Larson, D. K. Smith, A. Korgelb, K. Sokolov, A. Ben-Yakar, “Two-photon luminescence imaging for cancer cells using molecular targeted gold nanorods”, Nano Lett. 2007, 7, 941-945

[7] K. Imura, T. Nagahara, H. Okamoto， “Near-field optical imaging of plasmon modes in gold nanorods”, J. Chem Phys. 2005, 122, 154701

[8] K. Imura, T. Nagahara, H. Okamoto， “Near-field two-photoniunduced photoluminescence from single gold nanorods and imaging of plasmon modes”, J. Phys. Chem. B 2005, 109, 13214-13220

[9] P.K. Jain, X. H. Huang, I. H. El-Sayed, M. A. El-Sayed, “Noble metals on the nanoscale: optical and photothermal properties and some applications in imaging, sensing, biology, and medicine”, Acc. Chem. Res. 2008, 41, 1578–1586

[10] C. J. Murphy, A. M. Gole, J. W. Stone, P. N. Sisco, A. M. Alkilany, E. C. Goldsmith, S. C. Baxter, “Gold nanoparticles in biology: beyond toxicity to cellular imaging”, Acc. Chem. Res.2008, 41, 1721-1730

[11] X. H. Huang, I. H. El-Sayed, W. Qian, M. A. El-Sayed, “Cancer cell imaging and photothermal therapy in the near-infrared region by using gold nanorods”, J. Am. Chem. Soc. 2006, 128, 2115-2120

[12] K. S. Lee, M. A. El-Sayed, “Gold and silver nanoparticles in sensing and imaging: sensitivity of plsmon response to size, shape, and metal composition”, J. Phys. Chem. B 2006, 110, 19220-19225

[13] P.K. Jain, K. S. Lee, I. H. El-Sayed, M. A. El-Sayed, “Calculated absorption and scattering properties of gold nanoparticles of different size, shape, and composition: applications in biological imaging and biomedicine”, J. Phys. Chem. B 2006, 110, 14, 7238-7248

[14] H. F. Wang, T. B. Huff, D.A. Zweifei, P. S. Low, A. Wei, J. X. Cheng, “In vitro and in vivo two-photon luminescence imaging of single gold nanorods”, Proc. Natl. Acad. Sci. U.S.A. 2005, 102, 44, 15752

[15] N. Lewinski, V. Colvin, R. Drezek, “Cytotoxicity of nanoparticles”, Small, 2008, 4, 26-49

[16] H. J. Johnston,G. Hutchison, F. M. Christensen, S. Peters, S. Hankin, V. Stone, “A review of the *in vivo* and *in vitro* toxicity of silver and gold particulates: particle attributes and biological mechanisms responsible for the observed toxicity”, Rev. Toxicol. 2010, 40, 328-346

[17] M. Thomas, A. M. Klibanov, “Conjugation to gold nanoparticles enhances polyethylenimine’s transfer of plasmid DNA into mammalian cells”, Proc. Natl. Acad. Sci. U.S.A. 2003, 100, 9138-9143

[18] N. L. Rosi, D. A. Giljohann, C. S. Thaxton, A. K. R. Lytton-Jean, M. S. Han, C. A. Mirkin , “Oligonucleotide-modified gold nanoparticles for intracellular gene regulation”, Science 2006, 312, 1027-1030

[19] B. D. Chithrani, W. C. Chan W. C. W, “Elucidating the mechanism of cellular uptake and removal of protein-coated gold nanoparticles of different sizes and shapes”, Nano Lett. 2007, 7, 1542-1550

[20] Y. Pan, S. Neuss, M. Fischler, F. Wen, U. Simon, G. Schmid, W. Brandau, “Size-dependent cytotoxicity of gold nanoparticles”, Small 2007, 3, 1941-1949

[21] E. Boisselier, D. Astruc, “Gold nanoparticles in nanomedicine: preparations, imaging, diagnostics, therapies and toxcicity”, Chem. Soc. Rev. 2009, 38, 1759-1782

[22] X. H. Huang, P. K. Jain, I. H. El-Sayed, M. A. El-Sayed, “Gold nanoparticles: interesting optical properties and recent applications in cancer diagnostics and therapy”, Nanomedicine 2007, 2, 681-693

[23] W. J. Cui, J. R. Li, Y. K. Zhang, H. L. Rong, W.S. Lu, L. Jiang, “Effects of aggregation and the surface properties of gold nanoparticles on cytotoxicity and cell growth”, Nanomedicine 2012, 8, 46-53

[24] Y. Z. Hao, X. Y. Yang, S. Song, M. Huang, C. He, M. Y. Cui, J. Chen, “Exploring the cell uptake mechanism of phospholipid and polyethylene glycol coated gold nanoparticles”, Nanotechnology 2012, 23, 045103

[25] X. M. Jiang, L. M. Wang, C. Y. Chen, “Cellular uptake, intracellular trafficking and biological responses of gold nanoparticles”, J. Chin. Chem. Soc. 2011, 58, 273-281

[26] Y. Qiu, Y. Liu, L. M. Wang, L. G. Xu, R. Bai, Y. L. Ji, X. C. We, Y. L. Zhao, Y. F. Li, C. Y. Chen, “Surface chemistry and aspect ratio mediated cellular uptake of Au nanorods”, Biomaterials, 2010, 31, 7606-7619

[27] N. M. Schaeublin, L. K. Braydich-Stolle, E. I. Maurer, K. Park, R. I. MacCuspie, A. R. M. N. Afrooz, R. A. Vaia, N. B. Saleh, S. M. Hussain, “Does shape matter? Bioeffects of gold nanomaterials in a human skin cell model”, Langmuir, 2012, 28, 3248-3258

[28] B. Nikoobakht, M. A. El-Sayed, “Preparation and growth mechanism of gold nanorods (NRs) using seed-mediated growth method”, Chem. Mater. 2003, 15, 1957-1962

[29] C. J. Johnson, E. Dujardin, S. A. Davis, C. J. Murphy, S. Mann, “Growth and form of gold nanorods prepared by seed-mediated, surfactant-directed synthesis”, J. Mater. Chem. 2002, 12, 1765

[30] N. R. Jana, L. Gearheart, C. J. Murphy, “Wet chemical synthesis of high aspect ratio cylindrical gold nanorods”, J. Phys. Chem. B 2001, 105, 4065-4067

[31] S. G. Wang, W. T. Lu, O. Tovmachenko, U. S. Rai, H. T. Yu, P. C. Ray, "Challenge in understanding size and shape dependent toxicity of gold nanomaterials in human skin keratinocytes", Chem. Phys. Lett. 2008, 463, 145-149

[32] A. M. Alkilany, P. K. Nagaria, C. R. Hexel, T. J. Shaw, C. J. Murphy, M. D. Wyatt, "Cellular uptake and cytotoxicity of gold nanorods: molecular origin of cytotoxicity and surface effects", Small 2009, 5, 701-708

[33] T. Niidome, M. Yamagata, Y. Okamoto, Y. Akiyama, H. Takahashi, T. Kawano, Y. Katayama, Y. Nidome, "PEG-modified gold nanorods with a stealth character for *in vivo* applications", J. Control. Release 2006, 114, 343-347

[34] D. Mirska, K. Schirmer, S. S. Funari, A. Langner, B. Dobner, G. Brezesinski, "Biophysical and biochemical properties of a binary lipid mixture for DNA transfection", Colloids Surf. B 2005, 40, 51-59

[35] H. Takahashi, Y. Niidome, T. Niidome, K. Kaneko, H. Kawasaki, S. Yamada, "Modification of Gold Nanorods Using Phosphatidylcholine to Reduce Cytotoxicity", Langmuir 2005, 22, 1, 2-5

[36] E. Connor, J. Mwamuka, A. Gole, C. Murphy, M. Wyatt, "Gold nanoparticles are taken up by human cells but do not cause acute cytotoxicity", Small, 2005, 1, 325-327

[37] S. C. Boca, S. Astilean, "Detoxification of gold nanorods by conjugation with thiolated poly (ethylene glycol) and their assessment as SERS-active carriers of Raman tags", Nanotechnology, 21, 235601

[38] C. M. Grabinski, N. M. Schaeublin, A. Wijaya, H. D'Couto, S. A. Baxamusa, K. Hamad-Schifferli, S. M. Hussain, "Effect of gold nanorod surface chemistry on cellular response", ACS Nano 2011, 5, 2870-2879

[39] Y. Zhang, J. Yu, D. J. S. Birch, Y. Chen, "Gold nanorods for fluorescence lifetime imaging in biology", J. Biomed. Opt. 2010, 15, 020504-3

[40] Y. Zhang, D. J. S. Birch, Y. Chen, "Gold nanorods for applications in biological imaging", Proc. SPIE 2011, 7910 7910H

[41] Y. Zhang, D. J. S. Birch, Y. Chen, "Two-photon excited surface plasmon enhanced energy transfer between DAPI and gold nanoparticles:

opportunities in intra-cellular imaging and sensing", Appl. Phys. Lett. 2011, 99, 103701

[42] A. Leung, M. Trau, L. K. Nielsen, "Assembly of multilayer PSS/PAH membrane on coherent alginate/PLO microcapsule for long-term graft transplantation", J. Biomed Mater Res A. 2009, 88, 226-237

[43] D. J. Bergman, M. I. Stockman, " Surface plasmon amplification by stimulated emission of radiation: quantum generation of coherent surface plasmons in nanosystems", Phys. Rev. Lett. 2003, 90, 027402

[44] M. A. Noginov, G. Zhu, A. M. Belgrave, R. Bakker, V. M. Shalaev, E. E. Narimanov, S. Stout, E, Herz, T. Suteewong, U. Wiesner, "Demonstration of a spaser-based nanolaser", Nature 2009, 460, 1110-1112

[45] N. Omura, I. Uechi, S. Yamada, "Comparison of plasmonic sensing between polymer-and silica-coated gold nanorods", Anal. Sci. 2009, 25, 255-259

[46] J. Murphy, T. K. Sau, A. M. Gole, C. J. Orendorff, J. Gao, L. Gou, S. E. Huyadi, T. Li, "Anisotropic metal nanoparticles: synthesis, assembly, and optical applications", J. Phys. Chem. B 2005, 109, 13857-13870

[47] J. Kimling, M. Maier, B. Okenve, V. Kotaidis, H. Ballot, A. Plech, "Turkevich method for gold nanoparticle synthesis revisited", J. Phys. Chem. B 2006, 110, 15700-15707

[48] C. M. Goodman, C. D. McCusker, T. Yilmaz, V. M. Rotello, "Toxicity of gold nanoparticles functionalized with cationic and anionic side chains",Bioconjug. Chem. 2004 15, 897-900

[49] J. Lin, H. Zhang, Z. Chen, Y. Zheng, "Penetration of lipid membranes by gold nanoparticles: insights into cellular uptake, cytotoxicity, and their relationship", ACS Nano 2010, 4, 5421-5429

[50] T. Decker, M.-L. Lohmann-Matthes "A quick and simple method for the quantitation of lactate dehydrogenase release in measurements of cellular cytotoxicity and tumor necrosis factor (TNF) activity", J. Immun. Meth. 1998, 115, 61-69

[51] J. F. R. Kerr, A. H. Wyllie, A. R. Currie, "Apoptosis: A basic biologica phenomenon with wide ranging implications in tissue kinetics", Br. J. Cancer, 1972, 26, 239-257

[52] C. B. Thompson, “Apoptosis in the Pathogenesis and Treatment of Disease”, Science, 1995, 267, 1456-1462

Chapter7

Conclusion and future work

The work presented in this thesis has revealed that when combining with fluorescence techniques, gold nanoparticles can be excellent candidate in biological imaging and sensing research.

Gold nanorods can be synthesized by seeded-growth method, thorough which particle size and shape can be easily controlled by modifying synthesis recipe and reacting conditions. Changing particle size and shape will lead to tuning of surface plasmon structure. Spectroscopic study has shown that gold nanorods will provide strong and stable two-photon luminescence, which is governed by the localized surface plasmon and sensitive to incidence excitation polarization. And microscopic study has revealed that gold nanorods can be used as fluorescence probes in cell culture as their TPL is stronger than many commercial fluorophores. Furthermore,

Study of the imaging of gold nanorods in MDCK cells using fluorescence lifetime imaging microscopy (FLIM) has proved that FLIM image of gold nanorods can proved better contrast and sensitivity than intensity imaging. The characteristic fluorescence lifetime of gold nanorods is found to be less than 100ps, which can be used to distinguish gold nanorods from other fluorescent labels and endogenous fluorophores in lifetime imaging.

Work focused on energy transfer between DAPI, a commonly used DNA label, and gold nanoparticles under two-photon excitation in solution using fluorescence lifetime imaging microscopy (FLIM) has shown that with comparable size and concentration, gold nanorods are more efficient than gold nanospheres. We attribute this transfer enhancement effect to the longitudinal surface plasmon mode of GNRs

overlapping with the excitation wavelength. Energy transfer under two-photon excitation between GNRs and DAPI has also been observed in cell culture and found to be in accord with the solution phase results.

By monitoring interaction between gold nanoparticles and Fluor 405 dye in solution phase, a two-photon enhanced energy transfer effect has been detected, which may origin from the modification of nonradiative decay rate due to the resonance of longitudinal surface plasmon band and incidence light. FLIM-FRET study on cellular pathway has revealed that the uptake of gold nanorods into Hela cells is probably an endocytosis process.

It has been found that CTAB encapsulated gold nanorods were relatively higher cytotoxic than GNRs undergone polymer coating and citrate stabilized gold nanospheres. The toxicity of CTAB encapsulated GNRs was mainly caused by CTAB on GNRs' surface but not free CATB in the solution. No obvious difference was found among GNRs of different aspect ratios. Time-lapse study revealed that cell death caused by GNRs occurred predominately within one hour through apoptosis, whereas cell death by free CTAB was in a time and dose-dependent manner. Both positively and negatively surface charged polymer coated GNRs (PSS-GNRs and PAH-PSS-GNRs) showed similar levels of cytotoxic, suggesting the significance of surface functionality rather than surface charge in this case. The mechanism of cytotoxicity is found to be an apoptosis process.

In the future, at first, an enhanced energy transfer effect between gold nanoparticles and fluorophores has been detected in a qualitative way, but a further quantitative study would provide a thorough understanding into this new type of transfer effect model. This research can be carried out through multi-layer polymer coating experiments. By coating the gold particles layer by layer and link fluorophores to the polymer surface, the separation between 'donors' and 'acceptors' can be accurately controlled, which will make it possible to calculate the energy transfer rate at varying

distances and leading to a quantitative description of the transfer model relating to gold nanoparticles.

Gold nanoparticles can be applied to a new type of physical tool: the ‘Spaser”, which is short for surface plasmon amplification by stimulated emission of radiation. The spaser effect was pointed out by Dr. Stockman and Bergman, it is analogous to the conventional laser for three important reasons: first, surface plasmons are bosons which have spin 1 just as photons do; second, surface plasmons are electrically neutral excitations; third, surface plasmons are the most collective material oscillations known in nature. The most unique advantage of spaser compared to traditional optical sources is that it can generate dark modes, which means that a spaser will create highly intensive, localized field without any background radiation and radiative losses. If realized, a spaser can be applied to a variety of research fields ranging from sensing and biomedicine to imaging and information technology. The spaser system was first realized based on a silica-gold nanoparticle core shell structure in 2009, a spaser mode centring at 531nm was found. If gold nanorods based spaser system could be achieved, it would make the localized excitation source more powerful: as the surface plasmon band of gold nanorods can be tuned in a broad bandwidth, which means that the spaser mode and peaking position can be varied as well.

List of publication

[1] Y. Zhang, J. Yu, D. J. S. Birch, Y. Chen, “Gold nanorods for fluorescence lifetime imaging in biology”, J. Biomed. Opt. 2010, 15, 020504-3

[2] Y. Zhang, J. Yu, D. J. S. Birch, Y. Chen, “Gold nanorods for applications in biological imaging.” Proc. SPIE 2011, 7910 79101H

[3] Y. Zhang, D. J. S. Birch, Y. Chen, “Two-photon excited surface plasmon enhanced energy transfer between DAPI and gold nanoparticles: opportunities in intra-cellular imaging and sensing.”Appl. Phys. Lett. 2011, 99, 103701, (selected for the September 15, 2011 issue of Virtual Journal of Biological Physics Research)

[4] Y. Zhang, Y. Chen, “Plasmons: Structure, Properties and Applications, Chapter 5: Applications of Gold Nanorods Based on Localized Surface Plasmon Resonance.” in press by Nova Science Publishers, Inc. 2011

[5] Y. Zhang, D. Xu, W. Li, J. Yu, Y. Chen, “Effect of Size, Shape and Surface Modification on Cytotoxicity of Gold nanoparticles to Human HEp-2 and Canine MDCK Cells”, 2012, J. Nanomater. 2012, 375496.

[6] Y. Chen, Y. Zhang, D. J. S. Birch, A. S. Barnard, “Creation and Luminescence of Size-selected Gold Nanorods”, Nanoscale 2012, 4, 5017

[7] C. Racknor, M. R. Singh, Y. Zhang, D. J. S. Birch, Y. Chen, “Energy transfer between biological labelling dye and gold nanorods”, submitted to Appl. Phys. Lett. 2013